MATHEMATICAL MODELLING AND ANALYSIS OF DEFORMABLE PERTURBED CONTINUOUSLY STIRRED TANK REACTORS (CSTRs)

Muhirwa Jean Pierre

A Dissertation Submitted in Fulfilment of the Requirements for the Degree of Doctor of Philosophy in Mathematical and Computer Science and Engineering of the Nelson Mandela African Institution of Science and Technology

Arusha, Tanzania

July, 2022

ABSTRACT

In this dissertation, deterministic and stochastic mathematical models for a deformable perturbed continuously stirred tank reactor (CSTR) with exothermic and endothermic reactions have been developed and analysed. The Ordinary Differential Equations (ODEs) were obtained by using the Reynold transport theorem and Stochastic Differential Equations (SDEs) were derived in the Itô sense from the developed classical deterministic models. There were four types of SDEs formulation, namely, additive SDE, multiplicative SDE, parameter perturbation SDE and transition probabilities SDE. The numerical results of the developed models were obtained and analysed through statistical and Bayesian methods. These methods were Classical Least Squares (LSQ) and Markov chain Monte Carlo (MCMC) for ODES while the Euler-Maruyama technique was used to simulate the SDEs. The LSQ numerical findings showed that the measurements fit theoretical models well provided that the noise intensity ranges between 0 and 0.5. The MCMC results identified the parameters posterior means and the credible intervals in which models parameters must be oscillating. The PRCCs with Latin Hypercube Sampling technique were applied to check the sensitivity and uncertainty quantification of estimated parameters against the models' response. Some of the parameters of models were found to be highly and positively correlated with models' states and others were highly and negatively correlated with models' state variables. For example, seven parameters were found to be highly correlated with exothermic CSTR model whilst six parameters were identified to be highly correlated with endothermic CSTR model. This implies that those parameters have to be controlled and treated carefully as the increase or decrease in their values significantly impact the models' outcomes. For the case of stochastic part, simulations of SDEs revealed that high fluctuations notably affect trajectories of the variables. The overall numerical results obtained seem to be reliable and have shown an insight in describing the dynamics of the CSTR deterministic and stochastic models with detailed mathematical and statistical information. So, the formulated models were analysed, validated and can be used to model and describe various mechanical, biological and chemical processes such as filtration, anaerobic respiration and combustion among others.

APPROVAL

I, **Muhirwa Jean Pierre**, do hereby declare to the Senate of Nelson Mandela African Institution of Science and Technology that this thesis is my own original work and that it has neither been submitted nor being concurrently submitted for degree award in any other institution.

Muhirwa Jean Pierre

Name and signature of candidate — **Date** 01.07.2022

The above declaration is confirmed

Prof. Dr-Ing. Verdiana Grace MASANJA

Name and signature of supervisor 1 — **Date** 01.07.2022

Dr. Isambi Sailon MBALAWATA

Name and signature of supervisor 2 — **Date** 01.07.2022

DECLARATION

I, **Muhirwa Jean Pierre**, do hereby declare to the Senate of Nelson Mandela African Institution of Science and Technology that this thesis is my own original work and that it has neither been submitted nor being concurrently submitted for degree award in any other institution.

Muhirwa Jean Pierre

Name and signature of candidate — **Date** 01.07.2022

The above declaration is confirmed

Prof. Dr-Ing. Verdiana Grace MASANJA

Name and signature of supervisor 1 — **Date** 01.07.2022

Dr. Isambi Sailon MBALAWATA

Name and signature of supervisor 2 — **Date** 01.07.2022

COPYRIGHT

CERTIFICATION

The undersigned certify that they have read and found the dissertation entitled " Mathematical Modelling and Analysis of Deformable Perturbed Continuously Stirred Tank Reactors (CSTRs)" to be acceptable by the Nelson Mandela African Institution of Science and Technology, in the fulfilment of the requirements for the degree of Doctor of Philosophy in Mathematical and Computer Sciences and Engineering of the Nelson Mandela African Institution of Science and Technology.

Prof. Dr-Ing. Verdiana Grace MASANJA

Name and signature of supervisor 1 — **Date** 01.07.2022

Dr. Isambi Sailon MBALAWATA

Name and signature of supervisor 2 — **Date** 01.07.2022

ACKNOWLEDGEMENTS

My first acknowledgement is addressed to Lord, Almighty God who granted me peace and health to accomplish my PhD studies at Nelson Mandela African Institution of Science and Technology, Tanzania (NM-AIST).

My second gratitude and special thanks go to my enable, humble, smart, honest, courageous and selfless supervisors, Prof. Verdiana Grace MASANJA, Faculty member of Nelson Mandela African Institution of Science and Technology, Tanzania, School of Communication and Computational Science and Engineering, Department of Applied Mathematics and Computational Science and Dr. Isambi Sailon MBALAWATA, a senior researcher and scientific development manager at African Institute for Mathematical Sciences (AIMS)-global Secretariat in Kigali, Rwanda. I have been very lucky and a prestigious student among others to be supervised by that complementary team for which without them I could not finish my PhD studies on time. I really recognise their encouragements, assistance, advice, efforts, and maximum supervision that made my PhD studies and research go smoothly. They always advise, communicate and treat me like their own son. I found them to qualify for having that ability of understanding both social and academic issues for PhD students.

My sincere tribute is paid to my greatest sponsor, the German Academic Exchange Service (DAAD) for financial support to pursue my PhD studies at NM-AIST. Also, I acknowledge the financial support from AIMS to partially fund publication fees and flight ticket to Arusha - Tanzania. I am also thankful to my employer, the University of Rwanda, College of Science and Technology (UR-CST) for providing with me the study leave.

I can not thank my wife enough, Mrs. Uwamahoro Lea for being humble and tolerant for me while studying abroad. She has been patient and put herself on my side via comfort, encouragements and providing various ideas on how to overcome and manage both academic and social challenges. Her love and unstopped care to our family furnished me strengths to work hard to accomplish my tasks. At the same time, I thank my little son, Muhirwa Shimwa Perry who was very flexible to me and did not disturb me too much while working from home during the outbreaks of Covid-19 pandemic.

I wish to extend thanks to my beloved father, mother, brothers, sisters and all my in-laws for

their prayers and financial support. My last appreciations are given to my colleagues, staff, students from NM-AIST and my workmates from UR-CST for their motivations during my studies at NM-AIST. May almighty God bless you all.

DEDICATION

I dedicate this dissertation to my beloved wife, Mrs. Uwamahoro Lea

&

To my son, Muhirwa Shimwa Perry

TABLE OF CONTENTS

LIST OF TABLES

LIST OF FIGURES

LIST OF ABBREVIATIONS, ACRONYMS AND SYMBOLS

CSTR	Continuously Stirred Tank Reactor
CSTRs	Continuously Stirred Tank Reactors
MCMC	Markov chain Monte Carlo
DRAM	Delayed-Rejection Adaptive Metropolis
LSQ	Least Squares
Param	Parameters
ODE/ode	Ordinary Differential Equation
ODEs/odes	Ordinary Differential Equations
SDE/sde	Stochastic Differential Equation
SDEs/sdes	Stochastic Differential Equations
MSDE	Multiplicative Stochastic Differential Equation
PCC	Partial Correlation Coefficient
PRCCs	Partial Rank Correlation Coefficients
LHS	Latin Hypercube Sampling
Cov	Covariance
Var	Variance
std	Standard Deviation
NM-AIST	Nelson Mandela African Institution of Science and Technology
CoCSE	Communication and Computer Sciences and Engineering
UR	University of Rwanda
CST	College of Science and Technology
AIMS	African Institute for Mathematical Sciences

LIST OF APPENDICES

CHAPTER ONE

INTRODUCTION

1.1 Background of the Problem

From the 19th century until the middle of 20th century, Continuously Stirred Tank Reactors (CSTRs) were designed to be used for waste treatments, military tools to produce mustard gas, medical sample tubes to collect patients' samples, nuclear reactors to produce nuclear energies, hand-crafts tools in colour painting. All these reactors were in type of pots, vessels, tubes, chambers, containers, apparatuses and towers as stated in Rowse (2011) and Kockmann (2019). Before 21st century, there was no clear difference between reactors and all of them were categorised as reactors regardless their functionality behaviours (Kockmann, 2019). It is from 21st century where scientists, engineers and design engineers tried to distinguish these reactors depending on their functionalities and their production abilities ranging from batch processing to continuous stirred processing (Kockmann, 2019). Now, CSTRs are very useful chemical reactors that produce chemical products from the given inputs of reactants (Telen *et al.*, 2014). The complexity and the non-linearity dynamical behaviours of CSTRs have attracted many researchers, especially mathematicians who can contribute to determining, predicting, estimating parameters and controlling the states of these reactors. Examples of reactants and products include alcohols, polymers from monomers, fertilisers, pharmaceutical products and renewable energies from biogas process, among others. According to Vojtesek *et al.* (2008), mathematical understanding of how these tanks behave, is of great importance for solving, predicting and controlling them. It is moreover, important to analyse the effect of deformation and the perturbation that may be present in the CSTRs' models during processing. Different sources of deformation and perturbation which may be observed in CSTRs are from the change in feeding rates, environmental disturbances and measurements imperfect, among others.

1.2 Problem Statement

A great number of scholars reported that the mathematical formulation, the parameter estimation, methods to be used, control and the prediction of reactors seem to be a challenge due to reactors' non-linearity behaviour. To mention few from where the research idea in this study has been drawn, Oravec *et al.* (2018) revealed that robust model predictive control method is a good

method for CSTRs, however it is a challenging task for controlling and predicting CSTRs due to their non-linearities' behavior present in their models as well as time-varying uncertainties in its parameters. They further captioned that finding a suitable mathematical formulation for a complex process maybe a challenging task. Shakeri *et al.* (2018) have shown that over the past years, stochastic CSTRs models have been given little attention. They argued that there is a need to develop stochastic CSTRs models that may be able to describe and capture the randomness aspects in the system. Another challenge of having some of non-converging CSTRs' parameters is found in Muhirwa *et al.* (2017). Rowse (2011) claimed that choosing inappropriate range of CSTR's parameters impacts the expected yields from CSTRs while on the other hand, Karimi *et al.* (2014) mentioned that it is very important to take care of stochastic disturbance intensities into CSTR models by considering a wide range of parameter estimation problems with prior knowledge about the parameters. Many researchers ignored deformation which may alter the scale of production conversion (Yamamoto *et al.*, 2019). Others do not consider the perturbation of the tanks by not taking into consideration of noise which is a measure of how the process responds to the external disturbances like stochastic excitement and change in feeding rates (Karimi *et al.*, 2014). In the literature, a great number of scholars focus on only two or three states deterministic models with a first order simple exothermic irreversible models, for instance, Sinha *et al.* (2018). In addition, they considered very simplified assumptions such as constant volume, constant densities, and areas of the tanks as well as isothermal CSTRs (Sinha *et al.*, 2018). Therefore, this research aims at addressing some of these gaps by considering non-isothermal and both non-deterministic and deterministic models as the tanks may behave stochastically as can be found in Karimi *et al.* (2014). This research will further construct and display CSTR models that consider the first-order irreversible events with the variation of volumes. The other research gaps that will be addressed by the researchers is to solve and identify physical parameters of both variable-volume endothermic and exothermic CSTR models with four state variables namely, volumes, concentrations, reacting tanks' temperature and cooling or heating jackets'temperature.

1.3 Rationale of the Study

Most of the real life problems are modelled, solved and analysed using mathematical concepts. The same concepts are applied in chemical engineering, whereby the dynamics of the chemical reactors are modelled, solved, analysed, controlled and predicted mathematically. Hence, math-

ematical understandings of chemical industrial processes which ranges from industrial research, industrial development and extends to industrial operations are among the best approaches to minimize the risk of industrial's prototyping process. Cost for performing a physical-chemical laboratory experiment on the real chemical industry processes is inventively high. Combining laboratory experiments with mathematical modeling and computer experiments by simulations could lead to wastage of resources due to the tremendous cost. This may even lead to some unexpected hazards. As a result, a simple theoretical mathematical analysis provides a piece of very necessary and useful information for not only the global scientists, engineers and designers but also for the East-African scientists, engineers and designers as their countries are calling investors to install pharmaceutical industries, especially, Rwanda (Emmanuel, 2017). Such information assists them to design cost effectively and more appropriate prototypes and production systems. The focus of this research is neither the construction of prototypes nor the creation of the physical-chemical industries' tanks rather it is the development of a mathematical model and its simulations for the understanding of the behaviour of these tanks to generate knowledge that may help design engineers, chemical and process engineers to design suitable prototypes and produce physical tanks for chemical industries cost effectively.

1.4 Research Objectives

1.4.1 General Objective

The general objective of this research is to develop deterministic and stochastic deformable-perturbed CSTRs' models, and use Bayesian and statistical methods to analyse them.

1.4.2 Specific Objectives

This research has the following five specific objectives:

(i) To formulate perturbed exothermic and endothermic CSTRs' models both deterministic and stochastic;

(ii) To perform numerical simulations of the formulated CSTRs' models and determine the effectiveness of different numerical methods in solving these models;

(iii) To assess the effect of perturbation on the CSTRs' models;

(iv) To determine the impact of CSTRs' deformation;

(v) To simulate an actual real-life chemical problem as an application of CSTRs.

1.5 Research Questions

The following are the research questions that have to be addressed in this study:

(i) Can we formulate suitable and analysable non-deterministic and deterministic mathematical models for CSTR?

(ii) Can we find effective methods to solve CSTR models?

(iii) What is the effect of perturbations on CSTR models?

(iv) Is there deformation impact on CSTR models?

(v) Is there a real-life application of CSTR?

1.6 Significance of the Study

Continuously stirred tank reactor (CSTR) is very useful and important production tool in chemical engineering. This kind of tank reactor exhibits non-linear and complex dynamical behaviour which makes it to be very difficult to analyse, control and predict. Mathematical modelling and analysis of the CSTR help in determining the dynamical evolution of the CSTR's states. Combining experimental studies with numerical simulations of reactors mostly leads to unnecessary waste of resources and may cause unpredicted hazards. This dissertation numerically solves and analyses the dynamics of the CSTR's models which incorporate variable-volume and stochastic aspects, quantitatively. As a result, this study serves as a primary source of knowledge for chemical and design engineers towards the production of appropriate and suitable physical tank reactors with reasonable cost.

1.7 Delineation of the Study

In this study, deterministic and stochastic mathematical models for the CSTR with a variable-volume are formulated (Chapter 3) and numerically solved and analysed (Chapter 4). Due to unavailability of the CSTR's primary data, the numerical results obtained were not based on the actual real data but simulated data from the models using literature values.

It was very important for chemical and design engineers to know better about the estimate values of the physical quantities of the CSTR, namely, variables and parameters. In addition, to be aware about the magnitude of the effects of perturbation and deformation which may occur on the CSTR's models, from various sources was of a paramount benefit for the CSTR designing process. Even if the dynamical evolution of CSTR with cooling / heating process has been analysed in this dissertation, the following limitations were encountered:

(i) The formulated models both deterministic and stochastic were non-linear and have a great number of unknown parameters and hence complex, hence only numerical results of models have been obtained;

(ii) Due to unavailability of real data, data simulated from literature values have been used. With more time, real data can be sought and analysed to really identify CSTRs' models in future;

(iii) Due to computational facilities, the formulated models were not computed in parallel. However, this can be done in the presence of facilities like High Performance Computing (HPC).

CHAPTER TWO

LITERATURE REVIEW

2.1 Literature Review on Types of Chemical Reactors and their Descriptions

According to Foutch *et al.* (2003), Moran *et al.* (2000), Theodore (2012), Finlayson (2012) and Couper *et al.* (2009), there is no simple way of classifying chemical reactors due to the complexity, non-linearity term of the system and the variable of interest. However, there is a common way of classifying them depending on their operational behaviour, reaction phases namely homogeneous (one phase, either liquid phase, gas phase or solid phase) or heterogeneous (more than one phase, either liquid-gas, gas-liquid, solid-gas, gas-solid, solid-liquid-gas, gas-solid-liquid, gas-liquid-solid, etc.), reaction types (exothermic reactions which can release heat energy and endothermic reactions which can acquire heat energy to react). Advantages and disadvantages of these tanks which may be scientific or economical play a big role in differentiating the chemical reactors in terms of easiness of functioning, weaknesses, complications, production methods, as well as their physical properties which include size, shape and design. Even though there are many types of reactors, Barnard (1985) tried to show the most useful three types of reactors which are batch reactors, tubular reactors and CSTRs. They have highlighted some of the industrial advantages and disadvantages of these reactors based on their performance and treatment as well. Poulopoulos *et al.* (2006) have shown different ways of classifying reactors, and one way of doing this is to look at the number of reaction phases that are allowed in, which may be homogeneous, means a single phase that is either liquid-phase or gas-phase, heterogeneous, means two or three phases such as liquid-gas, liquid-solid, gas-solid, and vice-versa among others. Salmi *et al.* (2010) showed types of reactors that may be classified based on catalyst scraps and are called catalytic reactors. Among them are fluidized beds when these scraps are very tiny, trickle beds if scraps are immobile and slurry reactors if the catalyst scraps are suspended in the fluid. Therefore, Table 1 shows the main three types of chemical reactors which are commonly used in industries nowadays with the possibility of changing their names as stated above.

Table 1: Description of chemical reactors

Type	working behaviour	Number of phases	Reaction types	Advantages	Disadvantages
BATCH	Reactants and products are supplied and withdrawn once respectively	Homogeneous and heterogeneous	Exothermic and Endothermic	Easier to understand, low cost and low capital	Small conversion scale (most of cookers), not-flexible: no possibility to be changed over
SEMI-BATCH	It is a Batch but either reactants or products can be put or removed continuously	Homogeneous and heterogeneous	Exothermic and Endothermic	Medium firm tools, big in size compared to batch reactors, temperature and concentration prediction within time, some how easier to control	Batch and mid-CSTR, not practicable in many reactions
CSTR	Reactants and product are fed and removed continuously	Homogeneous and heterogeneous	Exothermic and Endothermic	High conversion scale, industrial tools, practicable for all most all reactions	Too complex to predict and control, normally operates at steady-state

2.2 General Literature Review on CSTRs

In the past decades, CSTRs have gained research momentum whereby most scientists and chemical engineers would like to know the theories and the mathematics behind these tanks due to the complexity and non-linearity operational behaviour that are present in these reactors during the production process (Naikwad *et al.*, 2009). Discussions about CSTRs that are found in literature seems to be broad, hence a non-exhaustive list of literature that consists of early and recent research on the matters related to the topic has been reviewed. Among others we have, robust feedback linearization of an isothermal continuous stirred tank reactor was conducted by Tofighi *et al.* (2017) using mixed sensitivity synthesis and iteration approaches in the presence of uncertainties. Also, the first-order and higher-order sliding mode observer methods have been used in Osorio *et al.* (2011) to design and estimate states and unknown inputs of the

CSTR, and it was shown that higher-order sliding mode may be adopted to reduce the noise into the system compared to first-order sliding mode.

The Luenberger fuzzy observer, Luenberger fuzzy observer with sliding modes, Walcott-Zak fuzzy observer and Utkin fuzzy observer were adopted and used as fault detection sensors of the CSTR, the more details are found in Ballesteros-Moncada *et al.* (2015). Again, a general model of the CSTR was developed and the transient behaviour for irreversible non-linear polymerization process in CSTR has been studied in Dias *et al.* (2005). Furthermore, a mathematical model and simulation of reactors with production experiment of Hexane from Benzene were performed in Prokopová *et al.* (2009). The experimental investigation of performance of CSTR as bioreactor for producing biohydrogen from water melon waste in the anaerobic diegester was done and explained in details by Cahyari *et al.* (2016). Zhang *et al.* (2013) identified the flow behaviours in the CSTR trough three-dimensional computational fluids dynamics (CFD) simulations. Furthermore, the effect of hydrodynamic shear on biogas production in the CSTR were analysed and discussed in the study of Jiang *et al.* (2016) using Metzner-Otto method.

The efficient Azo Dye colour identification in the CSTR with the built-in bio-electrochemical system was developed for Azo dye alizarin yellow R (AYR) which in turn help in wastewater treatment as mentioned in the work of Cui *et al.* (2016). The result has shown that the CSTR bio-electrochemical system could serve as a good strategy to add more value to the conventional existing anaerobic facilities compared to the refractory wastewater treatment approach. In the same way, different types of reactors and types of reactions in chemical engineering processes that may be used in production are widely defined and described in Nanda (2008). Limitations of CSTRs' performance due to cooling jacket dynamics with both open and closed loops are spoken out and discussed in the article of Russo *et al.* (1993).

The modelling and control of the CSTR were done based on a mixed logical dynamical model which resulted in satisfactory performance of the tank as revealed in the work of Jingjing *et al.* (2007). Another article on mathematical modeling and numerical simulations of two-phases which are gas-liquid flow in the CSTR was published by Karadimou *et al.* (2019). In addition, the non-parametric and non-linear stochastic dynamical model together with the behavior analysis of a class of the single state isothermal CSTR was studied and analysed in Tronci *et al.* (2009). Ahmed *et al.* (2013) used the cascade control strategy to control the temperature of the exothermic CSTR with cooling jacket. The stability analysis of the system was investigated

and achieved by using Routh-Hurwitz and Argand diagram. The adaptive method with recursive identification and the polynomial synthesis with placement of poles were applied on the CSTR system by Vojtesek *et al.* (2009) to study its dynamics, however, this method provided inappropriate control responses and overshoots.

The problem of characterizing the global dynamics of a single state non-linear stochastic CSTR system is addressed in Tronci *et al.* (2009) by using the Fokker-Plank as the state probability distribution function, but the study of several state non-linear stochastic system is of paramount as recommended in this article. The same approach of Fokker-Plank was applied for a two-state stochastic CSTR system as can be observed in Shakeri *et al.* (2018). Moreover, the effect of operating conditions on the CSTR's performance with saponification experiment was conducted in the research of Danish *et al.* (2015), and the result has shown that the increase in conversion scale depends on the increase in CSTR's volume. Besides that, the dynamical behaviour of the CSTR through a single first order reaction was researched on and analysed in the work of Uppal *et al.* (1974). It was mentioned that this method is one of among the best methods for the successful control of a system with the non-linearity behaviour.

Once more, the neural network approach was used to identify the dynamics of two-states namely the temperature and the concentration of the CSTR's model and the method has provided reasonable and precise results as can be found in Al-Araji (2015). The chemical process hazards, causes and proposed measures of safety of batch and semi-batch processes are as well discussed in Etchells (2005). In Karimi *et al.* (2015), the two-states CSTR stochastic model were studied and analysed by using the approximate expectation maximization (AEM) and Bayesian algorithms. It was revealed that Bayesian is an effective method to apply on CSTR's stochastic models since it provided more accurate parameter estimates compared to AEM, and it is even more applicable for an unknown system with a small number of data sets. López Buriticá *et al.* (2015) used Monod and Haldane kinetics methods to perform the stability analysis of a system that models the formation of biofilms inside the CSTR during the waste-water treatment process. Even though both methods performed well, still the Monod kinetics provided biofilms formation in a shorter time compared to the Haldane kinetics method. Likewise, the parameters estimation of non-linear chemical and biological processes with non-measured variables from a number of data sets was done by Jang *et al.* (2011) using Bayesian approach with examples of mammalian cell growth process, genetic regulatory network and JAK-STAT models.

From Buehler *et al.* (2016), the Lyapunov-based stochastic non-linear model predictive control was used to shape the state probability density functions in the CSTR with simple exothermic reaction $A \xrightarrow{k} B$. Rajagopalan *et al.* (1972) performed multivariate character and stability analysis of irreversible exothermic CSTRs, and the signal flow diagram and the equilibrium states were determined by taking into consideration of first and second-order reactions. The Bayesian approach was again used in Nicoulaud-Gouin *et al.* (2016) as the sorption parameters identifiability tool. The research outputs have shown that Bayesian inference is more preferable for the analysis of CSTR experiments as per numerical identification and sorption parameter identification as well. A modified CSTR model for the neutralization process was studied and analysed in the research of Ibrehem (2011). This CSTR model has been used to assess the effects of strong acid (HCL) and strong base (NaOH) on the flow rates of ionic concentrations and more discussions are found in Ibrehem (2011). A one state variable precisely temperature of a non-isothermal CSTR was analysed by using PID and Fuzzy logic controllers, and the results from simulation and temperature control shown that Fuzzy logic is a good controller compared to PID control as can be explored in Ramli *et al.* (2017).

However, due to the complexity and the non-linearity dynamical behaviour of CSTRs, the very important problem that the researchers are eager to address is to find a good parameter variation estimator for both deterministic and stochastic models. The identification of reliable methods that can provide converging solutions for a non-isothermal, four-states models of the perturbed and deformed exothermic and endothermic CSTRs is also addressed in this research.

CHAPTER THREE

MATERIALS AND METHODS

In this Chapter, there are discussions of materials employed in continuously stirred tank reactor (CSTR) models' formulation and descriptions of methods used to analyse those formulated models. The Chapter is split into three main Sections, whereby the first Section deals with deterministic CSTR models formulation while the second Section contains CSTR stochastic models formulation. The last Section describes the methods used to analyse the models.

3.1 Formulation of CSTRs Deterministic Models

The CSTR deterministic models are formulated using the schematic diagram represented in Fig. 1 for the exothermic reaction and Fig. 2 for the endothermic reaction within the tank.

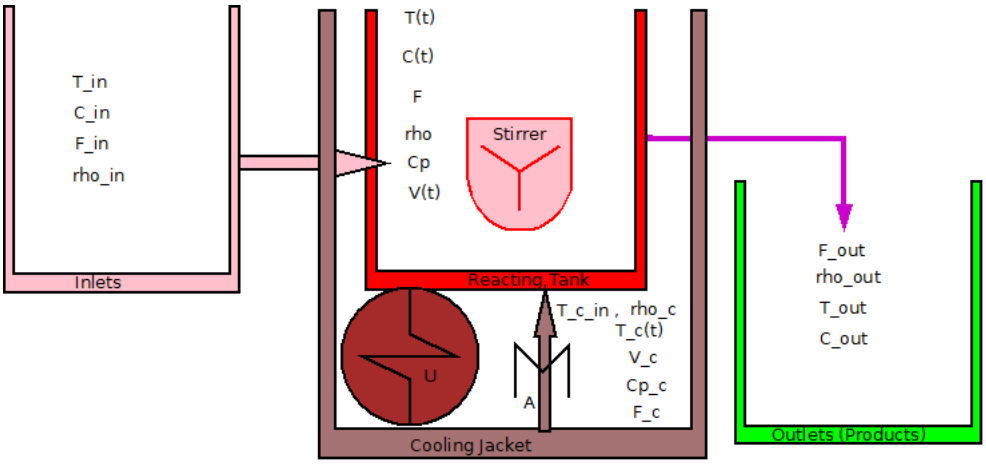

Figure 1: Schematic diagram that shows dynamics of exothermic CSTR system

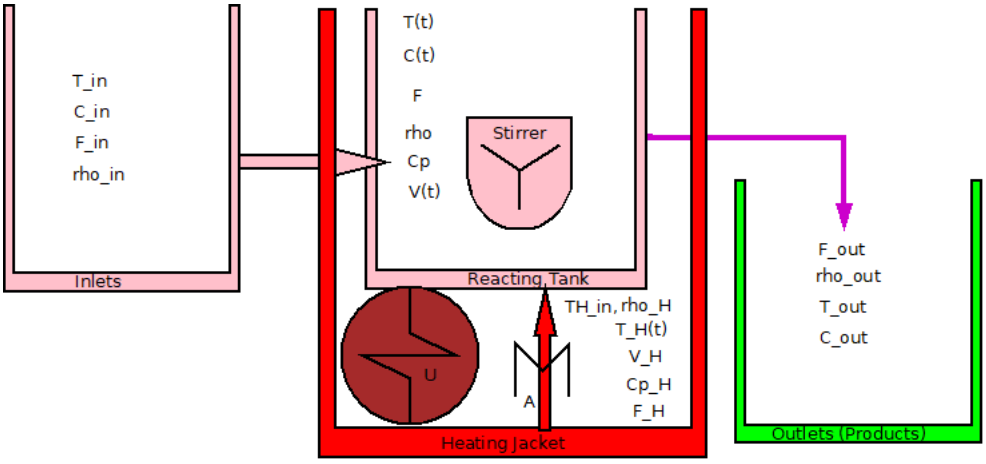

Figure 2: Schematic diagram that describes the dynamics of endothermic CSTR system

The variables, parameters and units of quantities that are shown in Fig. 1 and Fig. 2 are described in Table 2 and Table 3.

Table 2: Table of variables and parameters

Symbol	Units	Description
T_{in}	K	Temperature of the feeding reactants
C_{in}	$\frac{\text{kmol}}{\text{min}m^3}$	Concentration of the feeding reactants
F_{in}	$\frac{m^3}{\text{min}}$	Volumetric flow of the feeding reactants
ρ_{in}	$\frac{kg}{m^3}$	Density of the inlet reactant
$T_{c_{\text{in}}}$	K	Feeding cooling temperature
ρ	$\frac{kg}{m^3}$	Density of the substance inside the reacting tank
C_p	$\frac{\text{kcal}}{Kkg}$	Specific heat capacity of the reacting tank
A	m^2	Surface area of the reacting tank
$V(t)$	m^3	Volume of the reacting tank at time t
$T(t)$	K	Temperature of the substance inside the reacting tank at time t
$T_{H_{\text{in}}}$	K	Feeding heating temperature
$C(t)$	$\frac{\text{kmol}}{\text{min}m^3}$	Concentration of the product inside the reacting tank at time t
ρ_H	$\frac{kg}{m^3}$	Density of the heating substance
A_H	m^2	Cross-sectional area between the reacting tank and the heating jacket
V_H	m^3	Volume of the heating jacket

Table 3: Continued table of variables and parameters

Symbol	Units	Description
C_{p_H}	$\frac{\text{kcal}}{Kkg}$	Specific heat capacity of the heating jacket
F_H	$\frac{m^3}{\text{min}}$	Volumetric flow of the heating substance
ρ_{out}	$\frac{kg}{m^3}$	Density of the outlets (products)
F_{out}	$\frac{m^3}{\text{min}}$	Volumetric flow of the outlets (products)
T_{out}	K	Temperature of the outlets (products)
C_{out}	$\frac{\text{kmol}}{\text{min}m^3}$	Concentration of the outlets (products)
ρ_c	$\frac{kg}{m^3}$	Density of the coolant substance
$T_c(t)$	K	Temperature of the cooling jacket at time t
A_c	m^2	Cross-sectional area between the reacting tank and the cooling jacket
V_c	m^3	Volume of the cooling jacket
C_{p_c}	$\frac{\text{kcal}}{Kkg}$	Specific heat capacity of the cooling jacket
F_c	$\frac{m^3}{\text{min}}$	Volumetric flow of the coolant substance

To study the CSTRs behaviour as a whole system is complicated, that is why most of the researchers choose a unit and define a virtual control volume that may physically explain the transport phenomena in and out of the system by applying the Reynold transport theorem (RTT)(Lorenz, 2006; Baddour, 2008; Lee, 1969). Thus, instead of considering Fig. 1 and Fig. 2 for model formulation, the schematic diagram that is presented in Fig. 3 is used to explain the transport phenomena in and out of CSTRs.

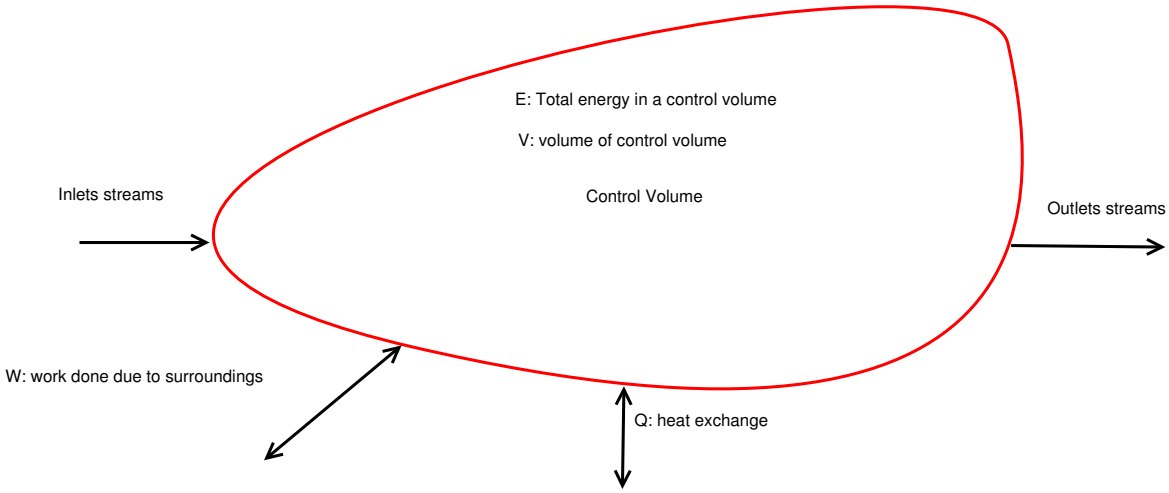

Figure 3: Control volume illustration

3.1.1 Formulation of Deterministic Model for Exothermic CSTR

During deterministic model formulation of the exothermic CSTR, the following assumptions were taken into considerations:

A.1 There is perfect mixing in CSTRs to avoid spatial gradients of velocity, temperature, concentration and of other properties of the mixture.

A.2 The shaft work produced by the stirring process is negligible.

A.3 No pressure drop happening in the CSTRs implies that CSTRs work at a constant pressure

A.4 Kinetic energy, potential energy and other forms of external energy are infinitesimal small compared to the heat exchange and the heat from the chemical reactions

A.5 The wall is isolated and its temperature is negligible. Only the heat exchange is channelled through the designed area between reacting tanks and jackets

A.6 The CSTRs' volume is a variable

A.7 The CSTRs' densities ρ, the specific heat capacities C_p are constants

A.8 There is negligible external stress acting on the system, hence negligible momentum on the system.

Based on the assumptions listed above and from the chemical reaction point of view, the derivation of the deterministic model for exothermic CSTR is done by considering the empirical

concentration which is given by

$$C = \frac{n}{V},$$

where n is the number of moles that are contained in molecules of substance and V is the volume occupied by that substance. The rate of production is given by

$$r = \frac{1}{V}\frac{\mathrm{d}n}{\mathrm{d}t} = \frac{\mathrm{d}C}{\mathrm{d}t} \equiv \frac{\mathrm{d}n}{\mathrm{d}t} = V\frac{\mathrm{d}C}{\mathrm{d}t}.$$

If we have a reactant to be converted into a product, then the rate of production becomes

$$r = -\frac{\mathrm{d}C}{\mathrm{d}t} = kC.$$

However, the reaction rate k has the temperature dependency which is shown in Van't Hoff equation and it is expressed as

$$\frac{\mathrm{d}(\ln k)}{\mathrm{d}T} = \frac{\triangle Hr}{RT^2} \equiv \mathrm{d}(\ln k) = \frac{\triangle Hr}{RT^2}\mathrm{d}T. \tag{1}$$

Solving Equation (1) for k by integrating both side with respect to T leads to

$$\int_{k_0}^{k} \mathrm{d}(\ln s) = \int_{T_{\text{mean}}}^{T} \frac{\triangle Hr}{Ry^2}\mathrm{d}y \equiv [\ln s]_{k_0}^{k} = -\frac{\triangle Hr}{R}\left[y^{-1}\right]_{T_{\text{mean}}}^{T}.$$

So,

$$\ln k - \ln k_0 = -\frac{\triangle Hr}{R}\left(T^{-1} - {T_{\text{mean}}}^{-1}\right) \equiv \ln(\frac{k}{k_0}) = -\frac{\triangle Hr}{R}\left(T^{-1} - {T_{\text{mean}}}^{-1}\right),$$

$$\frac{k}{k_0} = e^{-\frac{\triangle Hr}{R}\left(T^{-1} - {T_{\text{mean}}}^{-1}\right)} \equiv k = k_0 e^{-\frac{\triangle Hr}{R}\left(\frac{1}{T} - \frac{1}{T_{\text{mean}}}\right)}.$$

If we let $\triangle Hr = E$ be an activation energy, the energy required to activate the system, we get

$$k = k_0 e^{-\frac{E}{R}\left(\frac{1}{T} - \frac{1}{T_{\text{mean}}}\right)},$$

which is the Arrhenius equation with R being the gas law constant. As a result, the production rate is given by:

$$r = kC = k_0 e^{-\frac{E}{R}\left(\frac{1}{T} - \frac{1}{T_{\text{mean}}}\right)}C. \tag{2}$$

All derivations which lead to Equation (2) are done with the help of formulas found in Hill *et al.*

(1977) and Kandiyoti (2009).

The CSTRs' deterministic models are developed by using the fundamental principle of conservation of quantities. So, the accumulation of substance's property residing inside the system during a certain interval of time is equal to the amount of substance flows in subtract the amount of substance flows out plus the amount of substance produced inside the system subtract the amount of substance consumed in the system over that interval of time.

The substance property may represent the total mass, the individual (components) mass, the concentration, the volume, the total energy or the momentum. By applying the Raynold transport theorem (RTT) (Niven *et al.*, 2018), on the control volume in Fig. 3, then, the total mass balance (total continuity) in word equation is mathematically described as:

Accumulation of the total mass inside the system over time interval = mass flows in - mass flows out $\pm$ mass created or consumed inside the control volume by the reactions over the time interval. The equivalent mathematical equation to the above stated word equation is given in (3). From the molecular continuity equation i.e component mass balance, we have the time rate of change of moles of the components in the control volume = the components molar flows in - the components molar flows out $\pm$ the rate of components molar created or consumed by the reaction in the control volume. Mathematically, the total mass accumulation inside the system is described as,

$$\frac{\mathrm{d}}{\mathrm{d}t}\left(\int_{c.v} C_i V \mathrm{d}V\right) = \sum_{\text{inflows}} F_{\text{in}} C_{\text{in}_i} - \sum_{\text{outflows}} F_{\text{out}} C_{\text{out}_i} \pm \int_{c.v} r_i \mathrm{d}V. \tag{3}$$

Multiply Equation (3) by the molecular weight accumulations m_i of species i, the equation becomes

$$\frac{\mathrm{d}}{\mathrm{d}t}\left(\int_{c.v} C_i m_i V \mathrm{d}V\right) = \sum_{\text{inflows}} F_{\text{in}} m_i C_{\text{in}_i} - \sum_{\text{outflows}} F_{\text{out}} m_i C_{\text{out}_i} \pm \int_{c.v} r_i m_i \mathrm{d}V. \tag{4}$$

The terms $C_i m_i$, $C_{\text{in}_i} m_i$ and $C_{\text{out}_i} m_i$ are considered as mass densities of the mixture, the inlet and the outlet respectively. Thus, $C_i m_i = \rho$, $C_{\text{in}_i} m_i = \rho_{\text{in}}$ and $C_{\text{out}_i} m_i = \rho_{\text{out}}$. Therefore, the Equation (4) is simplified and becomes

$$\frac{\mathrm{d}}{\mathrm{d}t}\left(\int_{c.v} \rho V \mathrm{d}V\right) = \sum_{\text{inflows}} F_{\text{in}} \rho_{\text{in}} - \sum_{\text{outflows}} F_{\text{out}} \rho_{\text{out}} \pm \int_{c.v} r_i m_i \mathrm{d}V. \tag{5}$$

At the equilibrium state, the last integral term of Equation (5) becomes zero. By the assumption $A.7$ which considers the densities to be constants and equal throughout the process, yields,

$$\rho \frac{\mathrm{d}}{\mathrm{d}t}\left(\int_{c.v} V \mathrm{d}V\right) = \rho_{\text{in}} \sum_{\text{inflows}} F_{\text{in}} - \rho_{\text{out}} \sum_{\text{outflows}} F_{\text{out}}. \tag{6}$$

As a final result,

$$\rho \frac{\mathrm{d}V}{\mathrm{d}t} = \rho \left(F_{\text{in}} - F_{\text{out}}\right) \equiv \frac{\mathrm{d}V}{\mathrm{d}t} = F_{\text{in}} - F_{\text{out}}. \tag{7}$$

Again, the molar concentration rate is used to derive the concentration change inside the control volume and it is given by:

$$\frac{\mathrm{d}}{\mathrm{d}t}\left(\int_{c.v} n_i \mathrm{d}V\right) = \sum_{i=1}^{N_s} F_{\text{in}_i} C_{\text{in}_i} - \sum_{i=1}^{N_s} F_{\text{out}_i} C_{\text{out}_i} - \int_{c.v} r_i \mathrm{d}V, \tag{8}$$

$$\frac{\mathrm{d}}{\mathrm{d}t}\left(\int_{c.v} (C_i V) \mathrm{d}V\right) = \sum_{i=1}^{N_s} F_{\text{in}_i} C_{\text{in}_i} - \sum_{i=1}^{N_s} F_{\text{out}_i} C_{\text{out}_i} - \int_{c.v} r_i \mathrm{d}V, \tag{9}$$

$$\frac{\mathrm{d}(C_i V)}{\mathrm{d}t} = F_{\text{in}_i} C_{\text{in}_i} - F_{\text{out}_i} C_{\text{out}_i} - r_i V \equiv V \frac{\mathrm{d}C_i}{\mathrm{d}t} + C_i \frac{\mathrm{d}V}{\mathrm{d}t} = F_{\text{in}_i} C_{\text{in}_i} - F_{\text{out}_i} C_{\text{out}_i} - r_i V. \tag{10}$$

For simplicity and from the assumption $A.6$, Equation (10) can be written as:

$$V \frac{\mathrm{d}C_i}{\mathrm{d}t} + C_i \frac{\mathrm{d}V}{\mathrm{d}t} = F_{\text{in}_i} C_{\text{in}_i} - F_{\text{out}_i} C_{\text{out}_i} - r_i V \equiv V \frac{\mathrm{d}C}{\mathrm{d}t} + C \frac{\mathrm{d}V}{\mathrm{d}t} = F_{\text{in}} C_{\text{in}} - F_{\text{out}} C_{\text{out}} - rV. \tag{11}$$

Substituting Equation (7) into Equation (11) leads to Equation (12) below,

$$\begin{aligned} V \frac{\mathrm{d}C}{\mathrm{d}t} + C\left(F_{\text{in}} - F_{\text{out}}\right) &= F_{\text{in}} C_{\text{in}} - F_{\text{out}} C_{\text{out}} - rV, \\ V \frac{\mathrm{d}C}{\mathrm{d}t} &= F_{\text{in}} C_{\text{in}} - F_{\text{out}} C_{\text{out}} - rV - C F_{\text{in}} + C F_{\text{out}}. \end{aligned} \tag{12}$$

Since $C = C_{\text{out}}$ from the perfect mixing in the assumption $A.1$, and by division of V on the Equation (12), with $F_{\text{in}} = F$, these reduce the Equation (12) to Equation (13)

$$\frac{\mathrm{d}C}{\mathrm{d}t} = \frac{F}{V}(C_{\text{in}} - C) - r. \tag{13}$$

By substituting Equation (2) into Equation (13) yields,

$$\frac{\mathrm{d}C}{\mathrm{d}t} = \frac{F}{V}\left(C_{\text{in}} - C_{\text{out}}\right) - k_0 e^{\frac{E}{R}\left(\frac{1}{T} - \frac{1}{T_{\text{mean}}}\right)} C. \tag{14}$$

Finally, the derivation of the energy conservation of the system is attained by using the presented control volume in Fig. (3). From the first principle of thermodynamics on the open system with reactions which states that the energy is neither created nor destroyed but it is transformed into other form of energy. So, the total energy of the system is given by $E = U + K_E + P_E$ where, U is the total internal energy, K_E is the total kinetic energy and P_E is the total potential energy. Let consider the inlets streams' properties $F_{\text{in}},\ T_{\text{in}},\ V_{\text{in}},\ e_{\text{in}}$ and p_{in} to be volumetric flow, temperature, volume, partial molar energies and pressure of the inlet streams respectively. Also let $F_{\text{out}},\ T_{\text{out}},\ V_{\text{out}},\ e_{\text{out}}$ and p_{out} be the volumetric flow, the temperature, volume, partial molar energies and pressure of the outlet streams respectively. Hence, the change in energy of the system is mathematically formulated as:

$$\frac{\mathrm{d}E}{\mathrm{d}t} = F_{\text{in}}e_{\text{in}} - F_{\text{out}}e_{\text{out}} + Q + W + K_E + P_E. \tag{15}$$

However, W represents all form of energies due to surroundings and it is written as:

$$W = F_{\text{in}}V_{\text{in}}p_{\text{in}} - F_{\text{out}}V_{\text{out}}p_{\text{out}} - p\frac{\mathrm{d}V}{\mathrm{d}t} + W_{\text{shaft}} + W_f, \tag{16}$$

where $F_{\text{in}}V_{\text{in}}p_{\text{in}}$, $F_{\text{out}}V_{\text{out}}p_{\text{out}}$, $-p\frac{\mathrm{d}V}{\mathrm{d}t}$, W_{shaft} and W_f are the works done by inlet streams, the outlet streams, the change in volume of the control volume, the stirring process and other external forces respectively. Substitution of Equation (16) into Equation (15) produces Equation (17)

$$\begin{aligned}
\frac{\mathrm{d}E}{\mathrm{d}t} &= F_{\text{in}}e_{\text{in}} - F_{\text{out}}e_{\text{out}} + Q + F_{\text{in}}V_{\text{in}}p_{\text{in}} - F_{\text{out}}V_{\text{out}}p_{\text{out}} - p\frac{\mathrm{d}V}{\mathrm{d}t} + W_{\text{shaft}} + W_f + K_E + P_E, \\
\frac{\mathrm{d}E}{\mathrm{d}t} &= F_{\text{in}}\left(e_{\text{in}} + V_{\text{in}}p_{\text{in}}\right) - F_{\text{out}}\left(e_{\text{out}} + V_{\text{out}}p_{\text{out}}\right) + Q - p\frac{\mathrm{d}V}{\mathrm{d}t} + W_{\text{shaft}} + W_f + K_E + P_E.
\end{aligned} \tag{17}$$

After taking $e_{\text{in}} + V_{\text{in}}p_{\text{in}} = h_{\text{in}}$ and $e_{\text{out}} + V_{\text{out}}p_{\text{out}} = h_{\text{out}}$ to be specific enthalpies of inlet and outlet streams, then, Equation (17) becomes

$$\frac{\mathrm{d}E}{\mathrm{d}t} = F_{\text{in}}h_{\text{in}} - F_{\text{out}}h_{\text{out}} + W_{\text{shaft}} + W_f + Q - p\frac{\mathrm{d}V}{\mathrm{d}t} + K_E + P_E. \tag{18}$$

But from the assumptions $A.2$, $A.4$, and $A.8$, the kinetic energy, the potential energy, the shaft work and the external work done are infinitesimal small as compared to the heat exchange and the internal energy for chemical reactors. That means, $K_E,\ P_E,\ W_{\text{shaft}},\ W_f,\ \approx 0$. As a

consequence,

$$\frac{\mathrm{d}E}{\mathrm{d}t} = F_{\text{in}}h_{\text{in}} - F_{\text{out}}h_{\text{out}} + Q - p\frac{\mathrm{d}V}{\mathrm{d}t} \cong \frac{\mathrm{d}U}{\mathrm{d}t}. \tag{19}$$

Stepanov (2017) shows that, the enthalpy equation is given by:

$$H = U + pV. \tag{20}$$

Differentiation of Equation (20) with respect to t yields,

$$\frac{\mathrm{d}H}{\mathrm{d}t} = \frac{\mathrm{d}U}{\mathrm{d}t} + \frac{\mathrm{d}}{\mathrm{d}t}(pV) \equiv \frac{\mathrm{d}H}{\mathrm{d}t} = \frac{\mathrm{d}U}{\mathrm{d}t} + p\frac{\mathrm{d}V}{\mathrm{d}t} + V\frac{\mathrm{d}p}{\mathrm{d}t}. \tag{21}$$

The substitution of Equation (19) into Equation (21) gives Equation (22).

$$\frac{\mathrm{d}H}{\mathrm{d}t} = F_{\text{in}}h_{\text{in}} - F_{\text{out}}h_{\text{out}} + Q + V\frac{\mathrm{d}p}{\mathrm{d}t}. \tag{22}$$

The terms of Equation (22) can be expressed in partial molar enthalpies which are

$$F_{\text{in}}h_{\text{in}} = \sum_{i=1}^{N_s} F_{\text{in}_i}H_{\text{in}_i} \text{ and } F_{\text{out}}h_{\text{out}} = \sum_{i=1}^{N_s} F_{\text{out}_i}H_{\text{out}_i}. \tag{23}$$

Substitute Equation (23) into Equation (22) to obtain

$$\frac{\mathrm{d}H}{\mathrm{d}t} = \sum_{i=1}^{N_s} F_{\text{in}_i}H_{\text{in}_i} - \sum_{i=1}^{N_s} F_{\text{out}_i}H_{\text{out}_i} + Q + V\frac{\mathrm{d}p}{\mathrm{d}t}. \tag{24}$$

But also the CSTRs are designed in a such way that there is no pressure drop which implies that they operate at a constant pressure as stated in the assumption $A.3$. This implies the last term of Equation (24) to be zero. So,

$$\frac{\mathrm{d}H}{\mathrm{d}t} = \sum_{i=1}^{N_s} F_{\text{in}_i}H_{\text{in}_i} - \sum_{i=1}^{N_s} F_{\text{out}_i}H_{\text{out}_i} + Q. \tag{25}$$

It remains to establish the relationship between the enthalpy and the temperature. The overall differentiation of the enthalpy with no pressure drop is obtained from Bird *et al.* (2007), and it is expressed as

$$\frac{\mathrm{d}H}{\mathrm{d}t} = \rho C_p V\frac{\mathrm{d}T}{\mathrm{d}t} + \sum_{i=1}^{N_s} H_{\text{out}_i}\frac{\mathrm{d}n_i}{\mathrm{d}t} \text{ with } \frac{\mathrm{d}n_i}{\mathrm{d}t} = F_{\text{in}_i} - F_{\text{out}_i} + V\sum_{j=1}^{N_d} V_{j,i}r_j. \tag{26}$$

Therefore,

$$\frac{\mathrm{d}H}{\mathrm{d}t} = \rho C_p V \frac{\mathrm{d}T}{\mathrm{d}t} + \sum_{i=1}^{N_s} H_{\text{out}_i} \left(F_{\text{in}_i} - F_{\text{out}_i} + V \sum_{j=1}^{N_d} V_{j,i} r_j \right). \tag{27}$$

By equating the Equation (25) and the Equation (27), resulted in Equation (28)

$$\rho C_p V \frac{\mathrm{d}T}{\mathrm{d}t} + \sum_{i=1}^{N_s} H_{\text{out}_i} \left(F_{\text{in}_i} - F_{\text{out}_i} + V \sum_{j=1}^{N_d} V_{j,i} r_j \right) = \sum_{i=1}^{N_s} F_{\text{in}_i} H_{\text{in}_i} - \sum_{i=1}^{N_s} F_{\text{out}_i} H_{\text{out}_i} + Q. \tag{28}$$

After simplification and rearrangement of terms of Equation (28) and taking

$$\sum_{j=1}^{N_d} H_{\text{out}_i} V_{j,i} r_j = \triangle H_i r_i, \tag{29}$$

gives Equation (30)

$$\rho C_p V \frac{\mathrm{d}T}{\mathrm{d}t} = \sum_{i=1}^{N_s} F_{\text{in}_i} \left(H_{\text{in}_i} - H_{\text{out}_i} \right) + V \sum_{i=1}^{N_s} (- \triangle H_i) r_i + Q. \tag{30}$$

The Equation (30) can be further simplified by taking

$$\sum_{i=1}^{N_s} F_{\text{in}_i} = F, \ \sum_{i=1}^{N_s} (- \triangle H_i) r_i = -H^* r, \text{ and } \sum_{i=1}^{N_s} (H_{\text{in}_i} - H_{\text{out}_i}) = - \int_{T_{\text{in}}}^{T_{\text{out}}} \rho C_p \mathrm{d}T. \tag{31}$$

Upon inserting Equations from (31) into the Equation (30) displays

$$\rho C_p V \frac{\mathrm{d}T}{\mathrm{d}t} = V(-H^*) r + F \int_{T_{\text{out}}}^{T_{\text{in}}} \rho C_p \mathrm{d}T + Q. \tag{32}$$

Since ρ, C_p are constants from the assumption $A.7$, $Q = UA(T_c - T) = -UA(T - T_c)$ from the assumption $A.5$, and $r = k_0 e^{-\frac{E}{R}\left(\frac{1}{T} - \frac{1}{T_{\text{mean}}}\right)} C$, then the Equation (32) becomes

$$\frac{\mathrm{d}T}{\mathrm{d}t} = \frac{F}{V}(T_{\text{in}} - T) + \frac{-H^* k_0 e^{-\frac{E}{R}\left(\frac{1}{T} - \frac{1}{T_{\text{mean}}}\right)} C}{\rho C_p} - \frac{UA}{\rho C_p V}(T - T_c). \tag{33}$$

The dynamics of the heat in the cooling jacket can be deduced from Equation (33) since there is no reaction carried out inside. Then,

$$\frac{\mathrm{d}T_c}{\mathrm{d}t} = \frac{F_c}{V_c}(T_{c_{\text{in}}} - T_c) + \frac{UA}{\rho_c C_{p_c} V_c}(T - T_c). \tag{34}$$

Grouping together Equations (7), (14), (33) and (34), finally leads to the non-linear system of ODEs which governs the exothermic CSTRs deterministic model in the form of Equation (35)

$$\begin{cases} \frac{\mathrm{d}V}{\mathrm{d}t} = F_{\text{in}} - F_{\text{out}}, \\ \frac{\mathrm{d}C}{\mathrm{d}t} = \frac{F}{V}\left(C_{\text{in}} - C\right) - k_0 e^{-\frac{E}{R}\left(\frac{1}{T} - \frac{1}{T_{\text{mean}}}\right)} C, \\ \frac{\mathrm{d}T}{\mathrm{d}t} = \frac{F}{V}(T_{\text{in}} - T) + \frac{(-H^* k_0 e^{-\frac{E}{R}\left(\frac{1}{T} - \frac{1}{T_{\text{mean}}}\right)} C}{\rho C_p} - \frac{UA}{\rho C_p V}(T - T_c), \\ \frac{\mathrm{d}T_c}{\mathrm{d}t} = \frac{F_c}{V_c}(T_{c_{\text{in}}} - T_c) + \frac{UA}{\rho_c C_{p_c} V_c}(T - T_c). \end{cases} \tag{35}$$

3.1.2 Formulation of Deterministic Model for Endothermic CSTR

As for the deterministic model of the exothermic CSTR, a similar way is followed to formulate the variable-volume deterministic model for endothermic CSTR except that there is heating process that requires energy to be supplied on the system through the heating jacket which boosts the reaction. From the fundamental chemistry, the endothermic reactions have positive enthalpies. Therefore, on one hand, the temperature of the heating process diminishes while on the other hand the temperature of the mixture inside the tank increases. As a result, the four state variables endothermic CSTR's deterministic model is also governed by the following system of ordinary differential equations:

$$\begin{cases} \frac{\mathrm{d}V}{\mathrm{d}t} = F_{\text{in}} - F_{\text{out}}, \\ \frac{\mathrm{d}C}{\mathrm{d}t} = \frac{F}{V}(C_{\text{in}} - C) - k_0 e^{-\frac{E}{R}\left(\frac{1}{T} - \frac{1}{T_{\text{mean}}}\right)} C, \\ \frac{\mathrm{d}T}{\mathrm{d}t} = \frac{F}{V}(T_{\text{in}} - T) + \frac{H^* k_0 e^{-\frac{E}{R}\left(\frac{1}{T} - \frac{1}{T_{\text{mean}}}\right)} C}{\rho C_p} + \frac{UA(T_H - T)}{\rho_H C_{p_H} V_H}, \\ \frac{\mathrm{d}T_H}{\mathrm{d}t} = \frac{F_H}{V_H}(T_{H_{\text{in}}} - T_H) - \frac{UA(T_H - T)}{\rho_H C_{p_H} V_H}, \end{cases} \tag{36}$$

where H^* is the process temperature dependent enthalpy.

3.2 Formulation of CSTRs Stochastic Differential Equation Models

After the contribution made by Robert Brown who discovered the Brownian motion in 1827, stochastic modelling became a new direction of well describing the real physical, engineering, chemical and biological processes both experimentally and statistically. In the deterministic approach, models describe the system in the vicinity of its steady-state (local analysis) whereas the

study concerning about stochastic models is motivated by the fact that is due to capturing and characterising the effect of model uncertainty, which may influence the system outputs globally. Moreover, engineering, biological and chemical processes are often perturbed by small measurement errors and this has a great impact on the system outputs. Consequently, it is state-worth and of paramount to study and analyse various dynamical processes both deterministically and stochastically in order to be able to explore, characterise, control and quantify the randomness aspects that are not usually visible in the system deterministic model, but are often and in reality associated with the real system.

The time varying systems that are deterministically modeled by using the ordinary differential equations may be transformed into stochastic differential equations after introducing the "White noise" or its time derivative called "Wiener process" or Brownian motion in the deterministic model. The stochastic differential equation is composed by two parts, namely, "drift part" which describes the system deterministically and "diffusion part" which captures the random effect on the system. The general formula for stochastic differential equation is given by

$$\frac{\mathrm{d}X(t)}{\mathrm{d}t} = \mu(X(t),t) + \delta(X(t),t) \times \text{White noise}, \tag{37}$$

where $X(t)$ is the state variable, $\mu(X(t),t)$ is the drift part and $\delta(X(t),t) \times$ White noise is the diffusion part.

The problem of stochastic differential equation is to define, solve and characterise the properties of White noise. The White noise can mathematically be written as $\xi(t) = \frac{\mathrm{d}B(t)}{\mathrm{d}t}$ and so, after multiplying $\mathrm{d}t$ on both sides of Equation (37), then the stochastic differential equation becomes

$$\mathrm{d}X(t) = \mu(X(t),t)\mathrm{d}t + \delta(X(t),t)\mathrm{d}B(t). \tag{38}$$

Definition 1: Wiener process

According to Sauer (2012) and Øksendal (2003), a stochastic process $B(t)$ with $t \in [0,T]$ is called a Wiener process if the following properties hold:

(i) $B(0) = 0$ with almost surely (a.s);

(ii) $B(t)$ is a continuous function with respect to time;

(iii) The process increment $B(t) - B(s)$ has Gaussian distribution with $\mathbb{E}[B(t) - B(s)] = 0$ and $Var[B(t) - B(s)] = t - s$, for $0 \leq s < t \leq ... < T$;

(iv) The process increments $B(t_i) - B(s_i)$, for $i = 1, 2, ..., n$, are independent for the bounded time interval $0 \leq s_1 < t_1 \leq s_2 < t_2 \leq s_3 < t_3 \leq ... \leq s_n < t_n < T$.

The paths taken by a Wiener process can be plotted to show its trajectories. So, Fig. 4 and Fig. 5 illustrate the sample of single and six paths taken by the Wiener process respectively. From Fig. 5, it is seen that each trajectory among six shown trajectories of the Brownian motion follows its own path even if they are simulated by using the same initial values $B(0) = 0$ and the same parameter values.

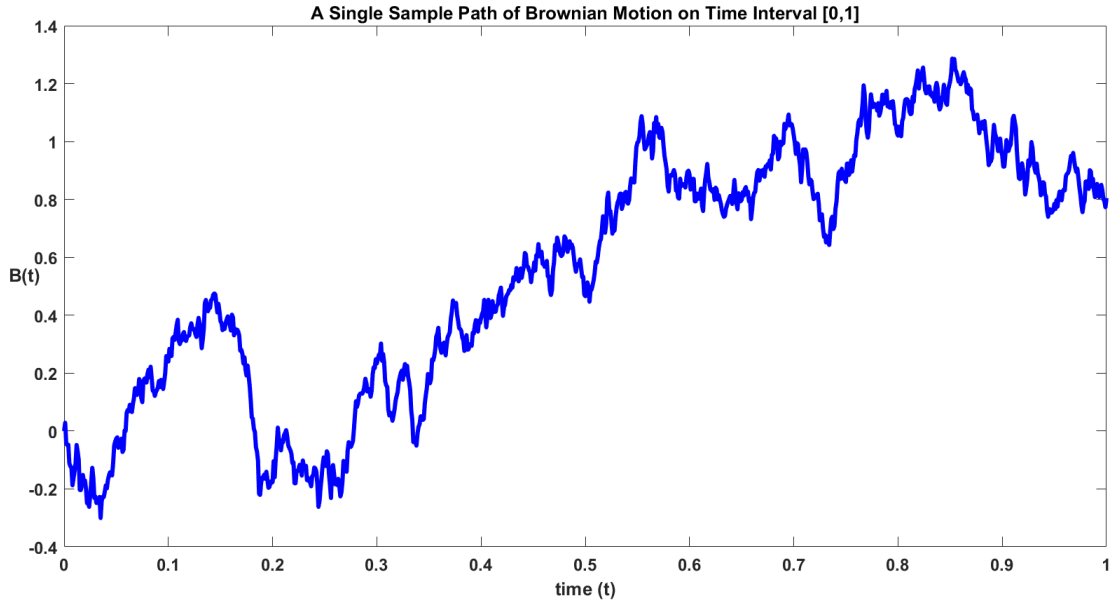

Figure 4: Example of a single trajectory taken by Brownian motion in the time interval $[0, 1]$. The sample size, $N = 1000$, sampling time $T = 1$ and discrete time step size $\mathrm{d}t = 1/1000$ are used here.

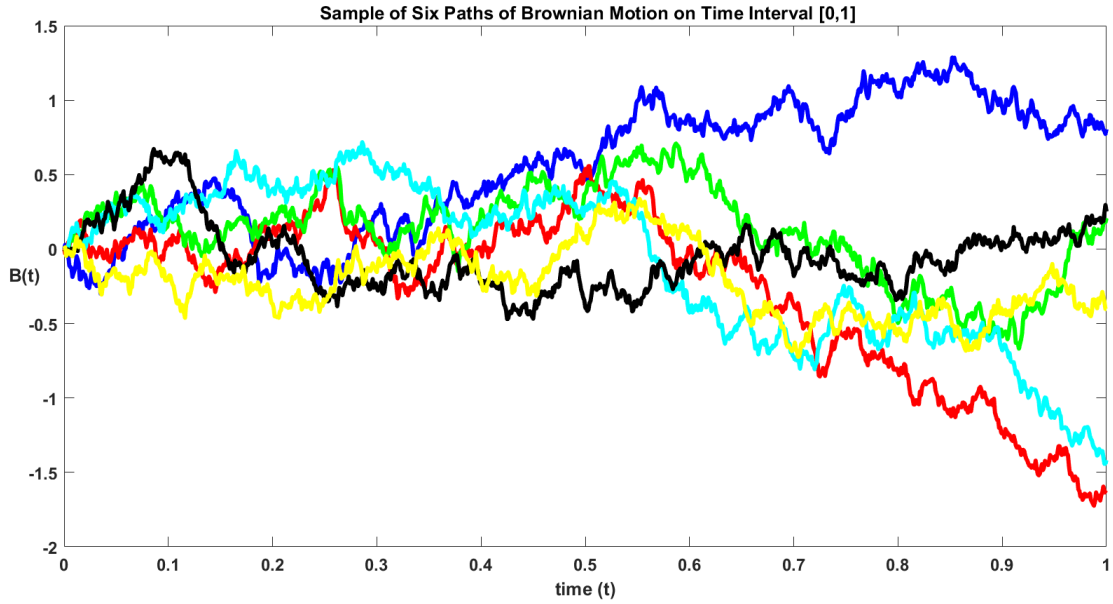

Figure 5: Sample of six trajectories of the Brownian motion in the time interval $[0, 1]$. All six trajectories have been generated by using the same sample size $N = 1000$, sampling time $T = 1$ and discrete time step size $\mathrm{d}t = 1/1000$

The solution of stochastic differential equation, if it exists, is also stochastic. If the stochastic process $X(t)$ with the initial condition $X(t_0) = X_0$ is the solution of SDE (38), then it may be weak or strong solution based on some properties. So, the solution can also be obtained in the integral form as:

$$X(t) = X_0 + \int_{t_0}^{t} \mu(X(s), s)\mathrm{d}s + \int_{t_0}^{t} \delta(X(s), s)\mathrm{d}B(s). \tag{39}$$

On the right hand side of Equation (39), there are two integrals. The first integral is an ordinary integral but the second one is not, simply because the Wiener process is not differentiable everywhere. To address the non-differentiable issue of the second integral, Itô and Stratonovich have developed two mathematical approaches to handle the integral $\int_{t_0}^{t} \delta(X(s), s)\mathrm{d}B(s)$. If δ is a constant, then

$$\int_{t_0}^{t} \delta(X(s), s)\mathrm{d}B(s) = \delta(B(t) - B(t_0)). \tag{40}$$

If δ is not a constant function, then the approximate solution of the diffusion part of the stochastic integral is obtained (Sethi *et al.*, 1981). In this dissertation, the Itô integral is considered because of the preservation of the martingale properties. The stochastic integral in Equation (39) is also called an Itô process.

Theorem 1: Itô Integral (Øksendal, 2003)

Assume that $X(t)$ is an Itô process such that

$$\mathrm{d}X(t) = \mu(X(t), t)\mathrm{d}t + \delta(X(t), t)\mathrm{d}B(t), \tag{41}$$

and chosen a function $f(t, x)$ to be twice continuously differentiable with respect to x and once differentiable in t. Thus,

$$Y(t) = f(t, X(t)), \tag{42}$$

is also Itô process with

$$\mathrm{d}Y(t) = \frac{\partial f(t, X(t))}{\partial t}\mathrm{d}t + \frac{\partial f(t, X(t))}{\partial x}\mathrm{d}X(t) + \frac{1}{2}\delta^2(X(t), t)\frac{\partial^2 f(X(t), t)}{\partial x^2}\mathrm{d}t, \tag{43}$$

obtained after applying the chain rule differentiation on $f(t, X(t))$ as well as considering the quadratic differentiation since the Wiener process has unbounded variation.

(i) Itô Integral Properties (Øksendal, 2003)

For all constants $\alpha, \gamma \in \mathbb{R}$ and $\forall$ functions $g, h \in \mathbb{L}^2(0, T)$, the following properties are obtained:

(i) $\int_0^T (\alpha h + \gamma g)\mathrm{d}B = \alpha \int_0^T h\mathrm{d}B + \gamma \int_0^T g\mathrm{d}B$ (Linearity property for step processes);

(ii) $\mathbb{E}[\int_0^T g\mathrm{d}B] = 0$ (Zero expectation property);

(iii) $\mathbb{E}[(\int_0^T g\mathrm{d}B)^2] = \mathbb{E}[\int_0^T g^2\mathrm{d}t] = 0$ (Isometric property);

(iv) $\mathbb{E}[\int_0^T g\mathrm{d}B \int_0^T h\mathrm{d}B] = \mathbb{E}[\int_0^T gh\mathrm{d}t] = 0$ (as $(\mathrm{d}B)^2 = dt$).

Example 1: Evaluate the integral $\int_0^t B(s)\mathrm{d}B(s)$ in the Itô sense.

From the calculus point of view, the term, $\frac{1}{2}B^2(t)$ is likely to be obtained. So, let choose $f(t, x) = \frac{1}{2}x^2$ and let $X(t) = B(t)$, by applying the Itô formula on Equation (44)

$$Y(t) = f(t, B(t)) = \frac{1}{2}B^2(t), \tag{44}$$

delivers Equation (45)

$$\mathrm{d}Y(t) = \frac{\partial f(t, B(t))}{\partial t}\mathrm{d}t + \frac{\partial f(t, B(t))}{\partial x}\mathrm{d}X(t) + \frac{1}{2}\delta^2(B(t), t)\frac{\partial^2 f(B(t), t)}{\partial x^2}\mathrm{d}t. \tag{45}$$

So,

$$\mathrm{d}Y(t) = 0 + B(t)\mathrm{d}B(t) + \frac{1}{2}\mathrm{d}t, \tag{46}$$

as $\delta^2(t, B(t)) = 1$. Integrating both side of the Equation (46), yields

$$Y(t) = \frac{1}{2}B^2(t) = \int_0^t B(s)\mathrm{d}B(s) + \frac{1}{2}\int_0^t \mathrm{d}s = \int_0^t B(s)\mathrm{d}B(s) + \frac{1}{2}t. \tag{47}$$

Hence,

$$\int_0^t B(s)\mathrm{d}B(s) = \frac{1}{2}B^2(t) - \frac{1}{2}t. \tag{48}$$

Example 2:

Let find the explicit solution of the geometric Brownian motion given by:

$$\begin{cases} \mathrm{d}X(t) = \mu X(t)\mathrm{d}t + \delta X(t)\mathrm{d}B(t), \\ X(0) = X_0 \end{cases} \tag{49}$$

by using the Itô theorem.

The Equation (49) can be written in the form of Equation (50)

$$\frac{\mathrm{d}X(t)}{X(t)} = \mu\mathrm{d}t + \delta\mathrm{d}B(t). \tag{50}$$

Integrate Equation (50) to obtain Equation (51)

$$\int_0^t \frac{\mathrm{d}X(s)}{X(s)} = \mu t + \delta B(t). \tag{51}$$

The Itô formula can be applied to function $Y(t) = f(t, x) = \log(x)$. So,

$$\mathrm{d}Y(t) = \mathrm{d}(\log(X)) = \frac{\partial f(t, X)}{\partial t}\mathrm{d}t + \frac{\partial f(t, X)}{\partial x}\mathrm{d}X + \frac{1}{2}\frac{\partial^2 f(X, t)}{\partial x^2}(\mathrm{d}X)^2. \tag{52}$$

Then,

$$\begin{aligned} \mathrm{d}(\log(X(t))) &= 0 + \frac{1}{X(t)}\mathrm{d}X(t) - \frac{1}{X^2(t)}(\mathrm{d}X(t))^2, \\ \mathrm{d}(\log(X(t))) &= \frac{1}{X(t)}(\mu X(t)\mathrm{d}t + \delta X(t)\mathrm{d}B(t)) - \frac{1}{X^2(t)}(\mu X(t)\mathrm{d}t + \delta X(t)\mathrm{d}B(t))^2. \end{aligned} \tag{53}$$

By using the increments properties that are $(\mathrm{d}t)^2 = \mathrm{d}t\mathrm{d}B(t) = 0$ and $(\mathrm{d}B(t))^2 = \mathrm{d}t$, Equation (54) is obtained as:

$$\begin{aligned} \mathrm{d}(\log(X(t))) = \mu\mathrm{d}t + \delta\mathrm{d}B - \frac{1}{2}\delta^2\mathrm{d}t = (\mu - \frac{1}{2}\delta^2)\mathrm{d}t + \delta B(t), \\ \log(X(t)) = (\mu - \frac{1}{2}\delta^2)t + \delta B(t), \\ X(t) = X_0 e^{((\mu - \frac{1}{2}\delta^2)t + \delta B(t))}. \end{aligned} \tag{54}$$

(ii) Stratonovic Integral (Øksendal, 2003)

The Stratonovich stochastic differential equation is given by:

$$\mathrm{d}X(t) = \mu(X(t), t)\mathrm{d}t + \delta(X(t), t)\ o\ \mathrm{d}B(t), s \tag{55}$$

where "o" in Equation (55) symbolises Stratonovich denotation.

By using the integral form, the Equation (55) becomes

$$X = X_0 + \int_0^t \mu(X(s), s)\mathrm{d}s + \int_0^t \delta(X(s), s)\ o\ \mathrm{d}B(s), \tag{56}$$

and then the Stratonovich suggests the evaluation of the function at the midpoint. That is to say if $f(t)$ is a twice differentiable continuous function, then the diffusion integral can be obtained by applying the infinite limiting of the Riemman sum as follow:

$$\int_a^b f(t)\ o\ \mathrm{d}B(t) = \lim_{m\to\infty} \sum_{i=0}^{m-1} \frac{1}{2}(f(t_i) + f(t_{i+1}))(B(t_{i+1} - B(t_i)). \tag{57}$$

The terms $\frac{1}{2}(f(t_i) + f(t_{i+1}))$ and $B(t_{i+1}) - B(t_i)$ under the summation in the Equation (57) are likely to be dependent. As a result, Stratonovich and Itô approaches have different results in general but possible transformation from Stratonovich to Itô can be made and vice-versa (Sethi *et al.*, 1981). Itô approach gains several applications in finance and economics since it has

martingale property that is future prediction will not solely be different from today's situation. Contrary, Stratonovich is not martingale and hence anticipating.

Example 3: Let also consider the Brownian motion problem presented in Example 1. Find its solution in the Stratonovich sense.

The Itô sense gives

$$\int_0^t B(s)\mathrm{d}B(s) = \frac{B^2(t)}{2} - \frac{t}{2}, \tag{58}$$

while the Stratonovich approach gives

$$\int_0^t B(s)\ o\ \mathrm{d}B(s) = \lim_{m\to\infty} \sum_{i=0}^{m-1} \frac{1}{2}(B(t_{i+1}) + B(t_i)(B(t_{i+1}) - B(t_i)) \tag{59}$$

$$= \lim_{m\to\infty} \sum_{i=0}^{m-1} \frac{1}{2}(B^2(t_{i+1}) - B^2(t_i)). \tag{60}$$

After expanding the summation and simplifying, the Equation (62) is obtained as:

$$\int_0^t B(s)\ o\ \mathrm{d}B(s) = \lim_{m\to\infty} \frac{1}{2}(B^2(t) - B^2(0)) \tag{61}$$

$$= \frac{B^2(t)}{2}. \tag{62}$$

So, the difference between the two approaches on the same problem is

$$\int_0^t B(s)\mathrm{d}B(s) - \int_0^t B(s)\ o\ \mathrm{d}B(s) = -\frac{t}{2}. \tag{63}$$

One of the biggest advantage of the Itô approach is that the evaluations of the function under integral are uncorrelated with the increments and their functions. That means $B(t_{i+1}) - B(t_i)$ is uncorrelated with $B(t_i)$ and it is also uncorrelated with any function of $B(t_i)$ and so $\mathbb{E}(B(t_{i+1}) - B(t_i)) = 0$.

Before discussing the existence and the uniqueness of a solution of the stochastic differential equation, let first discuss the Gronwall's Lemma.

(iii) Gronwall's Lemma (Oksendal, 2013)

Let Φ and f be continuous positive functions defined for $0 \leq t \leq T$, and let C_0 be a positive constant.

If

$$\Phi(t) \leq C_0 + \int_0^t f\Phi \mathrm{d}s, \ \forall\, 0 \leq t \leq T, \tag{64}$$

then

$$\Phi(t) \leq C_0 e^{\int_0^t f \mathrm{d}s}, \ \forall\, 0 \leq t \leq T. \tag{65}$$

Proof: Let $\phi(t) = C_0 + \int_0^t f\Phi \mathrm{d}s$, then $\frac{\mathrm{d}\phi}{\mathrm{d}s} = f\Phi \leq f\phi$ and so

$$\frac{\mathrm{d}}{\mathrm{d}s}(\phi e^{-\int_0^t f \mathrm{d}s}) = (\phi' - f\phi)e^{-\int_0^t f \mathrm{d}s} \leq (f\phi - f\phi)e^{-\int_0^t f \mathrm{d}s} = 0. \tag{66}$$

Therefore,

$$\phi(t)e^{-\int_0^t f \mathrm{d}s} \leq \phi(0)e^{-\int_0^t f \mathrm{d}s} = C_0, \tag{67}$$

and hence

$$\Phi(t) \leq \phi(t) \leq C_0 e^{\int_0^t f \mathrm{d}s}. \tag{68}$$

(iv) Existence and Uniqueness of Stochastic Solution (Lipschitz condition)

Consider the general stochastic differential equation presented in Equation (38) with the initial condition $X(0) = X_0$ and let $\mu : \mathbb{R}^n \times [0, T] \mapsto \mathbb{R}^n$ and $\delta : \mathbb{R}^n \times [0, T] \mapsto \mathbb{M}^{m \times n}$ are continuous and satisfy the following conditions:

(i) $\mid \mu(x,t) - \mu(y,t) \mid \leq L \mid x - y \mid$ and $\mid \delta(x,t) - \delta(y,t) \mid \leq L \mid x - y \mid$ for all $0 \leq t \leq T$ and $x, y \in \mathbb{R}^n$;

(ii) $\mid \mu(x,t) \mid \leq L(1 + \mid x \mid)$ and $\mid \delta(x,t) \mid \leq L(1 + \mid x \mid)$ for all $0 \leq t \leq T$ and $x \in \mathbb{R}^n$ for some constant L;

The above (i) and (ii) statements reveal that μ and δ are uniformally Lipschitz continuous in the variable x.

Let X_0 be any $\mathbb{R}^n-$ valued random variable such that

(iii) $\mathbb{E}(\mid X_0 \mid^2)$ is finite that means $\mathbb{E}(\mid X_0 \mid^2) < \infty$; and

(iv) X_0 is independent of $B(0)$, where $B(.)$ is $m-$dimensional Brownian motion. Then there exists a unique stochastic solution $X \in \mathbb{R}_n^2(0,T)$ for the SDE that is shown in the Equation (38).

Uniqueness implies that if $X, Y \in \mathbb{R}_n^2(0,T)$, with continuous sample paths almost surely (a.s) and both solve the SDE in Equation (38), then the probability $P(X(t) = Y(t)) = 1$, for all $0 \leq t \leq T$.

Proof (Uniqueness)

Let X and Y be two distinct solutions of SDE presented in Equation (38). Then for all $0 \leq t \leq T$,

$$X(t) - Y(t) = \int_0^t (\mu(X,s) - \mu(Y,s))\mathrm{d}s + \int_0^t (\delta(X,s) - \delta(Y,s))\mathrm{d}B. \tag{69}$$

From the inequality identity $(x+y)^2 = x^2 + 2xy + y^2 \leq 2(x^2+y^2)$, we have

$$\begin{aligned} \mathbb{E}(\mid (X(t) - Y(t) \mid^2) \leq 2[&\mathbb{E}(\mid \int_0^t (\mu(X,s) - \mu(Y,s))\mathrm{d}s \mid^2) \\ &+\mathbb{E}(\mid \int_0^t (\delta(X,s) - \delta(Y,s))\mathrm{d}B \mid^2)]. \end{aligned} \tag{70}$$

By using the Cauchy-Schwarz inequality which says that $\mid \int_0^t f\mathrm{d}s \mid^2 \leq t \int_0^t \mid f \mid^2 \mathrm{d}s$ for $0 < t$ and $f : [0,t] \mapsto \mathbb{R}^n$. From this, we can estimate the two expressions in Equation (70) as follow,

$$\begin{aligned} \mathbb{E}(\mid \int_0^t (\mu(X,s) - \mu(Y,s))\mathrm{d}s \mid^2) &\leq T\mathbb{E}(\int_0^t \mid (\mu(X,s) - \mu(Y,s)) \mid^2 \mathrm{d}s) \\ &\leq TL^2(\int_0^t \mathbb{E}[\mid X - Y \mid^2]\mathrm{d}s. \end{aligned} \tag{71}$$

and

$$\begin{aligned} \mathbb{E}(\mid \int_0^t (\delta(X,s) - \delta(Y,s))\mathrm{d}s \mid^2) &\leq L^2(\mathbb{E}(\int_0^t \mid (\delta(X,s) - \delta(Y,s)) \mid^2 \mathrm{d}s)) \\ &\leq L^2(\int_0^t \mathbb{E}[\mid X - Y \mid^2]\mathrm{d}s) \end{aligned} \tag{72}$$

Combining the Equations (71) and (72) to obtain Equation (73)

$$\mathbb{E}(\mid (X(t) - Y(t) \mid^2) \leq C(\int_0^t \mathbb{E}[\mid X - Y \mid^2]\mathrm{d}s), \tag{73}$$

where the constant $C = 2L^2(1+T)$ for all $0 \leq t \leq T$. If $\mathbb{E}(\mid (X(t) - Y(t) \mid^2) = \phi(t)$, so the Equation (73) becomes

$$\phi(t) \leq C \int_0^t \phi(t) \mathrm{d}s. \tag{74}$$

From Gronwall's Lemma presented above, choose $C = C_0 = 0$, thus $\phi(t) = 0$ which implies that $\mathbb{E}(\mid (X(t) - Y(t) \mid^2) = 0$. Therefore, $X(t) = Y(t)$ a.s and $P(X(t) = Y(t)) = 1$. $\Diamond$

Proof (Existence of a solution)

The existence of a solution is determined by proving the boundedness and the convergence of the solution. It is done as it is per ODEs. Hence without loss of generality, we this analogy is applied and followed to show the existence of the stochastic solution of the Equation (38).

Consider

$$X = X_0 + \int_0^t \mu(X, s)\mathrm{d}s + \int_0^t \delta(X, s)\mathrm{d}B, \tag{75}$$

to be the solution of the SDE (38). By applying the iterative method on the solution, gives

$$X^{n+1}(t) = X_0 + \int_0^t \mu(X^n, s)\mathrm{d}s + \int_0^t \delta(X^n, s)\mathrm{d}B, \tag{76}$$

for $n = 0, 1...$ and $0 \leq t \leq T$.

Let define

$$\phi^n(t) = \mathbb{E}(\mid X^{n+1}(t) - X^n(t) \mid^2) \tag{77}$$

and make an assumption that

$$\phi^n(t) \leq \frac{(Dt)^{n+1}}{(n+1)!} \text{ for all } n = 0, 1..., \ 0 \leq t \leq T \tag{78}$$

and for some constant D depending on L, T and X_0.

By the induction, for $n = 0$, the result becomes

$$\begin{aligned}
\phi^0(t) = \mathbb{E}(\mid X^1(t) - X^0(t) \mid^2) &= \mathbb{E}(\mid \int_0^t \mu(X_0, s)\mathrm{d}s + \int_0^t \delta(X_0, s)\mathrm{d}B \mid^2) \\
&\leq 2\mathbb{E}(\mid \int_0^t L(1+ \mid X_0 \mid)\mathrm{d}s \mid^2) + 2\mathbb{E}(\mid \int_0^t L(1+ \mid X_0 \mid) \mid^2 \mathrm{d}s) \\
&\leq 2L^2 t \int_0^t \mathbb{E}(1+ \mid X_0 \mid)^2 \mathrm{d}s + 2L^2 \int_0^t \mathbb{E}(1+ \mid X_0 \mid)^2 \mathrm{d}s \\
&\leq tD,
\end{aligned} \tag{79}$$

for some large enough constant D. This conforms the claim for $n = 0$.

Assume the claim remains true for $n - 1$, then

$$\begin{aligned}\phi^n(t) = \mathbb{E}(\mid X^{n+1}(t) - X^n(t) \mid^2) = \mathbb{E}(\mid \int_0^t (\mu(X^n, s) - \mu(X^{n-1}, s))\mathrm{d}s \\ + \int_0^t (\delta(X^n, s) - \delta(X^{n-1}, s))\mathrm{d}B \mid^2) \\ \leq 2TL^2(\int_0^t \mathbb{E}(\mid X^n - X^{n-1} \mid^2 \mathrm{d}s) + 2L^2(\int_0^t \mathbb{E}(\mid X^n - X^{n-1} \mid^2 \mathrm{d}s) \\ \leq 2L^2(1+T)(\int_0^t \mathbb{E}(\mid X^n - X^{n-1} \mid^2)\mathrm{d}s.\end{aligned} \tag{80}$$

But if

$$\phi^n(t) = \mathbb{E}(\mid X^{n+1} - X^n \mid^2) \leq \frac{(Dt)^{n+1}}{(n+1)!}, \tag{81}$$

thus,

$$\begin{aligned}\phi^n(t) \leq 2L^2(1+T) \int_0^t \frac{(Ds)^n}{n!}\mathrm{d}s \\ \leq \frac{D^{n+1}s^{n+1}}{(n+1)!},\end{aligned} \tag{82}$$

by choosing $2L^2(1+T) \leq D$. Finally, the claim is proved. So, the solution is proved to be bounded.$\Diamond$

The convergence of the stochastic solution is omitted as it can be found in Oksendal (2013), mainly on the page 70.

Mathematical modelling of chemical reactors are deterministically analysed by a large number of researchers due to the fact that several methods have been widely developed to tackle deterministic models that are popular and built based on ordinary differential equations. Hence Deterministic models become very easy to analyse over stochastic models (Hahl *et al.*, 2016). In addition, as can be found in Renard *et al.* (2013), deterministic solution is unique but sometimes unstable since small perturbation in its governing parameters or initial conditions can drastically lead to high variations of the results. Thus, where possible, stochastic models are naturally preferable as good descriptors of the physical, chemical and biological systems because of noise that is always associated with those processes (Hahl *et al.*, 2016). Even if the dynamics of a dynamical system can be well described and understood by the means of deterministic approach, it is generally good practice not to ignore the stochastic aspects which are

often present in any chemical, biological or physical process and maybe rooted from:

(i) Slight changes in dynamical systems input which can cause chaos in the system;

(ii) Likelihood that the system translates from one state to other within a short period of time;

(iii) Evolution of the system that starts with small variation of parameter and state values;

(iv) Estimation of parameters and states which is inseparable with uncertainty analysis.

Apart from the above enumerated general stochastic aspects, state variables of the chemical reactors such as concentration, temperature, volume of the mixture and the cooling temperature inside the tanks most commonly spread and mix randomly by the diffusive mixing phenomena (Fonseca, 2019; Mao *et al.*, 2017; Burghardt, 2008; Akiti, 2000; Wilhelm, 1962). Moraes (2015) has shown stochastic variability to be explored in chemical systems whereby a single or more than one species of molecules can be present in low numbers of molecule. In this regard, the classical description of the reaction into reactor by the approach of ordinary differential equations can not fully capture some phenomena like unexpected extinction of one of the interacting species in the mixture. Therefore, it is with the above reasons that the researchers are eager and forced to develop and simulate CSTR stochastic-based models in order to incorporating the randomness aspect that describes stochastic dynamics in the formulated deterministic models.

Stochastic models can be derived from deterministic models in the following four scenarios:
Scenario A: Additive of the diffusion part on each ODE of the system. The diffusion part is composed by the fluctuation constant times the white noise.
Scenario B: Additive of the diffusion part composed by fluctuation constant times state variable and white noise on each ODE of the system.
Scenario C: Perturbation of one or more important parameters of the model with the white noise.
Scenario D: Through transition probabilities.

Each of the stated four scenarios of formulating the stochastic models has its advantages and disadvantages. For the first scenario, the advantage is that formulation is simple but this technique increases the number of parameters in the model as disadvantage. The second scenario

also increases the number of parameters in the model as disadvantage but this is a good approach simply because of taking into account of the perturbation of the model and each of its respective state variable. The third scenario is good since it does not increase the number of parameters in the model but as disadvantage the perturbation may not affect each and every ordinary differential equation of the system. The fourth scenario is the most preferable technique but sometimes the covariance matrix obtained from small changes in the state variables may lead to a square root of the product of a complex expression and a derivative of Brownian term.

In this dissertation, the four scenarios are considered, analysed and compared with the corresponding deterministic models taken as benchmarks.

3.2.1 Exothermic CSTR Stochastic Models Formulation

(i) Scenario A: Diffusion part additive

Deterministic models always describe the system which evolves in only one direction. However, taking into consideration of the system that evolves in different directions rather than in one direction is very important and it helps to determine the behaviour of the system in any direction at any time. The stochastic models for the CSTRs considers fluctuations terms and are formulated by adding diffusion terms on the deterministic models. Therefore, the perturbed deformable stochastic models for the exothermic CSTRs is given by:

$$\begin{cases} \mathrm{d}V = (F_{\text{in}} - F_{\text{out}})\mathrm{d}t + \delta_V \mathrm{d}B_V(t), \\ \mathrm{d}C = \left(\frac{F}{V}(C_{\text{in}} - C) - k_0 e^{-\frac{E}{R}\left(\frac{1}{T}-\frac{1}{T_{\text{mean}}}\right)}C\right)\mathrm{d}t + \delta_C \mathrm{d}B_C(t), \\ \mathrm{d}T = \left(\frac{F}{V}(T_{\text{in}} - T) - \frac{H^* k_0 e^{-\frac{E}{R}\left(\frac{1}{T}-\frac{1}{T_{\text{mean}}}\right)}C}{\rho C_p} - \frac{UA(T-T_c)}{\rho C_p V}\right)\mathrm{d}t + \delta_T \mathrm{d}B_T(t), \\ \mathrm{d}T_c = \left(\frac{F_c}{V_c}(T_{c_{\text{in}}} - T_c) + \frac{UA(T-T_c)}{\rho_c C_{pc} V_c}\right)\mathrm{d}t + \delta_{T_c}\mathrm{d}B_{T_c}(t). \end{cases} \tag{83}$$

Note: Terms $\delta_V, \delta_C, \delta_T, \delta_{T_c}$ are fluctuation widths and are sometimes called volatility constants whilst $\mathrm{d}B_V(t), \mathrm{d}B_C(t), \mathrm{d}B_T(t), \mathrm{d}B_{T_c}(t)$ are one another mutually independent Wiener processes. This formulation is simple as advantage but it increases the number of parameters in the model as disadvantage.

(ii) Scenario B: Diffusion part additive times its corresponding state variable

For this scenario, the product of fluctuation constants, Wiener process and corresponding state variable is added to each of the deterministic differential equation of the system. This gives the system of stochastic differential equations shown in Equation (84).

$$\begin{cases} \mathrm{d}V = (F_{\text{in}} - F_{\text{out}})\mathrm{d}t + \delta_V V \mathrm{d}B_V(t), \\ \mathrm{d}C = \left(\frac{F}{V}(C_{\text{in}} - C) - k_0 e^{-\frac{E}{R}\left(\frac{1}{T} - \frac{1}{T_{\text{mean}}}\right)} C\right)\mathrm{d}t + \delta_C C \mathrm{d}B_C(t), \\ \mathrm{d}T = \left(\frac{F}{V}(T_{\text{in}} - T) - \frac{H^* k_0 e^{-\frac{E}{R}\left(\frac{1}{T} - \frac{1}{T_{\text{mean}}}\right)} C}{\rho C_p} - \frac{UA(T - T_c)}{\rho C_p V}\right)\mathrm{d}t + \delta_T T \mathrm{d}B_T(t), \\ \mathrm{d}T_c = \left(\frac{F_c}{V_c}(T_{c_{\text{in}}} - T_c) + \frac{UA(T - T_c)}{\rho_c C_{p_c} V_c}\right)\mathrm{d}t + \delta_{T_c} T_c \mathrm{d}B_{T_c}(t). \end{cases} \tag{84}$$

The formulation of this kind of stochastic models is simple as advantage but also it increases the number of parameters in the model as disadvantage. Another disadvantage for this kind of stochastic models formulation is to identify the numerical scheme which can be used to simulate them and provides accurate and reliable numerical results.

(iii) Scenario C: Parametric perturbation

Stochastic model driven by parametric perturbation is obtained after making one or more important deterministic model parameters to be random variables which is also another way of formulating a stochastic model. This process requires the thinking of one or more important parameters to be perturbed from the deterministic model. As it is well known, the reaction rate of a chemical reaction can be affected by a various number of external facets which may be taking place either from the environment like climate factors or from the functionality of the system itself such as the external cooling/heating system temperature, reactants impurities just to mention few. Then it is worthwhile and does make sense to introduce random perturbations on the reaction rate through the Arrhennius temperature dependent parameter k_0, so that $k_0\mathrm{d}t = k_0\mathrm{d}t + \delta\mathrm{d}B$. Therefore, for this scenario, the exothermic CSTR deterministic model

becomes stochastic model that is presented in Equation (85).

$$\begin{cases} \mathrm{d}V = (F_{\text{in}} - F_{\text{out}})\,\mathrm{d}t, \\ \mathrm{d}C = \left(\frac{F}{V}(C_{\text{in}} - C) - k_0 e^{-\frac{E}{R}\left(\frac{1}{T}-\frac{1}{T_{\text{mean}}}\right)}C\right)\mathrm{d}t - \delta e^{-\frac{E}{R}\left(\frac{1}{T}-\frac{1}{T_{\text{mean}}}\right)}C\mathrm{d}B, \\ \mathrm{d}T = \left(\frac{F}{V}(T_{\text{in}} - T) + \frac{-H^* k_0 e^{-\frac{E}{R}\left(\frac{1}{T}-\frac{1}{T_{\text{mean}}}\right)}C}{\rho C_p} - \frac{UA}{\rho C_p V}(T - T_c)\right)\mathrm{d}t + \frac{\delta(-H^*)e^{-\frac{E}{R}\left(\frac{1}{T}-\frac{1}{T_{\text{mean}}}\right)}C}{\rho C_p}\mathrm{d}B, \\ \mathrm{d}T_c = \left(\frac{F_c}{V_c}(T_{c_{\text{in}}} - T_c) + \frac{U_c A_c}{\rho_c C_{p_c} V_c}(T - T_c)\right)\mathrm{d}t. \end{cases} \tag{85}$$

The formulation of this kind of stochastic models is simple and it does not increase many number of parameters in the model as advantages. However, the thinking of sensitive model parameter may be a challenge and the stochastic behaviour may not been seen in each every equation that makes the CSTR's system.

(iv) Scenario D: Transition probability

According to Allen (2007, 2017), the stochastic modeling of the system can be achieved through transition probabilities by computing the mean of changes $\mathbb{E}((\vec{\triangle x})_i)$ and the covariance matrix of the changes as $\mathbb{E}((\vec{\triangle x})_i \vec{\triangle x})'_i)$. Let us define X_1, X_2, X_3 and X_4 to represent the state variables V, C, T and T_c respectively, and let pi be the transition probabilities from each of the terms of the system. The formulation of this type of SDEs is complicated as disadvantage but the results may be accurate as advantage. From the exothermic CSTR deterministic model shown in Equation (35), nine possible changes are counted and therefore, $i = 1, 2, 3..., 9$. So, the transitions and probabilities are displayed in Table 4.

Table 4: Transition probabilities for the exothermic model

Transition	**Probability**
$(\vec{\triangle x})_1 = [1,0,0,0]'$	$p_1 = F_{\text{in}} \triangle t$
$(\vec{\triangle x})_2 = [-1,0,0,0]'$	$p_2 = F_{\text{out}} \triangle t$
$(\vec{\triangle x})_3 = [0,1,0,0]'$	$p_3 = \frac{F}{V}(C_{\text{in}} - C) \triangle t$
$(\vec{\triangle x})_4 = [0,-1,0,0]'$	$p_4 = k_0 e^{-\frac{E}{R}\left(\frac{1}{T} - \frac{1}{T_{\text{mean}}}\right)} C \triangle t$
$(\vec{\triangle x})_5 = [0,0,1,0]'$	$p_5 = \frac{F}{V}(T_{\text{in}} - T) \triangle t$
$(\vec{\triangle x})_6 = [0,0,-1,0]'$	$p_6 = \frac{H^* k_0 e^{-\frac{E}{R}\left(\frac{1}{T} - \frac{1}{T_{\text{mean}}}\right)} C}{\rho C_p} \triangle t$
$(\vec{\triangle x})_7 = [0,0,-1,0]'$	$p_7 = \frac{UA(T - T_c)}{V \rho C_p} \triangle t$
$(\vec{\triangle x})_8 = [0,0,0,1]'$	$p_8 = \frac{F_c}{V_c}(T_{c_{\text{in}}} - T_c) \triangle t$
$(\vec{\triangle x})_9 = [0,0,0,1]'$	$p_9 = \frac{UA(T - T_c)}{V_c \rho_c C_{p_c}} \triangle t$

Hence, the expectation of the changes is given by:

$$\mathbb{E}(\vec{\triangle \mathbf{x}}) = \sum_{i=1}^{9} p_i (\vec{\triangle x})_i = p_1(\vec{\triangle x})_1 + p_2(\vec{\triangle x})_2 + p_3(\vec{\triangle x})_3 + p_4(\vec{\triangle x})_4 + p_5(\vec{\triangle x})_5 + p_6(\vec{\triangle x})_6 + p_7(\vec{\triangle x})_7 + p_8(\vec{\triangle x})_8 + p_9(\vec{\triangle x})_9.$$

$$\mathbb{E}(\vec{\triangle}\mathbf{x}) = F_{\text{in}} \begin{pmatrix} 1 \\ 0 \\ 0 \\ 0 \end{pmatrix} \triangle t + F_{\text{out}} \begin{pmatrix} -1 \\ 0 \\ 0 \\ 0 \end{pmatrix} \triangle t + \frac{F}{V}(C_{\text{in}} - C) \begin{pmatrix} 0 \\ 1 \\ 0 \\ 0 \end{pmatrix} \triangle t$$
$$+k_0 e^{-\frac{E}{R}\left(\frac{1}{T} - \frac{1}{T_{\text{mean}}}\right)} C \begin{pmatrix} 0 \\ -1 \\ 0 \\ 0 \end{pmatrix} \triangle t + \frac{F}{V}(T_{\text{in}} - T) \begin{pmatrix} 0 \\ 0 \\ 1 \\ 0 \end{pmatrix} \triangle t$$
$$+\frac{H^* k_0 e^{-\frac{E}{R}\left(\frac{1}{T} - \frac{1}{T_{\text{mean}}}\right)} C}{\rho C_p} \begin{pmatrix} 0 \\ 0 \\ -1 \\ 0 \end{pmatrix} \triangle t + \frac{UA(T - T_c)}{V \rho C_p} \begin{pmatrix} 0 \\ 0 \\ -1 \\ 0 \end{pmatrix} \triangle t$$
$$+\frac{F_c}{V_c}(T_{c_{\text{in}}} - T_c) \begin{pmatrix} 0 \\ 0 \\ 0 \\ 1 \end{pmatrix} \triangle t + \frac{UA(T - T_c)}{V_c \rho_c C_{p_c}} \begin{pmatrix} 0 \\ 0 \\ 0 \\ 1 \end{pmatrix} \triangle t.$$

So, the mean of the changes is obtained as follow:

$$\mathbb{E}(\vec{\triangle}\mathbf{x}) = \begin{pmatrix} F_{\text{in}} - F_{\text{out}} \\ \frac{F}{V}(C_{\text{in}} - C) - k_0 e^{-\frac{E}{R}\left(\frac{1}{T} - \frac{1}{T_{\text{mean}}}\right)} C \\ \frac{F}{V}(T_{\text{in}} - T) + \frac{(-H^* k_0 e^{-\frac{E}{R}\left(\frac{1}{T} - \frac{1}{T_{\text{mean}}}\right)} C}{\rho C_p} - \frac{UA}{\rho C_p V}(T - T_c) \\ \frac{F_c}{V_c}(T_{c_{\text{in}}} - T_c) + \frac{U_c A_c}{\rho_c C_{p_c} V_c}(T - T_c) \end{pmatrix} \triangle t = F(X_1, X_2, X_3, X_4) \triangle t.$$

The covariance matrix for the changes is given by:

$$\mathbb{E}(\vec{\triangle}\mathbf{x}\vec{\triangle}\mathbf{x}') = \sum_{i=1}^{9} p_i (\vec{\triangle}x)_i (\vec{\triangle}x)_i' = p_1 (\vec{\triangle}x)_1 (\vec{\triangle}x)_1' + ... + p_9 (\vec{\triangle}x)_9 (\vec{\triangle}x)_9'. \tag{86}$$

$$\mathbb{E}(\vec{\triangle}\mathbf{x}\vec{\triangle}\mathbf{x}') = p_1 \begin{pmatrix} 1 \\ 0 \\ 0 \\ 0 \end{pmatrix} \begin{pmatrix} 1 & 0 & 0 & 0 \end{pmatrix} + p_2 \begin{pmatrix} -1 \\ 0 \\ 0 \\ 0 \end{pmatrix} \begin{pmatrix} -1 & 0 & 0 & 0 \end{pmatrix} + p_3 \begin{pmatrix} 0 \\ 1 \\ 0 \\ 0 \end{pmatrix} \begin{pmatrix} 0 & 1 & 0 & 0 \end{pmatrix}$$
$$+p_4 \begin{pmatrix} 0 \\ -1 \\ 0 \\ 0 \end{pmatrix} \begin{pmatrix} 0 & -1 & 0 & 0 \end{pmatrix} + p_5 \begin{pmatrix} 0 \\ 0 \\ 1 \\ 0 \end{pmatrix} \begin{pmatrix} 0 & 0 & 1 & 0 \end{pmatrix} + p_6 \begin{pmatrix} 0 \\ 0 \\ -1 \\ 0 \end{pmatrix} \begin{pmatrix} 0 & 0 & -1 & 0 \end{pmatrix}$$
$$+p_7 \begin{pmatrix} 0 \\ 0 \\ -1 \\ 0 \end{pmatrix} \begin{pmatrix} 0 & 0 & -1 & 0 \end{pmatrix} + p_8 \begin{pmatrix} 0 \\ 0 \\ 0 \\ 1 \end{pmatrix} \begin{pmatrix} 0 & 0 & 0 & 1 \end{pmatrix} + p_9 \begin{pmatrix} 0 \\ 0 \\ 0 \\ 1 \end{pmatrix} \begin{pmatrix} 0 & 0 & 0 & 1 \end{pmatrix}.$$

The computations give

$$\mathbb{E}(\vec{\triangle}\mathbf{x}\vec{\triangle}\mathbf{x}') = p_1 \begin{pmatrix} 1 & 0 & 0 & 0 \\ 0 & 0 & 0 & 0 \\ 0 & 0 & 0 & 0 \\ 0 & 0 & 0 & 0 \end{pmatrix} + p_2 \begin{pmatrix} 1 & 0 & 0 & 0 \\ 0 & 0 & 0 & 0 \\ 0 & 0 & 0 & 0 \\ 0 & 0 & 0 & 0 \end{pmatrix} + p_3 \begin{pmatrix} 0 & 0 & 0 & 0 \\ 0 & 1 & 0 & 0 \\ 0 & 0 & 0 & 0 \\ 0 & 0 & 0 & 0 \end{pmatrix} + p_4 \begin{pmatrix} 0 & 0 & 0 & 0 \\ 0 & 1 & 0 & 0 \\ 0 & 0 & 0 & 0 \\ 0 & 0 & 0 & 0 \end{pmatrix}$$
$$+p_5 \begin{pmatrix} 0 & 0 & 0 & 0 \\ 0 & 0 & 0 & 0 \\ 0 & 0 & 1 & 0 \\ 0 & 0 & 0 & 0 \end{pmatrix} + p_6 \begin{pmatrix} 0 & 0 & 0 & 0 \\ 0 & 0 & 0 & 0 \\ 0 & 0 & 1 & 0 \\ 0 & 0 & 0 & 0 \end{pmatrix} + p_7 \begin{pmatrix} 0 & 0 & 0 & 0 \\ 0 & 0 & 0 & 0 \\ 0 & 0 & 1 & 0 \\ 0 & 0 & 0 & 0 \end{pmatrix} + p_8 \begin{pmatrix} 0 & 0 & 0 & 0 \\ 0 & 0 & 0 & 0 \\ 0 & 0 & 0 & 0 \\ 0 & 0 & 0 & 1 \end{pmatrix}$$
$$+p_9 \begin{pmatrix} 0 & 0 & 0 & 0 \\ 0 & 0 & 0 & 0 \\ 0 & 0 & 0 & 0 \\ 0 & 0 & 0 & 1 \end{pmatrix} = \begin{pmatrix} p_1 + p_2 & 0 & 0 & 0 \\ 0 & p_3 + p_4 & 0 & 0 \\ 0 & 0 & p_5 + p_6 + p_7 & 0 \\ 0 & 0 & 0 & p_8 + p_9 \end{pmatrix}$$
$$= \begin{pmatrix} q_1 & 0 & 0 & 0 \\ 0 & q_2 & 0 & 0 \\ 0 & 0 & q_3 & 0 \\ 0 & 0 & 0 & q_4 \end{pmatrix} \triangle t = Z(X_1, X_2, X_3, X_4)\triangle t, \tag{87}$$

where $q_1 = p_1 + p_2 = F_{\text{in}} + F_{\text{out}}, q_2 = p_3 + p_4 = \frac{F}{V}(C_{\text{in}} - C) + k_0 e^{-\frac{E}{R}\left(\frac{1}{T} - \frac{1}{T_{\text{mean}}}\right)} C, q_3 = p_5 + p_6 + p_7 = \frac{F}{V}(T_{\text{in}} - T) + \frac{(-H^* k_0 e^{-\frac{E}{R}\left(\frac{1}{T} - \frac{1}{T_{\text{mean}}}\right)} C}{\rho C_p} + \frac{UA}{\rho C_p V}(T - T_c), q_4 = p_8 + p_9 = \frac{F_c}{V_c}(T_{c_{\text{in}}} - T_c) + \frac{U_c A_c}{\rho_c C_{p_c} V_c}(T - T_c)$.

The SDE for the system can be formulated by using the square root of the obtained covariance matrix (Z). It follows that the stochastic differential equation is formulated as Equation (88).

$$\mathrm{d}\boldsymbol{X(t)} = F\left(\boldsymbol{X}(t), \theta\right) dt + Z^{\frac{1}{2}}\left(\boldsymbol{X}(t), \theta\right) \mathrm{d}\boldsymbol{B}(t), \tag{88}$$

where $\boldsymbol{X}(t) = [X_1, X_2, X_3, X_4]'$ and $\boldsymbol{B}(t) = [B_1(t), B_2(t), B_3(t), B_4(t)]'$.

Alternatively, one can find a matrix C so that $CC^T = Z$. As show by Allen (2017), a matrix C is not unique and can be obtained directly from the system of ODE as each of its column is the square root of the transition rates that are given in Table 4. It can be seen that C is 4×9 matrix and it is written as,

$$C = \begin{pmatrix} a_1 & a_2 & 0 & 0 & 0 & 0 & 0 & 0 & 0 \\ 0 & 0 & a_3 & a_4 & 0 & 0 & 0 & 0 & 0 \\ 0 & 0 & 0 & 0 & a_5 & a_6 & a_7 & 0 & 0 \\ 0 & 0 & 0 & 0 & 0 & 0 & 0 & a_8 & a_9 \end{pmatrix},$$

where

$$a_1 = \sqrt{F_{\text{in}}},\ a_2 = -\sqrt{F_{\text{out}}}\ , a_3 = \sqrt{\frac{F}{V}(C_{\text{in}} - C)},\ a_4 = -\sqrt{k_0 e^{-\frac{E}{R}(\frac{1}{T} - \frac{1}{T_{\text{mean}}})} C}$$

$$a_5 = \sqrt{\frac{F}{V}(T_{\text{in}} - T)},\ a_6 = -\sqrt{\frac{H^* k_0 e^{-\frac{E}{R}(\frac{1}{T} - \frac{1}{T_{\text{mean}}})} C}{\rho C_p}},\ a_7 = -\sqrt{\frac{UA(T - T_c)}{\rho C_p V}}$$

$$a_8 = \sqrt{\frac{F_c}{V_c}(T_{c_{\text{in}}} - T_c)},\ a_9 = \sqrt{\frac{UA(T - T_c)}{\rho_c C_{p_c} V_c}}.$$

Therefore, the corresponding system of SDE derived from model Equation (35) is given by a

system of Equations (89).

$$\begin{cases} \mathrm{d}V(t) = (F_{\text{in}} - F_{\text{out}})\mathrm{d}t + a_1\mathrm{d}B_1(t) + a_2\mathrm{d}B_2(t) \\ \mathrm{d}C(t) = \left(\frac{F}{V}(C_{\text{in}} - C) - k_0 e^{-\frac{E}{R}\left(\frac{1}{T} - \frac{1}{T_{\text{mean}}}\right)}C\right)\mathrm{d}t + a_3\mathrm{d}B_3(t) + a_4\mathrm{d}B_4(t) \\ \mathrm{d}T(t) = \left(\frac{F}{V}(T_{\text{in}} - T) - \frac{H^* k_0 e^{-\frac{E}{R}\left(\frac{1}{T} - \frac{1}{T_{\text{mean}}}\right)}C}{\rho C_p} - \frac{UA(T - T_c)}{\rho C_p V}\right)\mathrm{d}t + a_5\mathrm{d}B_5(t) + a_6\mathrm{d}B_6(t) \\ +a_7\mathrm{d}B_7(t) \\ \mathrm{d}T_c(t) = \left(\frac{F_c}{V_c}(T_{c_{\text{in}}} - T_c) + \frac{UA(T - T_c)}{\rho_c C_{p_c} V_c}\right)\mathrm{d}t + a_8\mathrm{d}B_8(t) + a_9\mathrm{d}B_9(t). \end{cases} \tag{89}$$

$B_i(t) \sim N(0, t)$, for $i = 1, 2, ..., 9$ is normally distributed random variable with mean zero and variance t that also means $\mathrm{d}B_i(t) \sim \mathbb{N}(0, \mathrm{d}t)$. The numerical simulations of the SDE (89) is carried out by using Euler-Maruyama method.

3.2.2 Endothermic CSTR Stochastic Models Formulation

Similarly, the four scenarios that were early considered for the formulation of the exothermic CSTR stochastic models are again taken into account in the formulation of the endothermic CSTR stochastic models. Therefore, the perturbed deformable endothermic CSTR stochastic models formulated are found in scenarios A-D as follow:

(i) Scenario A: Diffusion part additive

$$\begin{cases} \mathrm{d}V = (F_{\text{in}} - F_{\text{out}})\mathrm{d}t + \delta_V\mathrm{d}B_V(t), \\ \mathrm{d}C = \left(\frac{F}{V}(C_{\text{in}} - C) - k_0 e^{-\frac{E}{R}\left(\frac{1}{T} - \frac{1}{T_{\text{mean}}}\right)}C\right)\mathrm{d}t + \delta_C\mathrm{d}B_C(t), \\ \mathrm{d}T = \left(\frac{F}{V}(T_{\text{in}} - T) + \frac{H^* k_0 e^{-\frac{E}{R}\left(\frac{1}{T} - \frac{1}{T_{\text{mean}}}\right)}C}{\rho C_p} + \frac{UA(T_H - T)}{\rho_H C_{p_H} V_H}\right)\mathrm{d}t + \delta_T\mathrm{d}B_T(t), \\ \mathrm{d}T_H = \left(\frac{F_H}{V_H}(T_{H_{\text{in}}} - T_H) - \frac{UA(T_H - T)}{\rho_H C_{p_H} V_H}\right)\mathrm{d}t + \delta_{T_H}\mathrm{d}B_{T_H}(t), \end{cases} \tag{90}$$

where δ_{T_H} and $\mathrm{d}B_{T_H}(t)$ are also fluctuation width and wiener process.

(ii) Scenario B: Diffusion part additive times its corresponding state variable

The system of SDEs for this scenario is given in Equation (91).

$$\begin{cases} \mathrm{d}V = (F_{\text{in}} - F_{\text{out}})\mathrm{d}t + \delta_V V \mathrm{d}B_V(t) \\ \mathrm{d}C = \left(\frac{F}{V}(C_{\text{in}} - C) - k_0 e^{-\frac{E}{R}\left(\frac{1}{T} - \frac{1}{T_{\text{mean}}}\right)} C\right)\mathrm{d}t + \delta_C C \mathrm{d}B_C(t) \\ \mathrm{d}T = \left(\frac{F}{V}(T_{\text{in}} - T) + \frac{H^* k_0 e^{-\frac{E}{R}\left(\frac{1}{T} - \frac{1}{T_{\text{mean}}}\right)} C}{\rho C_p} + \frac{UA(T_H - T)}{\rho_H C_{p_H} V_H}\right)\mathrm{d}t + \delta_T T \mathrm{d}B_T(t) \\ \mathrm{d}T_H = \left(\frac{F_H}{V_H}(T_{H_{\text{in}}} - T_H) - \frac{UA(T_H - T)}{\rho_H C_{p_H} V_H}\right)\mathrm{d}t + \delta_{T_H} T_H \mathrm{d}B_{T_H}(t) \end{cases} \tag{91}$$

(iii) Scenario C: Parametric perturbation

This scenario leads to a system of SDEs written as Equation (92).

$$\begin{cases} \mathrm{d}V = (F_{\text{in}} - F_{\text{out}})\,\mathrm{d}t \\ \mathrm{d}C = \left(\frac{F}{V}\,(C_{\text{in}} - C) - k_0 e^{-\frac{E}{R}\left(\frac{1}{T} - \frac{1}{T_{\text{mean}}}\right)} C\right)\mathrm{d}t - \delta e^{-\frac{E}{R}\left(\frac{1}{T} - \frac{1}{T_{\text{mean}}}\right)} C \mathrm{d}B \\ \mathrm{d}T = \left(\frac{F}{V}(T_{\text{in}} - T) + \frac{H^* k_0 e^{-\frac{E}{R}\left(\frac{1}{T} - \frac{1}{T_{\text{mean}}}\right)} C}{\rho C_p} + \frac{UA}{\rho C_p V}(T_H - T)\right)\mathrm{d}t + \frac{\delta H^* e^{-\frac{E}{R}\left(\frac{1}{T} - \frac{1}{T_{\text{mean}}}\right)} C}{\rho C_p}\mathrm{d}B \\ \mathrm{d}T_H = \left(\frac{F_H}{V_H}(T_{H_{\text{in}}} - T_H) - \frac{U_H A_H}{\rho_H C_{p_H} V_H}(T_H - T)\right)\mathrm{d}t \end{cases} \tag{92}$$

(iv) Scenario D: Transition probability

As per scenario D of the exothermic CSTR stochastic model, the transitions and probabilities that help in the formulation of the endothermic CSTR stochastic model are shown in Table 5.

Table 5: Transition probabilities for the endothermic model

Transition	**Probability**
$(\vec{\triangle x})_1 = [1,0,0,0]'$	$p_1 = F_{\text{in}} \triangle t$
$(\vec{\triangle x})_2 = [-1,0,0,0]'$	$p_2 = F_{\text{out}} \triangle t$
$(\vec{\triangle x})_3 = [0,1,0,0]'$	$p_3 = \frac{F}{V}(C_{\text{in}} - C) \triangle t$
$(\vec{\triangle x})_4 = [0,-1,0,0]'$	$p_4 = k_0 e^{-\frac{E}{R}\left(\frac{1}{T} - \frac{1}{T_{\text{mean}}}\right)} C \triangle t$
$(\vec{\triangle x})_5 = [0,0,1,0]'$	$p_5 = \frac{F}{V}(T_{\text{in}} - T) \triangle t$
$(\vec{\triangle x})_6 = [0,0,1,0]'$	$p_6 = \frac{H^* k_0 e^{-\frac{E}{R}\left(\frac{1}{T} - \frac{1}{T_{\text{mean}}}\right)} C}{\rho C_p} \triangle t$
$(\vec{\triangle x})_7 = [0,0,1,0]'$	$p_7 = \frac{UA(T_H - T)}{V \rho C_p} \triangle t$
$(\vec{\triangle x})_8 = [0,0,0,1]'$	$p_8 = \frac{F_H}{V_H}(T_{H_{\text{in}}} - T_H) \triangle t$
$(\vec{\triangle x})_9 = [0,0,0,-1]'$	$p_9 = \frac{UA(T_H - T)}{V_H \rho_H C_{p_H}} \triangle t$

Thus, the expectation of the possible changes is given by:

$$\mathbb{E}(\vec{\triangle \mathbf{x}}) = \sum_{i=1}^{9} p_i (\vec{\triangle x})_i = p_1(\vec{\triangle x})_1 + p_2(\vec{\triangle x})_2 + p_3(\vec{\triangle x})_3 + p_4(\vec{\triangle x})_4 + p_5(\vec{\triangle x})_5 + p_6(\vec{\triangle x})_6 + p_7(\vec{\triangle x})_7 + p_8(\vec{\triangle x})_8 + p_9(\vec{\triangle x})_9.$$

$$\mathbb{E}(\vec{\triangle \mathbf{x}}) = F_{\text{in}} \begin{pmatrix} 1 \\ 0 \\ 0 \\ 0 \end{pmatrix} \triangle t + F_{\text{out}} \begin{pmatrix} -1 \\ 0 \\ 0 \\ 0 \end{pmatrix} \triangle t + \frac{F}{V}(C_{\text{in}} - C) \begin{pmatrix} 0 \\ 1 \\ 0 \\ 0 \end{pmatrix} \triangle t$$
$$+k_0 e^{-\frac{E}{R}\left(\frac{1}{T} - \frac{1}{T_{\text{mean}}}\right)} C \begin{pmatrix} 0 \\ -1 \\ 0 \\ 0 \end{pmatrix} \triangle t + \frac{F}{V}(T_{\text{in}} - T) \begin{pmatrix} 0 \\ 0 \\ 1 \\ 0 \end{pmatrix} \triangle t$$
$$+\frac{H^* k_0 e^{-\frac{E}{R}\left(\frac{1}{T} - \frac{1}{T_{\text{mean}}}\right)} C}{\rho C_p} \begin{pmatrix} 0 \\ 0 \\ 1 \\ 0 \end{pmatrix} \triangle t + \frac{UA(T_H - T)}{V \rho C_p} \begin{pmatrix} 0 \\ 0 \\ 1 \\ 0 \end{pmatrix} \triangle t$$
$$+\frac{F_H}{V_H}(T_{H_{\text{in}}} - T_H) \begin{pmatrix} 0 \\ 0 \\ 0 \\ 1 \end{pmatrix} \triangle t + \frac{UA(T_H - T)}{V_H \rho_H C_{p_H}} \begin{pmatrix} 0 \\ 0 \\ 0 \\ -1 \end{pmatrix} \triangle t.$$

So, the expectation of the changes in the process is given by:

$$\mathbb{E}(\vec{\triangle \mathbf{x}}) = \begin{pmatrix} F_{\text{in}} - F_{\text{out}} \\ \frac{F}{V}(C_{\text{in}} - C) - k_0 e^{-\frac{E}{R}\left(\frac{1}{T} - \frac{1}{T_{\text{mean}}}\right)} C \\ \frac{F}{V}(T_{\text{in}} - T) + \frac{(H^* k_0 e^{-\frac{E}{R}\left(\frac{1}{T} - \frac{1}{T_{\text{mean}}}\right)} C}{\rho C_p} + \frac{UA}{\rho C_p V}(T_H - T) \\ \frac{F_H}{V_H}(T_{H_{\text{in}}} - T_H) - \frac{UA}{\rho_H C_{p_H} V_H}(T_H - T) \end{pmatrix} \triangle t = F(X_1, X_2, X_3, X_4) \triangle t.$$

The covariance matrix for the changes in the endothermic process that is represented in Equation model (36) is also given by:

$$\mathbb{E}(\vec{\triangle \mathbf{x}} \vec{\triangle \mathbf{x}}') = \sum_{i=1}^{9} p_i (\vec{\triangle x})_i (\vec{\triangle x})_i' = p_1 (\vec{\triangle x})_1 (\vec{\triangle x})_1' + ... + p_9 (\vec{\triangle x})_9 (\vec{\triangle x})_9'. \tag{93}$$

$$\mathbb{E}(\vec{\triangle}\mathbf{x}\vec{\triangle}\mathbf{x}') = p_1 \begin{pmatrix} 1 \\ 0 \\ 0 \\ 0 \end{pmatrix} \begin{pmatrix} 1 & 0 & 0 & 0 \end{pmatrix} + p_2 \begin{pmatrix} -1 \\ 0 \\ 0 \\ 0 \end{pmatrix} \begin{pmatrix} -1 & 0 & 0 & 0 \end{pmatrix} + p_3 \begin{pmatrix} 0 \\ 1 \\ 0 \\ 0 \end{pmatrix} \begin{pmatrix} 0 & 1 & 0 & 0 \end{pmatrix}$$
$$+p_4 \begin{pmatrix} 0 \\ -1 \\ 0 \\ 0 \end{pmatrix} \begin{pmatrix} 0 & -1 & 0 & 0 \end{pmatrix} + p_5 \begin{pmatrix} 0 \\ 0 \\ 1 \\ 0 \end{pmatrix} \begin{pmatrix} 0 & 0 & 1 & 0 \end{pmatrix} + p_6 \begin{pmatrix} 0 \\ 0 \\ 1 \\ 0 \end{pmatrix} \begin{pmatrix} 0 & 0 & 1 & 0 \end{pmatrix}$$
$$+p_7 \begin{pmatrix} 0 \\ 0 \\ 1 \\ 0 \end{pmatrix} \begin{pmatrix} 0 & 0 & 1 & 0 \end{pmatrix} + p_8 \begin{pmatrix} 0 \\ 0 \\ 0 \\ 1 \end{pmatrix} \begin{pmatrix} 0 & 0 & 0 & 1 \end{pmatrix} + p_9 \begin{pmatrix} 0 \\ 0 \\ 0 \\ -1 \end{pmatrix} \begin{pmatrix} 0 & 0 & 0 & -1 \end{pmatrix}.$$

The computation leads to

$$\mathbb{E}(\vec{\triangle}\mathbf{x}\vec{\triangle}\mathbf{x}') = p_1 \begin{pmatrix} 1 & 0 & 0 & 0 \\ 0 & 0 & 0 & 0 \\ 0 & 0 & 0 & 0 \\ 0 & 0 & 0 & 0 \end{pmatrix} + p_2 \begin{pmatrix} 1 & 0 & 0 & 0 \\ 0 & 0 & 0 & 0 \\ 0 & 0 & 0 & 0 \\ 0 & 0 & 0 & 0 \end{pmatrix} + p_3 \begin{pmatrix} 0 & 0 & 0 & 0 \\ 0 & 1 & 0 & 0 \\ 0 & 0 & 0 & 0 \\ 0 & 0 & 0 & 0 \end{pmatrix} + p_4 \begin{pmatrix} 0 & 0 & 0 & 0 \\ 0 & 1 & 0 & 0 \\ 0 & 0 & 0 & 0 \\ 0 & 0 & 0 & 0 \end{pmatrix}$$
$$+p_5 \begin{pmatrix} 0 & 0 & 0 & 0 \\ 0 & 0 & 0 & 0 \\ 0 & 0 & 1 & 0 \\ 0 & 0 & 0 & 0 \end{pmatrix} + p_6 \begin{pmatrix} 0 & 0 & 0 & 0 \\ 0 & 0 & 0 & 0 \\ 0 & 0 & 1 & 0 \\ 0 & 0 & 0 & 0 \end{pmatrix} + p_7 \begin{pmatrix} 0 & 0 & 0 & 0 \\ 0 & 0 & 0 & 0 \\ 0 & 0 & 1 & 0 \\ 0 & 0 & 0 & 0 \end{pmatrix} + p_8 \begin{pmatrix} 0 & 0 & 0 & 0 \\ 0 & 0 & 0 & 0 \\ 0 & 0 & 0 & 0 \\ 0 & 0 & 0 & 1 \end{pmatrix}$$
$$+p_9 \begin{pmatrix} 0 & 0 & 0 & 0 \\ 0 & 0 & 0 & 0 \\ 0 & 0 & 0 & 0 \\ 0 & 0 & 0 & 1 \end{pmatrix} = \begin{pmatrix} p_1 + p_2 & 0 & 0 & 0 \\ 0 & p_3 + p_4 & 0 & 0 \\ 0 & 0 & p_5 + p_6 + p_7 & 0 \\ 0 & 0 & 0 & p_8 + p_9 \end{pmatrix}$$
$$= \begin{pmatrix} q_1 & 0 & 0 & 0 \\ 0 & q_2 & 0 & 0 \\ 0 & 0 & q_3 & 0 \\ 0 & 0 & 0 & q_4 \end{pmatrix} \triangle t = Z(X_1, X_2, X_3, X_4)\triangle t, \tag{94}$$

where $q_1 = p_1 + p_2 = F_{\text{in}} + F_{\text{out}}, q_2 = p_3 + p_4 = \frac{F}{V}(C_{\text{in}} - C) + k_0 e^{-\frac{E}{R}\left(\frac{1}{T} - \frac{1}{T_{\text{mean}}}\right)} C, q_3 = p_5 + p_6 + p_7 = \frac{F}{V}(T_{\text{in}} - T) + \frac{(H^* k_0 e^{-\frac{E}{R}\left(\frac{1}{T} - \frac{1}{T_{\text{mean}}}\right)} C}{\rho C_p} + \frac{UA}{\rho C_p V}(T_H - T), q_4 = p_8 + p_9 = \frac{F_H}{V_H}(T_{H_{\text{in}}} - T_H) + \frac{UA}{\rho_H C_{p_H} V_H}(T_H - T)$.

Therefore, stochastic differential equation of the endothermic CSTR formulated using transitions and probabilities is given below as:

$$\mathrm{d}\boldsymbol{X(t)} = F\left(\boldsymbol{X}(t), \theta\right) dt + Z^{\frac{1}{2}}\left(\boldsymbol{X}(t), \theta\right) \mathrm{d}\boldsymbol{B}(t), \tag{95}$$

where $\boldsymbol{X}(t) = [X_1, X_2, X_3, X_4]'$ and $\boldsymbol{B}(t) = [B_1(t), B_2(t), B_3(t), B_4(t)]'$.

From Table 5, it can be seen that C is also 4×9 matrix which is written as:

$$C = \begin{pmatrix} b_1 & b_2 & 0 & 0 & 0 & 0 & 0 & 0 & 0 \\ 0 & 0 & b_3 & b_4 & 0 & 0 & 0 & 0 & 0 \\ 0 & 0 & 0 & 0 & b_5 & b_6 & b_7 & 0 & 0 \\ 0 & 0 & 0 & 0 & 0 & 0 & 0 & b_8 & b_9 \end{pmatrix},$$

where

$$b_1 = \sqrt{F_{\text{in}}},\ b_2 = -\sqrt{F_{\text{out}}}\ , b_3 = \sqrt{\frac{F}{V}(C_{\text{in}} - C)},\ b_4 = -\sqrt{k_0 e^{-\frac{E}{R}(\frac{1}{T} - \frac{1}{T_{\text{mean}}})} C}$$

$$b_5 = \sqrt{\frac{F}{V}(T_{\text{in}} - T)},\ b_6 = \sqrt{\frac{H^* k_0 e^{-\frac{E}{R}(\frac{1}{T} - \frac{1}{T_{\text{mean}}})} C}{\rho C_p}},\ b_7 = \sqrt{\frac{UA(T_H - T)}{\rho C_p V}}$$

$$b_8 = \sqrt{\frac{F_H}{V_H}(T_{H_{\text{in}}} - T_H)},\ b_9 = -\sqrt{\frac{UA(T_H - T)}{\rho_H C_{p_H} V_H}}.$$

Therefore, the corresponding system of SDEs derived from model Equation (36) is given by the

system of stochastic differential equations (96).

$$\begin{cases} \mathrm{d}V(t) = (F_{\text{in}} - F_{\text{out}})\mathrm{d}t + b_1\mathrm{d}B_1(t) + b_2\mathrm{d}B_2(t), \\ \mathrm{d}C(t) = \left(\frac{F}{V}(C_{\text{in}} - C) - k_0 e^{-\frac{E}{R}\left(\frac{1}{T} - \frac{1}{T_{\text{mean}}}\right)}C\right)\mathrm{d}t + b_3\mathrm{d}B_3(t) + b_4\mathrm{d}B_4(t), \\ \mathrm{d}T(t) = \left(\frac{F}{V}(T_{\text{in}} - T) - \frac{H^* k_0 e^{-\frac{E}{R}\left(\frac{1}{T} - \frac{1}{T_{\text{mean}}}\right)}C}{\rho C_p} + \frac{UA(T_H - T)}{\rho C_p V}\right)\mathrm{d}t + b_5\mathrm{d}B_5(t) + b_6\mathrm{d}B_6(t) \\ +b_7\mathrm{d}B_7(t), \\ \mathrm{d}T_H(t) = \left(\frac{F_H}{V_H}(T_{H_{\text{in}}} - T_H) - \frac{UA(T_H - T)}{\rho_H C_{p_H} V_H}\right)\mathrm{d}t + b_8\mathrm{d}B_8(t) + b_9\mathrm{d}B_9(t), \end{cases} \tag{96}$$

where $B_i(t) \sim N(0, t)$ is also normally distributed random variable with mean zero and variance t or $\mathrm{d}B_i(t) \sim N(0, \mathrm{d}t)$ with $i = 1, 2, ..., 9$. The numerical simulations of the SDE (96) is again carried out by using Euler-Maruyama method.

3.3 Parameters Estimation, Sensitivity and Uncertainty Analysis Methods

This Section deals with the descriptions of the least squares and Markov chain Monte Carlo methods used for parameters estimation as well as the sensitivity and uncertainty analysis methods used for quantifying the effect of estimated model parameters' variation on models' response.

3.3.1 Least Squares Method

The models that are presented in Equations (35) and (36) are of the time dependent differential equations with the following form:

$$\frac{\mathrm{d}X_p}{\mathrm{d}t}(X_p, \theta, t_i) = 0,$$

where p is the number of state variables and X_p is the vector of state variables. For the model Equations (35) and (36), $p = 4$, t_i is the discrete time sampling, $X_p = [V, C, T, T_c]'$ and $X_p = [V, C, T, T_H]'$ are state variables of both models respectively, and θ is the set of parameters of the models to be identified. So, in this dissertation, fourteen unknown parameters to be identified for models (35) and (36) are $\theta = [F_{\text{out}}, F, k_0, E, T_{\text{mean}}, H^*, \rho, C_p, U, A, F_c, V_c, \rho_c, C_{p_c}]$ and $\theta = [F_{\text{out}}, F, k_0, E, T_{\text{mean}}, H^*, \rho, C_p, U, A, F_H, V_H, \rho_H, C_{p_H}]$, respectively. The least squares method is the classical optimization methods that minimizes the sum of squared residuals of the given models. Suppose $Y_{p,i}$ is a predictive model and $g(X_{p,i}, \theta, t_i)$ is the numerical solutions.

Then the residuals defined as $r_{p,i}$ can be computed as follows:

$$r_{p,i} = Y_{p,i} - g(X_{p,i}, \theta, t_i).$$

Thus, the sum of squared residuals function is obtained by taking the sum of squares of $r_{p,i}$. Mathematically it is written as:

$$S.S.R = \sum_{i=1}^{m} (r_{p,i})^2 = \sum_{i=1}^{m} (Y_{p,i} - g(X_{p,i}, \theta, t_i))^2. \tag{97}$$

The least squares method searches the best fitting parameters that minimise the $S.S.R$ function which is taken as the likelihood function. This implies that the fitting set of parameters $\hat{\theta}$ of the model Equations (35) and (36) can be obtained after solving Equation (98)

$$\frac{\partial(S.S.R)}{\partial\theta} = 0 \equiv \frac{\partial\left(\sum_{i=1}^{m}(Y_{p,i} - g(X_{p,i}, \theta, t_i))^2\right)}{\partial\theta} = 0, \tag{98}$$

simultaneously. Most of chemical processes are intractable and complex due to their non-linearity behaviours and the number of parameters involved. In such situation, it is difficult to find the exact solution for Equation (98). For model Equations (35) and (36), there are fourteen parameters. This implies that there should be fourteen equations. Solving those equations analytically, simultaneously, is a complicated task. As a simplification, the numerical simulations become a usual way of solving that problem.

3.3.2 Markov chain Monte Carlo Method

Markov chain Monte Carlo (MCMC) is one of the numerical methods that are presently used by most researchers as statistical and Bayesian techniques to identify the complex differential equations' parameters that fit the dynamics of chemical and biological models (Valderrama Bahamondez *et al.*, 2019; Niederberger, 2012; Masoumi *et al.*, 2013). The Bayesian inference has been qualified to be a very powerful statistical technique and has been widely used to identify the model's parameters θ which are obtained after evaluating the parameters' posterior density $p(\theta/X_{p_1}, X_{p_2}, ..., X_{p_N})$, where $X_{p_1}, X_{p_2}, ..., X_{p_N}$ are measurement points of the chemical process.

The overall implementation process, as stated in Remo *et al.* (2018), starts from proposing a

suitable distribution, called proposal distribution, and drawing samples from it. The proposal distribution sometimes depends on the present value to form the chain, which in turn is considered as a Markov chain. The acceptance or rejection mechanisms are employed in the simulation to rectify the trial proposal distribution which ends up with the target distribution. In the end, a simulated chain of parameters (drawn samples, $\theta_1, \theta_2, ..., \theta_N$) can be used to approximate the intractable integral (distribution), as

$$\mathbb{E}\left[f(\theta)/X_{p_1}, X_{p_2}, ..., X_{p_N}\right] \approx \frac{1}{N}\sum_{j=1}^{N} f(\theta_j), \tag{99}$$

where $\mathbb{E}\left[f(\theta)/X_{p_1}, X_{p_2}, ..., X_{p_N}\right]$ is the expectation, and $f(\theta_j)$ is the density function. According to Mbalawata *et al.* (2013) and Laine (2008), Metropolis algorithm, Metropolis Hastings, Hamiltonian Monte Carlo, Gibbs Sampler, Reversible Jump Monte Carlo, Metropolis Adjusted Langevin, Slice Sampling, Multiple Try Metropolis, and Delayed Rejection Metropolis are among the most used MCMC algorithms. But, in this dissertation, the adaptive version of Delayed Rejection Metropolis (DRAM) which is presented in Algorithm 3.1 will be used to estimate the unknown parameters of the model Equations (35) and (36). This method has nice features of tuning the reliable proposal distribution without defining it manually (Remo *et al.*, 2018; Ndanguza *et al.*, 2019). This method overcomes a tedious task of trial and error of tuning a suitable proposal distribution that may appear in the Metropolis-Hastings technique (Mbalawata *et al.*, 2015). The Gaussian distribution as a proposal distribution with initial mean 0 and covariance Σ_0 is used. For a start up, MCMC needs initial parameter values which are computed by using the classical least squares method.

Algorithm 3.1 (1) Draw the initial point θ_0 from initial distribution $p_0(\theta)$. Set an initial non-adaptive period N_0 and initial covariance matrix Σ_0.

(2) For $j = 1, 2, ...$ perform the following:

(i) Sample a current point $\hat{\theta}$ from the proposal distribution $q(\hat{\theta}/\theta_{j-1})$

(ii) Compute the acceptance probability using

$$\alpha(\theta_{j-1}, \hat{\theta}) = \min\{1, \frac{p(\hat{\theta}/X_{p_1}, X_{p_2}, ..., X_{p_N})q(\theta_{j-1}/\hat{\theta})}{p(\theta_{j-1}/X_{p_1}, X_{p_2}, ..., X_{p_N})q(\hat{\theta}/\theta_{j-1})}\}$$

(iii) Acceptance/rejection rule by setting

$$\theta_j = \begin{cases} \hat{\theta}, \text{ if } u < \alpha(\theta_{j-1}, \hat{\theta}), \text{ where } u \sim \mathbb{U}(0,1) \\ \theta_{j-1}, \text{ otherwise.} \end{cases}$$

(iv) If $n_0 \leqslant j$ (or after every n_0^{th} iterations), then update the covariance matrix by using the formula

$$\Sigma_j = \text{Cov}(\theta_0, \theta_1, ..., \theta_j) + \epsilon I_d,$$

where I_d is an $d \times d$ identity matrix and ϵ is a small positive number that makes the matrix Σ_j to be non-singular matrix (Haario *et al.*, 1999, 2001; Remo *et al.*, 2018).

(v) $j \leftarrow j + 1$.

3.3.3 Sensitivity and Uncertainty Analysis Method

Sensitivity analysis is a technique that quantifies the uncertainty in the responsive model from the uncertainties of input initial conditions and parameters. Thus, to validate the proposed deterministic model Equations (35) and (36), the global sensitivity analysis of the models which is necessary and important tool to quantify the effects of uncertainties of the parameters' variations on the responsive variables of the model is performed. Based on the nature of a formulated mathematical model, various methods for the sensitivity analysis have been proposed. For linear mathematical models, the standardized linear regression correlation coefficients, the partial correlation coefficients and Pearson correlation coefficients are sufficient to draw a conclusion about the model uncertainties. For non-linear models, methods that are based on decomposition of the output variance of the model like sobol method are used to quantify the model uncertainty but this is applicable for non-monotonic models. For the case of nonlinear and monotonic models, spearman rank correlation coefficients, standardized rank regression coefficients and the partial rank correlation coefficients (PRCCs) are preferably to be used but PRCCs are the most accurate and adequate to measure and quantify the uncertainty in the outputs of the model (Marino *et al.*, 2008). PRCCs vary in the range of ± 1 with significant correlation for the values approaching -1 or +1 (values ≥ 0.5 or ≤ -0.5) and low correlation for the values that are far from -1 or +1 (values < 0.5 or > -0.5). The model systems that are shown in Equations (35) and (36) are nonlinear and monotonic, so the Latin Hypercube Sampling ((LHS) method with

the PRCCs are to be implemented to qualitatively and quantitatively performing the sensitivity analysis to examine the effects of estimated parameters on model responsive variables.

(i) Latin Hypercube Sampling and Partial rank correlation coefficients

The following are three steps for implementing both LHS and PRCCs.

Step 1: Sampling model parameters from a specified distributions.

Consider a mathematical model given by

$$\frac{\mathrm{d}X}{\mathrm{d}t} = h(X, \theta), \tag{100}$$

where $X \in \mathbb{R}^m$ is an m^{th}-dimensional state space and $\theta \in \mathbb{R}^n$ is an n^{th}-dimensional parameter space, then the expected outputs of the model is given by

$$y = f(X, \theta). \tag{101}$$

For example, let the parameter space be $\mathbb{R}^2$ means $\theta = (a, b)$ and then let the sample size be $N = 4$. So, four samples of each parameter is to be sampled from a certain distribution. Consider two cases of distributions where uniform distribution and normal distribution are chosen to be used as proposal distributions. Minimum and maximum values of the parameter are needed for the case of uniform distribution and mean and standard deviation of the parameter are also needed for the case of normal distribution.

Let a be sampled from a uniform distribution that is to say $a \sim \mathbb{U}(a_{\text{min}}, a_{\text{max}})$, so the picture of its samples can be as follow:

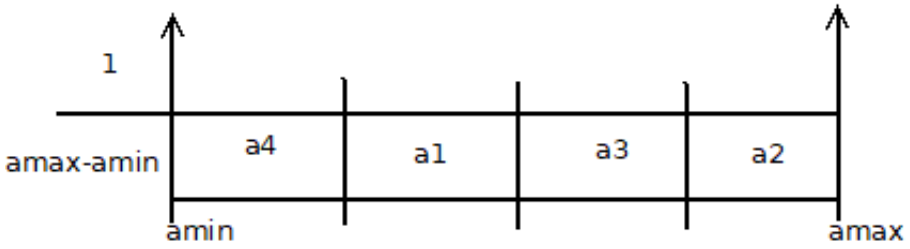

Let the parameter b be sampled from the normal distribution, that is to say $b \sim \mathbb{N}(\mu_b, \sigma_b)$, then the picture of its samples will be looking like

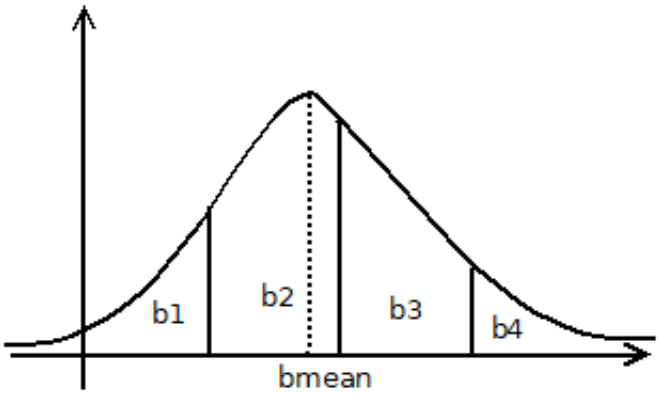

Step 2: Obtaining LHS Matrix

The LHS matrix of the sampled parameters is a matrix that contains all samples of parameters and is for example given by X, where

$$X = \begin{pmatrix} a_1 & b_1 \\ a_2 & b_2 \\ a_3 & b_3 \\ a_4 & b_4 \end{pmatrix} \tag{102}$$

and the output matrix Y is given by row matrix that contains model responses from sampled parameters obtained in matrix X. So,

$$Y = \begin{bmatrix} y_1 = f(a_1, b_1) = \text{value}_1 \\ y_2 = f(a_2, b_2) = \text{value}_2 \\ y_3 = f(a_3, b_3) = \text{value}_3 \\ y_4 = f(a_4, b_4) = \text{value}_4 \end{bmatrix} \tag{103}$$

The ranking for X and Y matrices is based on low values obtained for samples. For example, the ranking matrix X_R can be as:

$$X_R = \begin{bmatrix} 2 & 3 \\ 4 & 1 \\ 1 & 2 \\ 3 & 4 \end{bmatrix} \tag{104}$$

and the ranking matrix Y_R as:

$$Y_R = \begin{bmatrix} 3 \\ 4 \\ 1 \\ 2 \end{bmatrix} \tag{105}$$

Step 3: Computing the correlation coefficients

The possibility of computing the Pearson, Spearman and the partial rank correlation coefficients are in the following way: Pearson ((X, Y)), Spearman ((X_R, Y_R)) and PRCC ((X_R, Y_R)).

The correlation measures the magnitude of the linear association between model outputs and model inputs. Let x_i represents inputs for $i = 1, 2, ..., k$ and y be the outputs. Then the measure of the linear association between x_i and y is given by:

$$R_{x_i,y} = \frac{\text{Cov}(y, x_i)}{\sqrt{\text{Var}(y)\text{Var}(x_i)}}, \tag{106}$$

with $\text{Cov}(y, x_i) = \sum_{j=1}^{N}(x_{ij} - \bar{x})(y_j - \bar{y})$ being the covariance and $\text{Var}(y) = \sum_{j=1}^{N}(y_j - \bar{y})^2$ and $\text{Var}(x_i) = \sum_{j=1}^{N}(x_{ij} - \bar{x})^2$ being variances of outputs and inputs respectively. Partial correlation coefficient (PCC) determines the linear relationship between the input x_i and the output y after excluding other linear effects of the remaining inputs. So, the PCC is obtained by computing the correlation coefficient between two residuals $x_i - \bar{x_i}$ and $y - \bar{y}$, where

$$\bar{x_i} = a_0 + \sum_{p=1\neq i}^{k} a_p x_p \tag{107}$$

and

$$\bar{y} = b_0 + \sum_{p=1\neq i}^{k} b_p x_p \tag{108}$$

are the linear regression models. Like PCC, PRCC performs a PCC on a rank-transformed data x_i and y with the same procedure of computing the correlation between residuals using built regression models as presented in Equations (107) and (108). Thus, these techniques are used to perform the sensitivity and uncertainty analysis of parameters estimates of model Equations (35) and (36) on models' response.

3.3.4 Euler-Maruyama Method

The general Euler-Maruyama numerical scheme for a single SDE

$$\mathrm{d}X(t) = f(X(t))\mathrm{d}t + g(X(t))\mathrm{d}B(t) \tag{109}$$

is given by the iterative formula in Equation (110),

$$X_{n+1} = X_n + \Delta_t f(X_n) + g(X_n)(B(\tau_{n+1}) - B(\tau_n)). \tag{110}$$

The Euler-Maruyama scheme for the system of SDEs which are in Equation (83), and can be adopted for any of the rest of SDEs appearing in this dissertation is described in Equation (111) as:

$$\begin{cases} V_{n+1} = V_n + \big(F_{\text{in}} - F_{\text{out}}\big)\Delta_t + \delta_V V_n\big(B_V(\tau_{n+1}) - B_V(\tau_n)\big) \\ C_{n+1} = C_n + \left(\dfrac{F}{V_n}(C_{\text{in}} - C_n) - k_0 e^{-\frac{E}{R}(\frac{1}{T_n} - \frac{1}{T_{\text{mean}}}}C_n\right)\Delta_t \\ \qquad\qquad +\delta_C C_n\big(B_C(\tau_{n+1}) - B_C(\tau_n)\big) \\ T_{n+1} = T_n + \left(\dfrac{F}{V_n}(T_{\text{in}} - T_n) - \dfrac{k_0 e^{-\frac{E}{R}(\frac{1}{T_n} - \frac{1}{T_{\text{mean}}}}C_n}{\rho C_p}\right. \\ \left. -\dfrac{UA(T_n - T_{c_n})}{\rho C_p V_n}\right)\Delta_t + \delta_T T_n\big(B_T(\tau_{n+1}) - B_T(\tau_n)\big) \\ T_{c_{n+1}} = T_{c_n} + \left(\dfrac{F_c}{V_c}(T_{c_{\text{in}}} - T_{c_n}) + \dfrac{UA(T_n - T_{c_n})}{\rho_c C_{p_c} V_c}\right)\Delta_t \\ \qquad\qquad +\delta_{T_c} T_{c_n}\big(B_{T_c}(\tau_{n+1}) - B_{T_c}(\tau_n)\big) \end{cases} \tag{111}$$

CHAPTER FOUR

RESULTS AND DISCUSSIONS

The numerical analysis of all models obtained in Chapter 3 of this dissertation are well analysed, explained and discussed in this chapter. Results obtained and its discussions are split into five main parts, where the first part is found in Section 4.1 and deals with results and discussions of model Equation (35) and the second part contains results and discussions of model Equation (36) which are in Section 4.2. The third and the fourth part of this chapter that are in Section 4.3 and Section 4.4 discuss results of stochastic models that describe the dynamics of CSTR with exothermic reactions (model Equations (83), (84), (85) and (89)) and the dynamics of CSTR with endothermic reactions (Equations (90), (91), (92) and (96)) respectively while Section 4.5 which is the last part shows the real life application of CSTRs.

For testing the formulated models, synthetic data are used. The idea here was to see if the model, together with the numerical methods for parameters estimation can lead to parameters identifiability.

4.1 Numerical Analysis and Parameters Estimation of Deterministic Model for Exothermic CSTR

To obtain the numerical solutions of the model Equation (35) while performing numerical analysis, Runge-Kutta method of fourth order has been used. The least squares and Markov chain Monte Carlo methods have been also used to estimate unknown parameters of CSTR model. Furthermore, sensitivity and uncertainty analysis was carried out to validate the formulated deterministic model by identifying parameters which are very sensitive to the model output. The software employed during numerical analysis is MATLAB of version R2016b.

4.1.1 Numerical Solutions

Due to lack of actual information (real data) about the functionality of CSTR, the model Equation (35) was simulated by using values that are found in Table 6 and Table 7, where nineteen out of twenty six parameters equivalent to 73% were obtained from literature, 12% of them equivalent to three parameters out of twenty six have been estimated and four of them equals

15% were state variables and their values have been simulated. The discrete sampling time points used were 100 and 100×4 numerical solutions of the model have been obtained. The numerical results from subplot 1 of Fig. 6 have revealed that the volume of tank reactor increases from 100 m^3 to approximately 126 m^3 and this is an indication of having non-constant flow rates of reactants due to change of both inlets and outlets. Figure 6 have shown that the reactants were consumed inside the reacting tank as its concentration approached zero. This has shown a complete mixing and at the same time symbolised a non-partial conversion of reactants into products that may lead to time residence distribution analysis as one of the inconveniences of CSTRs. Along this process, there was a covering cooling jacket that communicated with the reacting tank through a designed cross-sectional area (A) of $0.015m^2$, to cool down the rising temperature inside the reacting tank. The covering cooling jacket contained the substance whose temperature was initially lower than the starting temperature of the reacting tank to disable the explosion of the reaction. During this process, the temperature of the reacting tank rose from 298.35^oK to its operating working temperature that was 373.48^oK. Meanwhile, the cooling temperature of the covering cooling jacket also rose from its initial temperature (288.15^oK) until it reached 363.14^oK. As a result, if this scenario is selected to be a piloting tank, then all the simulated information and the working conditions that are described above have to be taken into consideration quantitatively. The numerical solutions of the model Equation (35) and are obtained in Fig. 6 below,

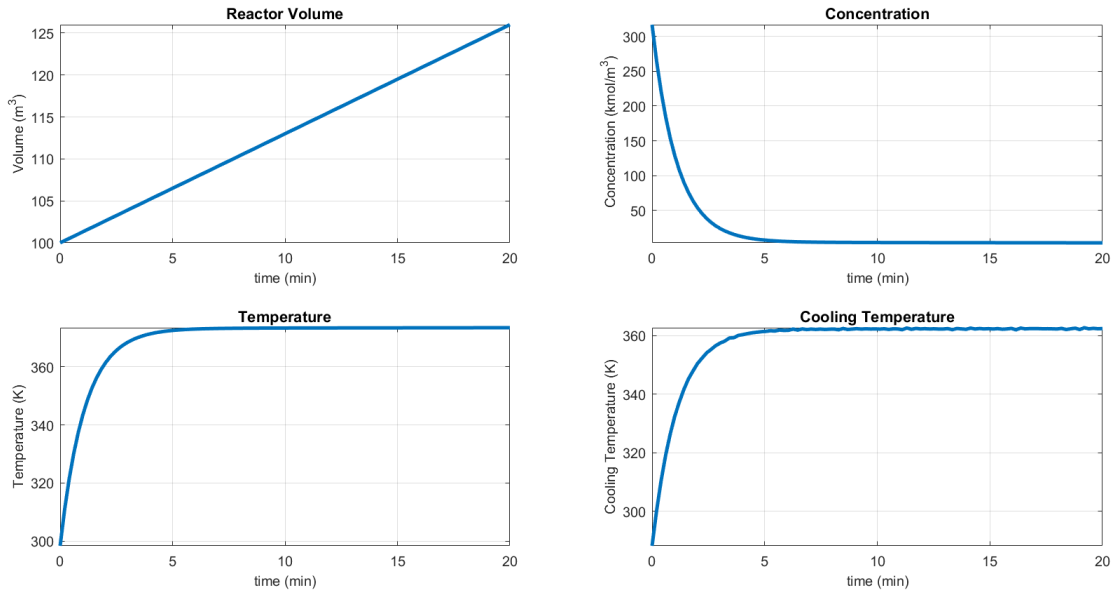

Figure 6: Numerical solutions of model Equation (35)

Table 6: Table of variables, parameters and constants

Param symbol (unit)	Param name	Value	Reference
$C_{in}(kmol\ min^{-1}m^{-3})$	Feeding concentration	316.8	Muhirwa *et al.* (2017)
$C_0(kmol\ min^{-1}m^{-3})$	Initial concentration	316.8	Muhirwa *et al.* (2017)
$C(kmol\ min^{-1}m^{-3})$	Mixture concentration	State variable	to be simulated
$T_{in}(^oK)$	Feeding temperature	341.37	Karimi *et al.* (2015)
$T_0(^oK)$	Initial temperature	298.35	Muhirwa *et al.* (2017)
$T(^oK)$	Mixture temperature	State variable	to be simulated
$H^*(kcal\ kmol^{-1})$	Enthalpy	-1004.3×10^3	Muhirwa *et al.* (2017)
$T_{c_0}(^oK)$	Initial cool temperature	299.97	Lu *et al.* (2017)
$T_{c_{in}}(^oK)$	Feed cool temperature	293	Vojtesek *et al.* (2008)
$T_c(^oK)$	Jacket temperature	State variable	to be simulated
$R(kJ\ kmol^{-1}\ ^oK^{-1})$	Gas constant	8.314	Muhirwa *et al.* (2017)
$V_0(m^3)$	Initial tank volume	100	Aboelela *et al.* (2018)
$V(m^3)$	Volume of the tank	State variable	to be simulated
$k_0(min^{-1})$	Pre-Arrhenius frequency	0.9	Muhirwa *et al.* (2017)
$E(kJ\ kmol^{-1})$	Activation energy	0.5	Muhirwa *et al.* (2017)
$T_{\text{mean}}(^oK)$	Reference temperature	298.15	Muhirwa *et al.* (2017)

Table 7: Continuation of table of variables, parameters and constants

Param symbol (unit)	Param name	Value	Reference
$F = F_{in}(m^3\ min^{-1})$	Feeding velocity	130×10^{-2}	Muhirwa *et al.* (2017)
$\rho(kg\ m^{-3})$	Density	1000	Muhirwa *et al.* (2017)
$C_p(kcal\ kg^{-1}\ {}^oK^{-1})$	Heat capacity	4186	Muhirwa *et al.* (2017)
$U(kJ\ min^{-1}\ {}^oK^{-1}\ m^{-2})$	Heat transfer coefficient	100 000	Muhirwa *et al.* (2017)
$A(m^2)$	Cross-sectional area	0.015	Muhirwa *et al.* (2017)
$F_c(m^3\ min^{-1})$	Cooling velocity	46.5×10^{-6}	to be estimated
$V_c(m^3)$	Cooling reactor volume	50×10^{-6}	to be estimated
$\rho_c(kg\ m^{-3})$	Density of the coolant	1000	Aboelela *et al.* (2018)
$C_{p_c}(kcal\ kg^{-1o}K^{-1})$	Cooling heat capacity	4.168×10^3	Muhirwa *et al.* (2017)
$F_{\text{out}}(m^3 min^{-1})$	Outlet velocity	130×10^{-6}	to be estimated

Note: Param means parameter

4.1.2 Least Squares Results

For estimating the model parameters by using Least Squares, the numerical solutions obtained in Section 4.1.1 are corrupted by using five different noise intensities which are $[0.01, 0.05, 0.1, 0.5, 1]$ to obtain the experimental datasets taken as the real measurements of CSTR system. This technique is used for identifying the unknown physical system as an inverse problem. As results, the Least Squares estimates of parameters were computed five times by varying the intensity of noise σ. It means the parameters of model Equation (35) were estimated five times; when $\sigma = [0.01, 0.05, 0.1, 0.5, 1]$. After estimation of parameters, the model was fitted with various values of estimates. Figures 7, 8, 9, 10, 11 show the experimental data with five fitted graphs while Tables 8, 9, 10, 11, 12 show parameters estimates for five different values of σ.

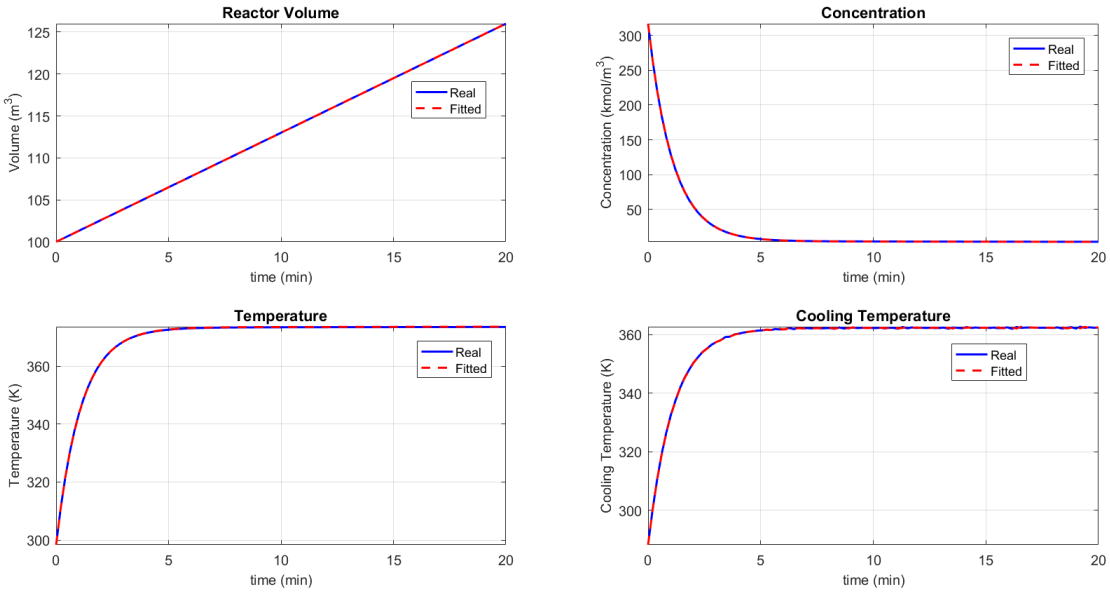

Figure 7: Fitted model when $\sigma = 0.01$

Based on the results in Table 8, all estimated parameter values are in good agreement with their initial values. But also it is observed from Fig. 7 that the distance between the predictive solutions (in red color) and the exact model solutions (blue color) seems to be minimised, and hence the system model is fitting the measurements very well, simply because both colors are in coincidence. One may point out that if the model is influenced by the noise of magnitude $\sigma = 0.01$, the exothermic reacting tank's model still performs very well and provide the optimal converging solutions. It can be seen that the volume of the reactor is linearly increasing from 100 m^3 to almost 126 m^3. The concentration of the reactant is exhausted towards zero which describes the total conversion of reactant into product. As the reaction goes on, the temperature inside the reacting tank increases from 298.35 K to 373.48 K and be cooled by the cooling system to avoid the reaction explosion. During the cooling process the temperature in the cooling jacket increases from 288.15 K to 363.14 K and both CSTR and jacket's temperatures stabilise after 5 minutes of the reaction. The least squares results reveal that the estimated values of the volume, concentration, temperature and cooling temperature of the CSTR system are the same as numerical results of the model.

Table 8: Table of estimated model parameters when $\sigma = 0.01$

Parameter symbol	Parameter Physical Meaning	Initial value	Estimated
F_{out}	Outlet Velocity	130×10^{-6}	120.271×10^{-6}
F	Feeding Velocity	130×10^{-2}	126.799×10^{-2}
k_0	Pre-Arrhenius Frequency	0.9	0.896129106
E	Activation Energy	0.5	0.555990875
T_{mean}	Reference Temperature	298.15	280.5678233
H^*	Enthalpy	-1004.3×10^3	-1 004 013.891
ρ	Density	1000	1009.793374
C_p	Heat Capacity	4186	4140.326
U	Heat Transfer Coefficient	100 000	100 948.8166
A	Cross-sectional Area	0.015	0.014337536
F_c	Cooling Velocity	46.5×10^{-6}	48.0×10^{-6}
V_c	Cooling Reactor Volume	50×10^{-6}	51.9×10^{-6}
ρ_c	Density of the Coolant	1000	973.7494767
C_{p_c}	Cooling Heat Capacity	4168	4044.644492

The experimental data obtained by using $\sigma = 0.05$ give the results that is shown in Fig. 8 and Table 9.

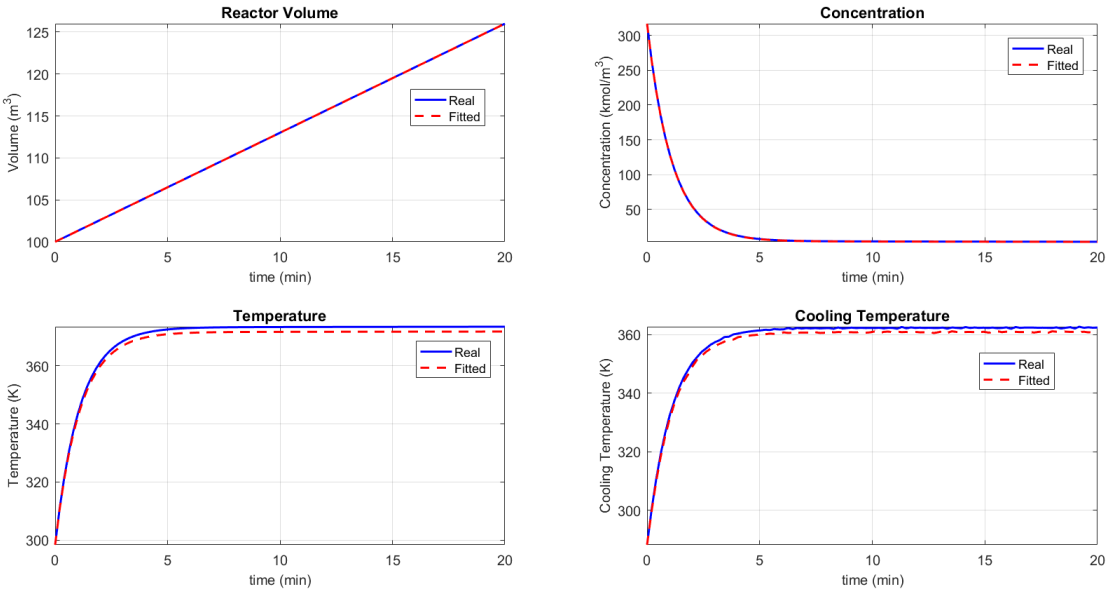

Figure 8: Fitted model when $\sigma = 0.05$

According to the results in Table 9, all parameters are also converging to its initial values and the measurements are highly fitting the exothermic CSTR model as can be viewed from Fig.

8. Thus the noise of intensity $\sigma = 0.05$ still does affect the optimality working conditions of the proposed exothermic CSTR deterministic model as all four state variables of the system are well fitted by the experimental data. The volume and the concentration of the CSTR are well fitted and vary from 100 m^3 to 126m^3 and 316 towards zero respectively. The Least Squares results show that the temperature and the cooling temperature of reacting and cooling tanks are very close to their numerical solutions which vary from 298.35 K to 373.48 K and from 288.15 K to 363.14 K, respectively.

Table 9: Table of estimated model parameters when $\sigma = 0.05$

Parameter symbol	**Parameter Physical Meaning**	**Initial value**	**Estimated**
F_{out}	Outlet Velocity	130×10^{-6}	130.016×10^{-6}
F	Feeding Velocity	130×10^{-2}	130.09×10^{-2}
k_0	Pre-Arrhenius Frequency	0.9	0.900553
E	Activation Energy	0.5	0.493183
T_{mean}	Reference Temperature	298.15	298.147
H^*	Enthalpy	-1004.3×10^3	-1026.03×10^3
ρ	Density	1000	1017.16
C_p	Heat Capacity	4186	4231.14
U	Heat Transfer Coefficient	100 000	100 681
A	Cross-sectional Area	0.015	0.0151979
F_c	Cooling Velocity	46.5×10^{-6}	46.7705×10^{-6}
V_c	Cooling Reactor Volume	50×10^{-6}	49.6872×10^{-6}
ρ_c	Density of the Coolant	1000	987.751
C_{p_c}	Cooling Heat Capacity	4168	4134.6

Figure 9 and Table 10 show the least square results of model Equation (35) after using experimental data obtained via $\sigma = 0.1$.

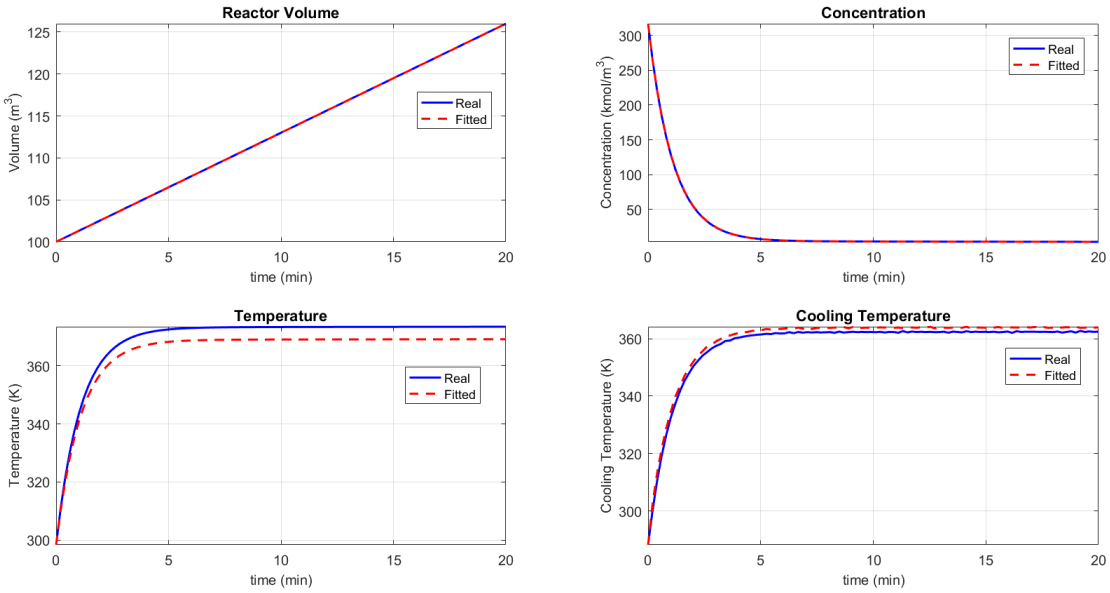

Figure 9: Fitted model when $\sigma = 0.1$

Similarly, the results in the Table 10 show that all model parameters are fairly converging to their initial values and the measurements are somehow close to the so-called real exothermic CSTR deterministic model. This is a sign of a fair fitting as can be viewed from Fig. 9. Thus the noise of intensity $\sigma = 0.1$ also does not highly affect the optimality working conditions of the formulated exothermic CSTR deterministic model. The numerical results for the volume and the concentration and their corresponding Least Squares results are the same. However, the Least Squares results for the temperature become slightly lower and start from 298.35 K to approximately 370 K and the Least Squares results for cooling temperature become greater than the corresponding numerical results and range from 288.15 K to approximately 364 K.

Table 10: Table of estimated model parameters when $\sigma = 0.1$

Parameter symbol	Parameter Physical Meaning	Initial value	Estimated
F_{out}	Outlet Velocity	130×10^{-6}	153.489×10^{-6}
F	Feeding Velocity	130×10^{-2}	128.400×10^{-2}
k_0	Pre-Arrhenius Frequency	0.9	0.896055403
E	Activation Energy	0.5	0.441415996
T_{mean}	Reference Temperature	298.15	304.7208549
H^*	Enthalpy	-1004.3×10^3	-907 216.0504
ρ	Density	1000	1045.936659
C_p	Heat Capacity	4186	3835.799667
U	Heat Transfer Coefficient	100 000	111 325.8035
A	Cross-sectional Area	0.015	0.016932493
F_c	Cooling Velocity	46.5×10^{-6}	32.9×10^{-6}
V_c	Cooling Reactor Volume	50×10^{-6}	52.1×10^{-6}
ρ_c	Density of the Coolant	1000	833.0925744
C_{p_c}	Cooling Heat Capacity	4168	4442.755181

The investigation of how the experimental data obtained by using perturbation constant $\sigma = 0.5$ fits the formulated model in Equation (35) is shown in Fig. 10 and their corresponding estimated parameters are found in Table 11.

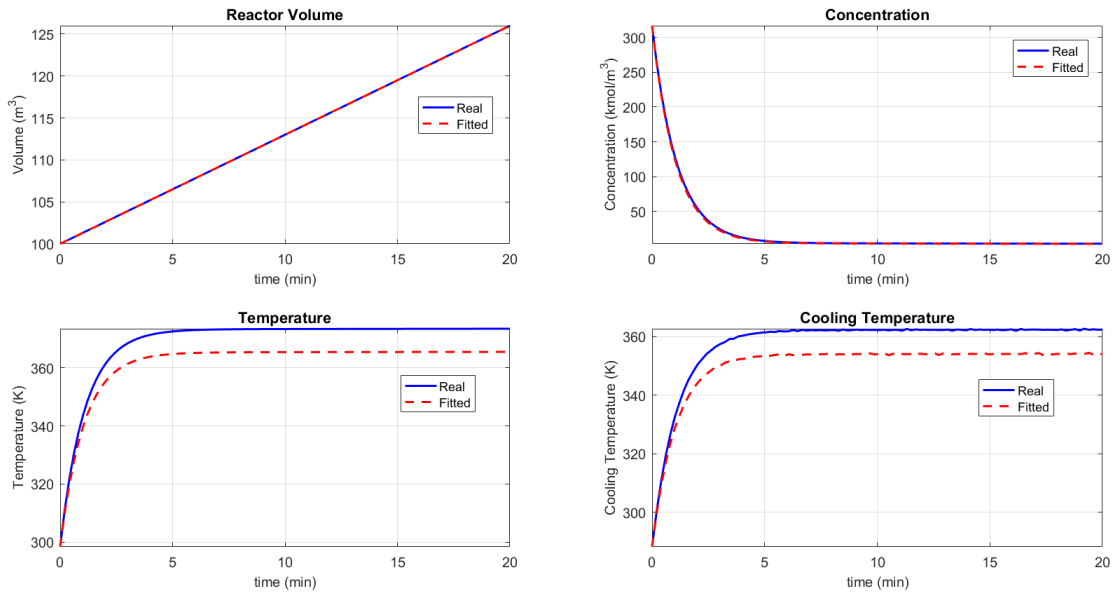

Figure 10: Fitted model when $\sigma = 0.5$

From the results presented in Table 11 and from Fig. 10, it is seen that the parameters are fairly

converging and only two state variables (reactor volume and concentration) are well fitted by the experimental data while the other two state variables namely, the temperature and the cooling temperature are not well fitted. Therefore, on one hand the noise of intensity $\sigma = 0.5$ greatly affects the temperature of the reacting tank and the cooling temperature of the cooling jacket as compared with the volume and the concentration on the other hand. Physically, the Least Squares results for the temperature and the cooling temperature becomes very lower than their corresponding numerical results and range from 298.35 k to approximately 362 K and 288.15 K to approximately 350 K, respectively.

Table 11: Table of estimated model parameters when $\sigma = 0.5$

Parameter symbol	**Parameter Physical Meaning**	**Initial value**	**Estimated**
F_{out}	Outlet Velocity	130×10^{-6}	128.726×10^{-6}
F	Feeding Velocity	130×10^{-2}	126.662×10^{-2}
k_0	Pre-Arrhenius Frequency	0.9	0.930134156
E	Activation Energy	0.5	0.492520992
T_{mean}	Reference Temperature	298.15	287.5494455
H^*	Enthalpy	-1004.3×10^3	-987 991.6235
ρ	Density	1000	1096.742511
C_p	Heat Capacity	4186	4203.713355
U	Heat Transfer Coefficient	100 000	96 750.38837
A	Cross-sectional Area	0.015	0.014126652
F_c	Cooling Velocity	46.5×10^{-6}	49.3×10^{-6}
V_c	Cooling Reactor Volume	50×10^{-6}	46.4×10^{-6}
ρ_c	Density of the Coolant	1000	1031.560661
C_{p_c}	Cooling Heat Capacity	4168	3950.953476

Finally, the noise of intensity $\sigma = 1$ is used to produce experimental data for which the obtained fitted model and the estimated model parameter values are pointed out in Fig. 11 and Table 12 accordingly.

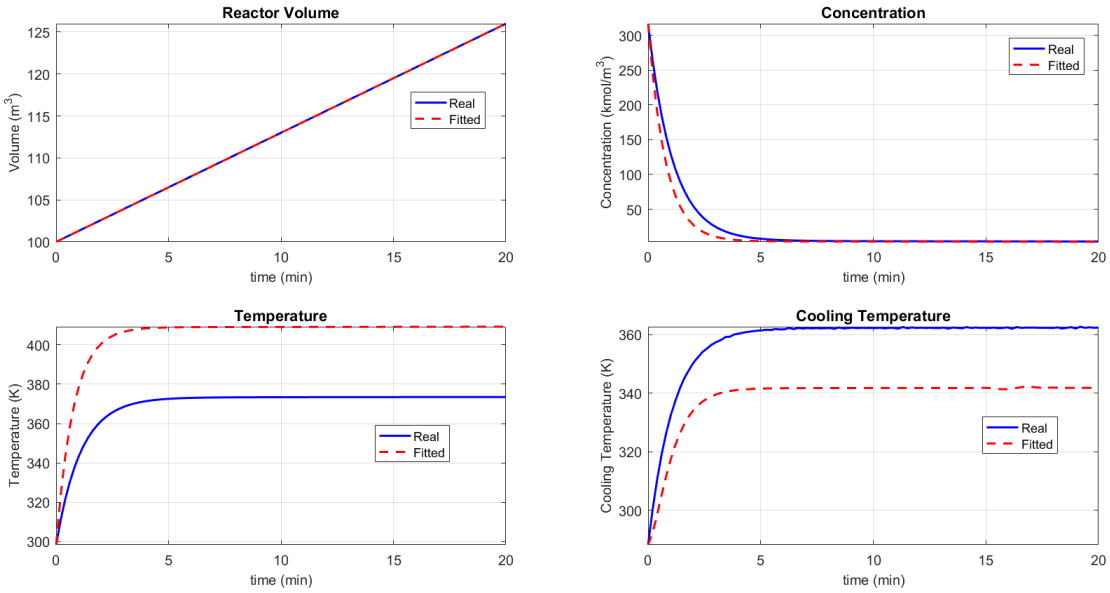

Figure 11: Fitted model when $\sigma = 1$

From Fig. 11, it is seen that the noise intensity, $\sigma = 1$ highly affects the system temperature and the cooling temperature. However, the reason behind it cannot be explained to the best of knowledge of researchers. So, the only explanation is that if a random noise of intensity $\sigma = 1$ is presented in the formulated exothermic CSTR model, this will highly affect the optimality working conditions of the reacting tank and we can expect defective products from the tank as a consequence. Therefore, if one chooses to design a reacting tank that implements the proposed exothermic CSTR model, there must an additional design in such a way that the noise of intensity which is closer or greater than unity is sensed and has to be directly filtered from the working process. Most of all optimal parameter values somewhat deviate from its initial parameter values which resulted in poor model fitting as can be explored from the results in Table 12 and from Fig. 11. The poor fitting results are due to introducing high value of uncertainty in the numerical solutions of the CSTR model Equation (35).

Table 12: Table of estimated model parameters when $\sigma = 1$

Parameter symbol	Parameter Physical Meaning	Initial value	Estimated
F_{out}	Outlet Velocity	130×10^{-6}	123.66×10^{-6}
F	Feeding Velocity	130×10^{-2}	158.502×10^{-2}
k_0	Pre-Arrhenius Frequency	0.9	1.2701104
E	Activation Energy	0.5	0.446481364
T_{mean}	Reference Temperature	298.15	178.5052479
H^*	Enthalpy	-1004.3×10^3	-999 186.9285
ρ	Density	1000	899.102053
C_p	Heat Capacity	4186	3144.842237
U	Heat Transfer Coefficient	100 000	77 062.50444
A	Cross-sectional Area	0.015	0.008857562
F_c	Cooling Velocity	46.5×10^{-6}	67.0×10^{-6}
V_c	Cooling Reactor Volume	50×10^{-6}	50.3×10^{-6}
ρ_c	Density of the Coolant	1000	1267.008926
C_{p_c}	Cooling Heat Capacity	4168	4473.862286

4.1.3 Markov Chain Monte Carlo Results

The very important and necessary question that one keeps in mind while using MCMC method is to know whether or not the method provides convergent and accurate posterior samples of parameters. Therefore, a varied number of MCMC diagnostic tests has been used.

4.1.4 MCMC diagnostic tests

There are several common statistical and graphical convergence tests for the MCMC method that are found in Brooks (1998); Sinharay (2003); Roy (2020); Sharma (2017). In this dissertation, the trace (time series plots), scatter plots, autocorrelation plots, probability plots (quantile-quantile plots) and the marginal density distributions for each drawn sample of the parameters were used to identify the accuracy of the formulated model parameters and diagnose whether or not the convergence of the generated MCMC samples is reached. The identifiability of

the model parameters is mainly based on the convergence of the MCMC method. For model Equation (35), the initial number of samples generated was 100 000, Gaussian distribution was considered to have mean 0 and covariance matrix $\Sigma_0 = \frac{0.00001 \times I_{p\times p}}{\sqrt{p}}$, where p represents the number of parameters to be identified, and $I_{p\times p}$ is the $p \times p$ identity square matrix. The least squares results obtained when $\sigma = 0.05$ have been used as prior values for the MCMC method.

(i) Trace plots

One way of analysing the convergence of the MCMC method is to check the mixing of the generated sample of posteriors through trace plots. If the generated chain of posteriors becomes stationary for several initial values, and there are no obvious spikes, then this is an indication of having a good mixing which is a good sign of convergence. From Fig. 12, it can be observed that the mixing of samples with the exception of F_c and V_c is very good so the chain converges, and the sampling parameter values of posteriors are means (centres) of the generated chain of samples.

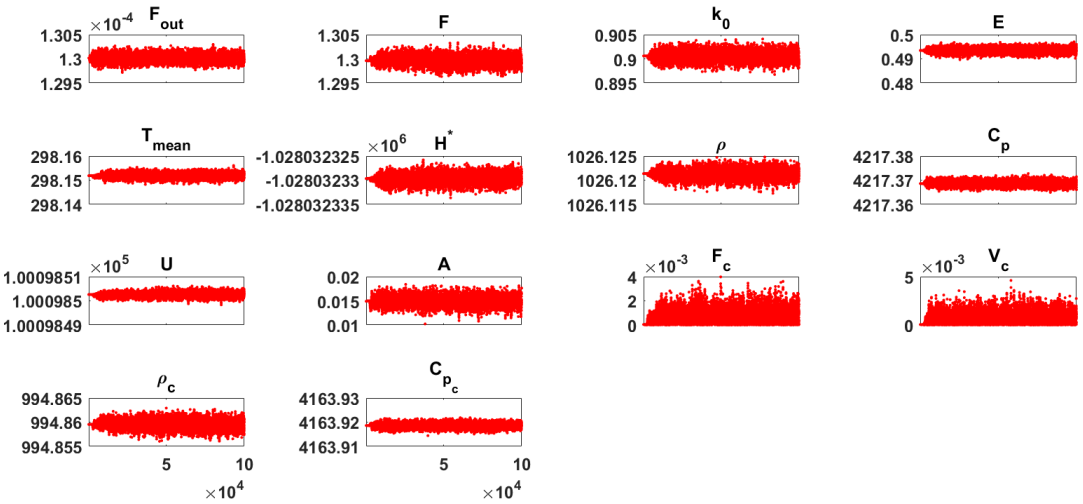

Figure 12: MCMC samples of posteriors

(ii) Scatter plots (pairs)

A poor convergence of MCMC method inventively leads to high correlation between estimated parameters. Since there are fourteen parameters to be identified, then there are 91 scatter plots for which we need to investigate if there are strong correlations between them. Due to the big number of parameters, it has been able to explore the scatter plots for the first ten parameters and

Fig. 13 shows how couples of posterior samples of the selected parameters correlate each other. According to Fig. 13, it is observed that there is no high correlation between pairs of estimated parameters and so the parameters of the model Equation (35) are adequately identified.

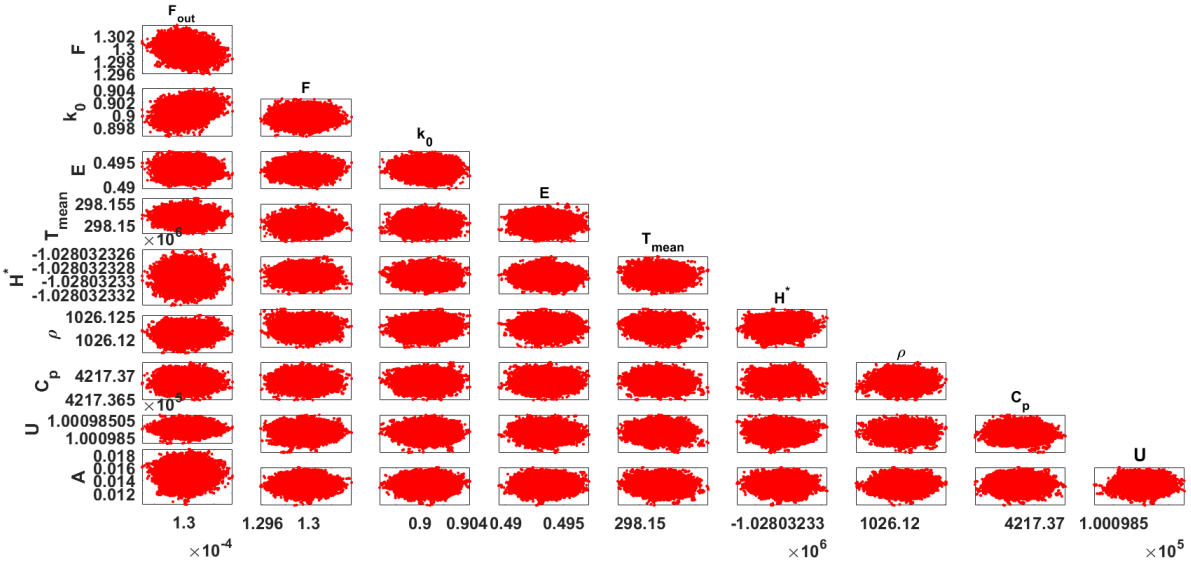

Figure 13: MCMC pairs plot of samples

(iii) Autocorrelation plots

Figure 14 determines and examines the correlation between consecutive samples during posteriors chain sampling. From Fig. 14, it is explored that the coefficients of autocorrelation functions of all generated samples tend to zero as the number of lags increases and get stationary around zero after 100 lags. That is an indication of having a good mixing. Bad mixing will conventionally lead to non-decaying coefficients of autocorrelation functions.

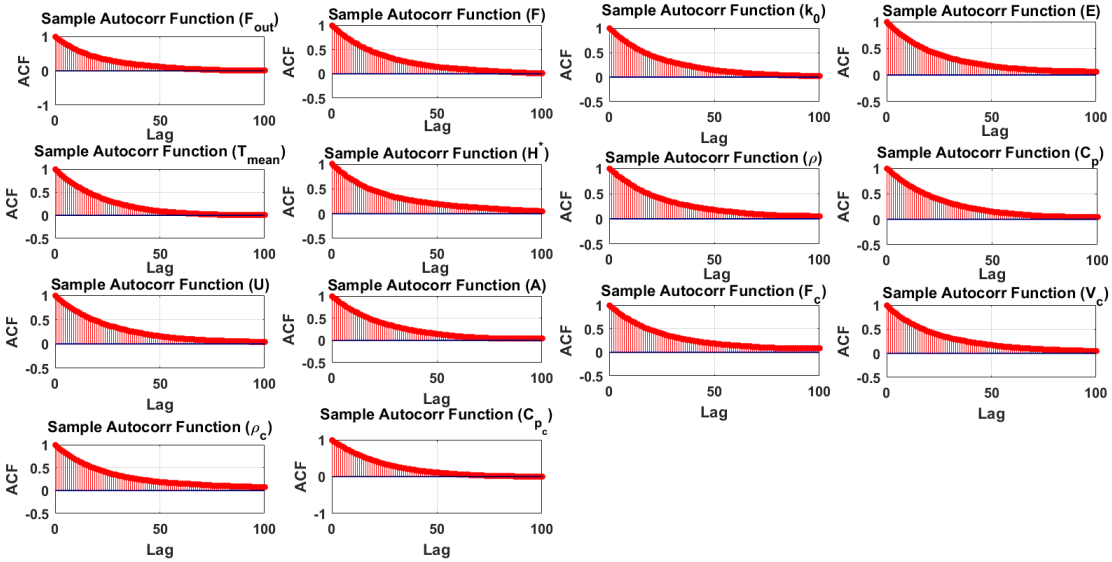

Figure 14: MCMC autocorrelation plots of sampled posteriors

(iv) Histograms for posterior distributions

To be sure that posterior distributions of parameters are well sampled from a suitable proposal distributions, one has to plot distributions of all generated chains of posterior parameters and observe if those chains are fairly following normal distributions. It can be seen from Fig. 15 that all of them do follow the mentioned distribution except for the chains of parameter F_c and V_c which are somehow right-skewed.

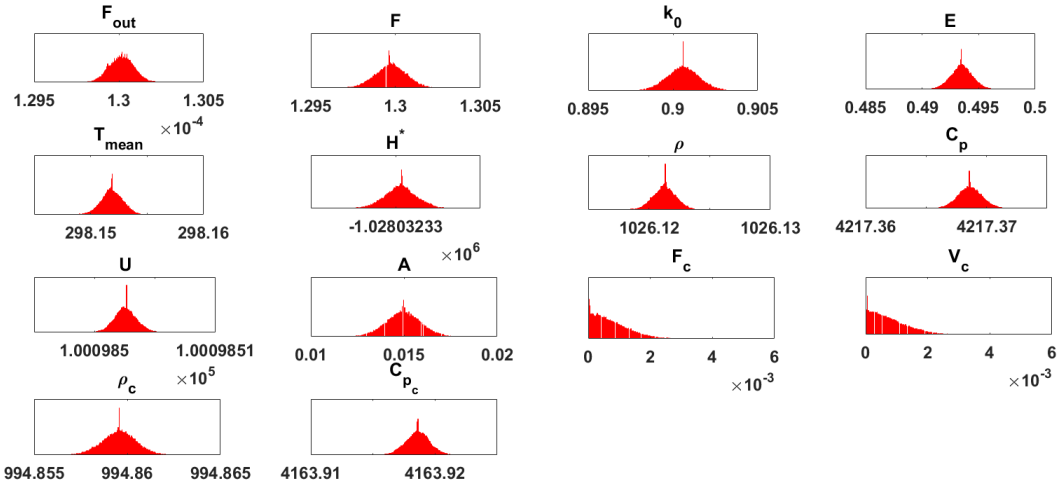

Figure 15: MCMC histograms plots of posterior samples

(v) Marginal density of posterior distributions

Another diagnostic test is to plot the posteriors density distributions. Normally for a better mixing and for a well sampled posteriors, we expect the histograms of all density estimations to follow a Gaussian distribution. Figure 16 depicts that density distributions of all fourteen estimated parameters follow Gaussian distribution and their values are taken as means of distributions of the chains except for the values of F_c and V_c.

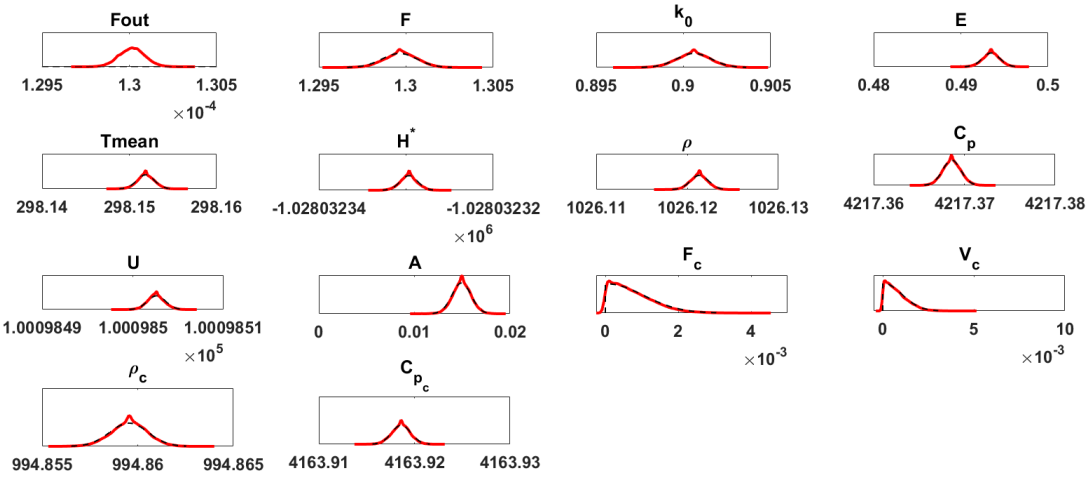

Figure 16: MCMC density distributions plots of sampled chain of parameters

(vi) Empirical probability plot of posteriors

To explore whether the empirical quantiles of posteriors are matching with the theoretical quantiles also requires probability plots of posteriors or quantile-quantile plots (Q-Q plots). Thus, Fig. 17 illustrates the Q-Q plots for the model Equation (35).

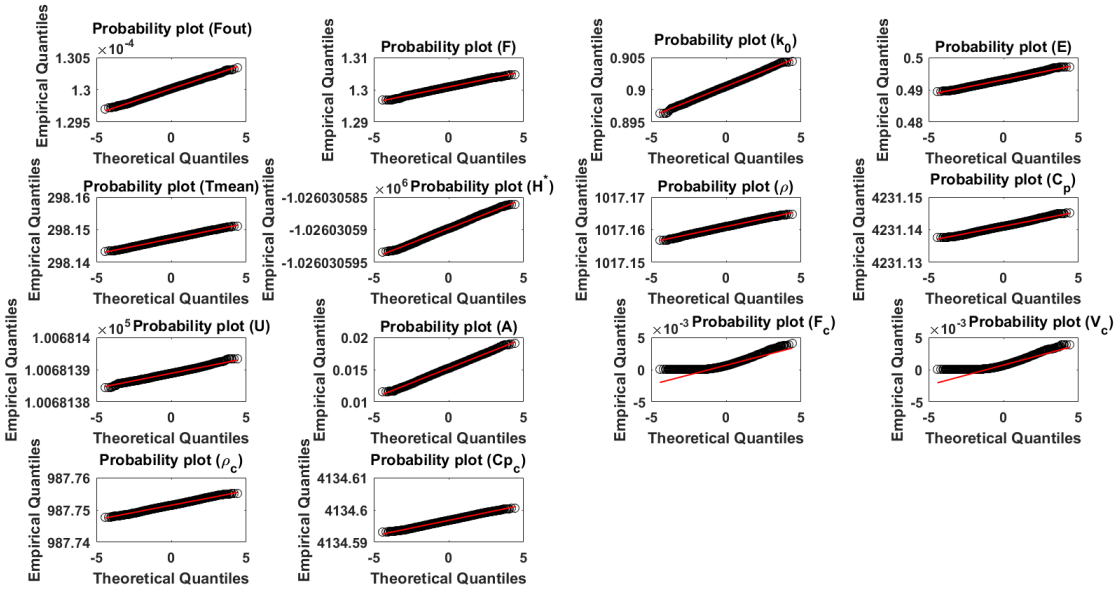

Figure 17: Probability plots for 100 000 posterior samples for each of identified fourteen model parameters of Equation (35).

As previously mentioned, it can be seen from this Fig. 17 that quantiles of posteriors of parameters F_c and V_c are not matching with their theoretical quantiles very well in the interval -5 to 0.

Table 13: MCMC and LSQ estimated parameters of the model Equation (35) and their and statistical inferences

Param	**Initial values**	**LSQ**	**Post mean**
F_{out}	130×10^{-6}	130.016×10^{-6}	130.015×10^{-6}
F	130×10^{-2}	130.09×10^{-2}	$129.971139 \times 10^{-2}$
k_0	0.9	0.900553	0.900592376
E	0.5	0.493183	0.493486288
T_{mean}	298.15	298.147	298.151888471
H^*	-1004.3×10^3	-1026.03×10^3	-1028032.329702401
ρ	1000	1017.16	1026.121280804
C_p	4186	4231.14	4217.368624072
U	100 000	100 681	100 098.502552738
A	0.015	0.0151979	0.014959065
F_c	46.56×10^{-6}	46.7705×10^{-6}	74.7936×10^{-5}
V_c	50×10^{-6}	49.6872×10^{-6}	76.2673×10^{-5}
ρ_c	1000	987.751	994.859555082
C_{p_c}	4186	4134.6	4163.918586616

Table 14: Table of standard deviation, Markov chain error, posterior median and credible interval

Std	**MCerr**	**Post Median**	**Credible Interval**
7.32×10^{-8}	1.0633×10^{-9}	130.016×10^{-6}	$[130.015 \times 10^{-6}, 130.16 \times 10^{-6}]$
0.00093	3.9735×10^{-5}	$129.9704569 \times 10^{-2}$	$[129.9705396 \times 10^{-2}, 129.9716882 \times 10^{-2}]$
0.000951	2.2856×10^{-5}	0.900596750	[0.900586482, 0.900598270]
0.0009525	1.7754×10^{-5}	0.493470050	[0.493480384, 0.493492191]
0.00095466	1.9926×10^{-5}	298.151879315	[298.151882554, 298.151894388]
0.00095973	3.2217×10^{-5}	-1028032.329677610	$-[1028032.329708349, 1028032.3296966452]$
0.00094236	2.9081×10^{-5}	1026.121304498	[1026.121274963, 1026.121286644]
0.00098619	2.1133×10^{-5}	4217.368601824	[4217.368617960, 4217.368630185]
0.00091663	4.2388×10^{-5}	100 098.502551528	[100 098.502547056, 100 098.502558419]
0.00095668	3.0706×10^{-5}	0.014962113	[0.014953136, 0.014964995]
0.00058698	3.7635×10^{-5}	62.4641×10^{-5}	$[74.4298 \times 10^{-5}, 75.1574 \times 10^{-5}]$
0.00059791	3.2879×10^{-5}	63.7067×10^{-5}	$[75.8967 \times 10^{-5}, 76.6379 \times 10^{-5}]$
0.00092534	2.464×10^{-5}	994.859566589	[994.859549347, 994.859560817]
0.00095621	1.7679×10^{-5}	4163.918608754	[4163.918580689, 4163.918592542]

Table 15: Table of autocorrelation time, geweke, kurtosis and skewness

tau	Geweke	Kurtosis	Skewness
41.003	0.99994	2.9626	-0.0630
62.713	0.99997	3.0915	-0.0225
50.329	0.99994	3.0930	-0.0016
46.313	0.9985	3.1854	0.0934
58.812	1	3.0988	-0.0220
57.28	1	3.1340	0.0125
59.644	1	3.0811	-0.0299
48	1	3.3398	0.0578
69.113	1	3.2362	0.0790
53.978	0.99458	3.0965	-0.0279
85.568	0.21093	3.9661	1.0355
69.882	0.41264	3.8227	1.0014
63.819	1	3.2461	0.0145
45.604	1	3.0466	-0.0150

Results that are presented in Tables 13, 14 and 15 show the estimated parameters values and statistical quantifications of the model Equation (35). Among the used statistical quantifications measure of the parameter values, there are measure of central tendencies (posterior mean, posterior median and credible interval with their lower bounds and upper bounds), measure of dispersions (standard deviation (std) and Markov Chain error (MCerr)), measure of shapes (Kurtosis and Skewness) and measure of correlations (autocorrelation time (tau) and Geweke). It can be observed that estimated parameters of the model agree with their initial values and hence parameters variations of the model are well identified to lie in their credible intervals (lower values and upper values for which parameters can take). As can be seen, LSQ estimates agree with MCMC estimates and therefore parameter values of the said model are statistically quantified and determined.

4.1.5 Sensitivity and Uncertainty Analysis Results

Sensitivity and uncertainty analysis of the estimated parameters on the formulated model presented in Equation (35) have been carried out with $X \in \mathbb{R}^4$ and $\theta \in \mathbb{R}^{14}$. The Gaussian distribution was assigned to be the the initial distribution for each of parameters. The obtained PRCCs results are displayed in Fig. 18 and Table 16.

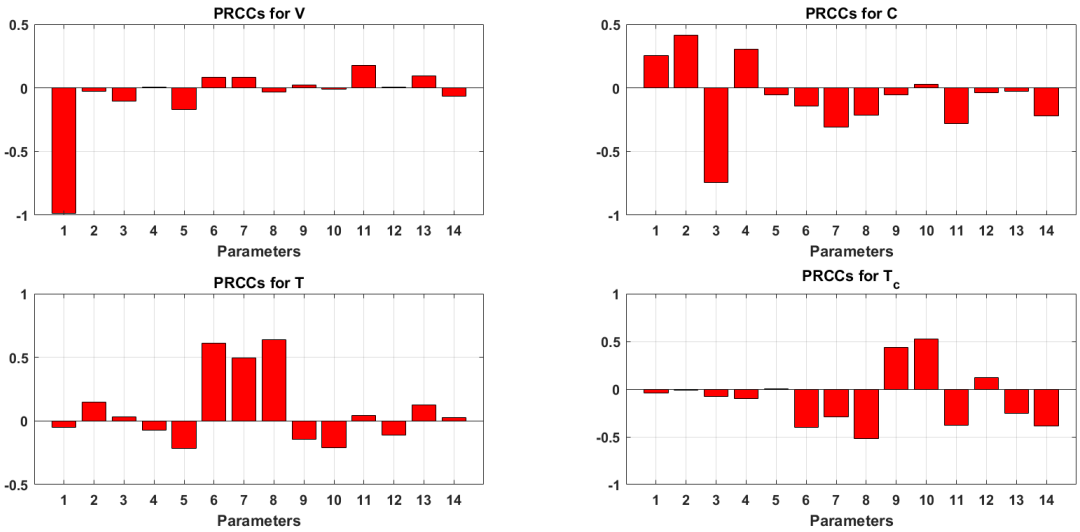

Figure 18: PRCCs plot for model Equation (35). The parameters 1,2,3...,14 correspond to parameters that are shown in Table 16, respectively.

Table 16: PRCCs results for model Equation (35)

Parameter		**PRCCs values for each state variable**		
Symbol	V	C	T	T_c
F_{out}	$-0.9847^{(*)}$	0.2545	-0.0479	-0.0429
F	-0.0269	0.4127	0.1482	-0.0119
k_0	-0.1060	$-0.7418^{(*)}$	0.0302	-0.0761
E	0.0070	0.3054	-0.0743	-0.0973
T_{mean}	-0.1713	-0.0515	-0.2141	0.0032
H^*	0.0813	-0.1444	$0.6114^{(*)}$	-0.3979
ρ	0.0819	-0.3102	$0.5000^{(*)}$	-0.2924
C_p	-0.0345	-0.2137	$0.6391^{(*)}$	$-0.5186^{(*)}$
U	0.0232	-0.0547	-0.1470	0.4348
A	-0.0091	0.0298	-0.2086	$0.5232^{(*)}$
F_c	0.1761	-0.2802	0.0415	-0.3810
V_c	0.0038	-0.0401	-0.1139	0.1187
ρ_c	0.0928	-0.0246	0.1285	-0.2502
C_{p_c}	-0.0655	-0.2189	0.0294	-0.3894

The results in Table 16 and Fig. 18 show that the first parameter which is the volumetric flows out (F_{out}) is significantly and negatively affecting the volume response as a state variable of the model Equation (35). On one side, the increase in that parameter values will significantly decrease the products volume in the tank whereas the slight decrease in F_{out} values will increase the volume of products in the tank which may lead to a catastrophic hazard like a destruction (deformation) of the tank if there are no other control measures. In this regard, deformable

CSTRs can be proposed as they may deform with the change of the volume. Similarly, the results show that the second parameter (k_0) is negatively correlated with the concentration. So, the decrease in its values increases the concentration and the other way around. One can observe that the tank temperature profiles in the model Equation (35) are specifically determined by the increase of reaction heat energy (H^*), density (ρ) and the specific heat capacity (C_p). The cooling jacket temperature is also negatively and positively affected by C_p and the cross-sectional area (A) between the reacting tank and the jacket respectively. Consequently, seven parameters in total may be found to have a great effect on the formulated model response.

4.1.6 Conclusion

The formulated model Equation (35) has been numerically solved by using fourth order Runge-Kutta method that is implemented in Matlab version 2016b. The identifiability of physical parameters of the model was also numerically carried out by using the least squares and DRAM methods. The least square parameters estimates converged to the literature values and were treated as prior information for the DRAM method. The generated DRAM samples were graphically and statistically analysed to test the convergence of the MCMC results. The results show that the parameters of the model were well identified as can be seen in Table 13. The uncertainty and sensitivity analysis of the model parameters variations on model variables using LHS and PRCCs have been further conducted. It was found that seven parameters among fourteen estimated parameters of the model have a great impact on model response and therefore control of those parameters are of great importance.

4.2 Numerical Analysis and Parameters Estimation of Deterministic Model for Endothermic CSTR

The numerical analysis of the formulated model that is presented in Equation (36) was done by using the same methods used in Section 4.1.

4.2.1 Numerical Solutions

Similarly, the numerical simulations and the parameters identification of the endothermic CSTR deterministic model which is presented in the model Equation (36) were done by following the same previous concepts. But simulations require parameters and initial values of the model Equation (36) as well. Table 17 and Table 18 show variables, parameters and initial values used to obtain the numerical solutions of the model. Quantitative results and the graphical representations of the solutions were performed and are found in Fig. 19.

Table 17: Table of variables, parameters and constants

Param symbol (unit)	**Param name**	**Value**	**Reference**
$C_{in}(kmol\ min^{-1}m^{-3})$	Feeding concentration	316.8	Muhirwa *et al.* (2017)
$C_0(kmol\ min^{-1}m^{-3})$	Initial concentration	316.8	Muhirwa *et al.* (2017)
$C(kmol\ min^{-1}m^{-3})$	Mixture concentration	State variable	to be simulated
$T_{in}(^oK)$	Feeding temperature	298.35	Muhirwa *et al.* (2017)
$T_0(^oK)$	Initial temperature	298.35	Muhirwa *et al.* (2017)
$T(^oK)$	Mixture temperature	State variable	to be simulated
$H^*(kcal\ kmol^{-1})$	Enthalpy	1004.3×10^3	Muhirwa *et al.* (2017)
$T_{H_0}(^oK)$	Initial heating temperature	288.15	Lu *et al.* (2017)
$T_{H_{in}}(^oK)$	Feeding heating temperature	293	Vojtesek *et al.* (2008)
$T_H(^oK)$	Jacket heating temperature	State variable	to be simulated
$R(kJ\ kmol^{-1}\ ^oK^{-1})$	Gas law constant	8.314	Muhirwa *et al.* (2017)
$V_0(m^3)$	Initial tank volume	100	Aboelela *et al.* (2018)
$V(m^3)$	Volume of the tank	State variable	to be simulated
$k_0(min^{-1})$	Pre-Arrhenius frequency	0.9	Muhirwa *et al.* (2017)
$E(kJ\ kmol^{-1})$	Activation energy	0.5	Muhirwa *et al.* (2017)
$T_{\text{mean}}(^oK)$	Reference temperature	298.15	Muhirwa *et al.* (2017)

Table 18: Continued table of variables, parameters and constants

Param symbol (unit)	Param name	Value	Reference
$F = F_{in}(m^3\ min^{-1})$	Feeding velocity	130×10^{-2}	Muhirwa *et al.* (2017)
$\rho(kg\ m^{-3})$	Density	1000	Muhirwa *et al.* (2017)
$C_p(kcal\ kg^{-1}\ ^oK^{-1})$	Specific Heat capacity	4186	Muhirwa *et al.* (2017)
$U(kJ\ min^{-1}\ ^oK^{-1}\ m^{-2})$	Heat transfer coefficient	100 000	Muhirwa *et al.* (2017)
$A(m^2)$	Cross-sectional area	0.015	Muhirwa *et al.* (2017)
$F_H(m^3\ min^{-1})$	Heating velocity	46.5×10^{-6}	to be estimated
$V_H(m^3)$	Heating reactor volume	50×10^{-6}	to be estimated
$\rho_H(kg\ m^{-3})$	Density of the heater	1000	Aboelela *et al.* (2018)
$C_{p_H}(kcal\ kg^{-1o}K^{-1})$	Heater heat capacity	4.168×10^3	Muhirwa *et al.* (2017)
$F_{\text{out}}(m^3min^{-1})$	Outlet velocity	130×10^{-6}	to be estimated

Note: Param means parameter

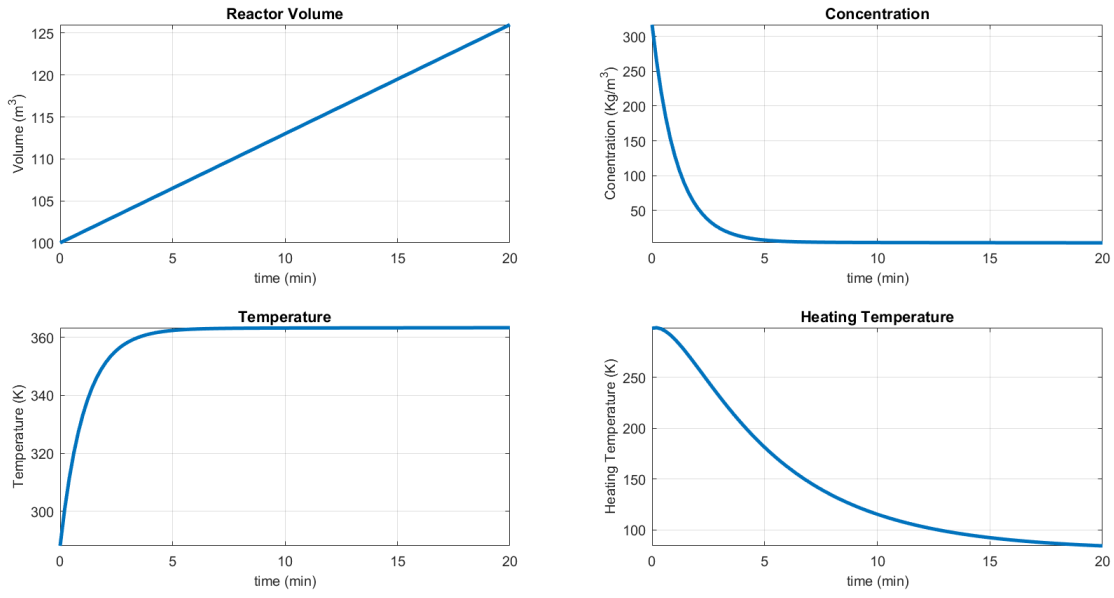

Figure 19: Numerical solutions of model Equation (36)

From Fig. 19, it is seen that the concentration of the reactants is decreasing inside the tank from 316.8 and approaching zero. When the reactants are fed continuously into the tank they are consumed and this is an indication of having a complete conversion of reactant's concentration into

product's concentration. The temperature of the system is observed to increase exponentially from 298.35^oK to 360^oK due to the heating process alongside the reacting tank. Consequently, the temperature of the heating tank decreases slightly from 288.15^oK to almost zero after 5 minutes. From sub-plot 1 of Fig. 19, it can further be observed that the volume of the reacting tank increases as the feeding rates become more and greater than the removal rates. This has a significance in designing the reacting tank which may deform continuously to adapt to the increase of the production conversion rate from $100m^3$ to approximately $126m^3$.

4.2.2 Least Squares Results

As it was previously done for the CSTR with the exothermic reaction, the numerical solutions of model Equation (36) are corrupted with five different noise intensity $\sigma = [0.01, 0.05, 0.1, 0.5, 1]$ to obtain 5 data points which are considered as the experimental measurements of the CSTR system with the endothermic reaction. By using the obtained experimental measurements, in Fig. 20 - Fig. 24, there are estimated solutions (dashed red color) and the exact model solutions (blue color) as well as the estimated values of parameters of model Equation (36) which are presented in Table 19 - Table 23.

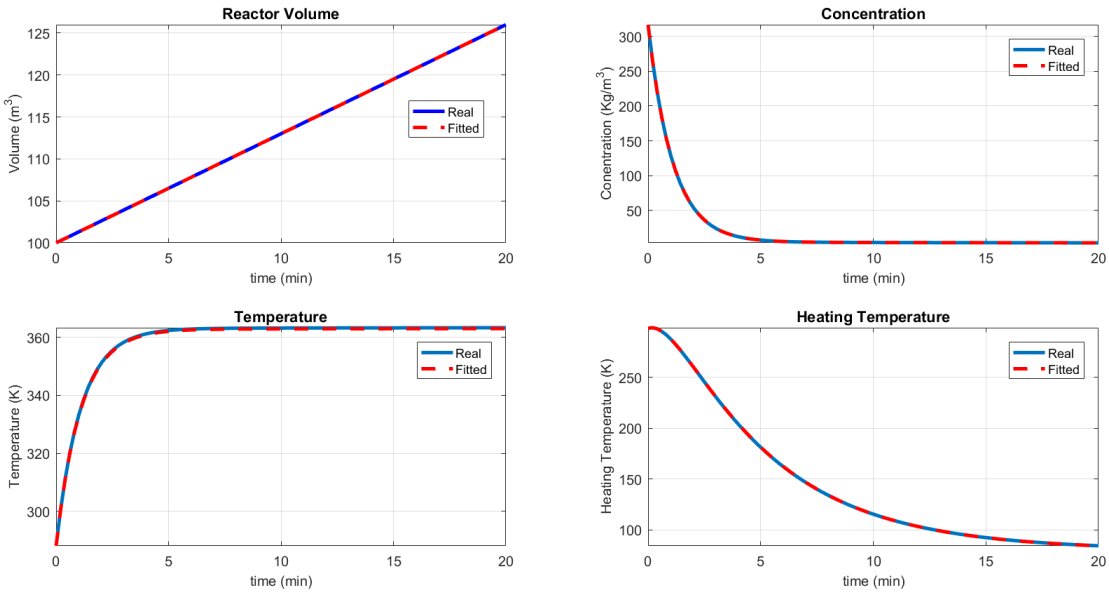

Figure 20: Fitted CSTR model Equation (36) when $\sigma = 0.01$

From Fig. 20, the measurements are fitting the model very well and all parameters seem to converge to its true parameter values as can be also observed in Table 19. Therefore, the corruption

of the CSTR model (36) solutions by using $\sigma = 0.01$ will have no big impact on the predictive results from the model since all measurements are almost overlapping with the estimated values of the model. The Least Squares results show that the estimated values of the volume, the concentration, the temperature and the heating temperature remain the same as their numerical solutions due to low noise introduced in the numerical results of the model.

Table 19: Table of estimated model parameters when $\sigma = 0.01$

Parameter symbol	**Parameter Physical Meaning**	**Initial value**	**Estimated**
F_{out}	Outlet Velocity	130×10^{-6}	129.105×10^{-6}
F	Feeding Velocity	130×10^{-2}	129.273×10^{-2}
k_0	Pre-Arrhenius Frequency	0.9	0.898036713
E	Activation Energy	0.5	0.498149772
T_{mean}	Reference Temperature	298.15	297.5395333
H^*	Enthalpy	1004.3×10^3	992 722.1594
ρ	Density	1000	998.2500704
C_p	Heat Capacity	4186	4161.567828
U	Heat Transfer Coefficient	10 000	9892.834025
A	Cross-sectional Area	0.015	0.014838739
F_H	Heating Velocity	46.5×10^{-6}	46.2×10^{-6}
V_H	Heating Reactor Volume	50×10^{-6}	49.5×10^{-6}
ρ_H	Density of the Heating Substance	1000	992.4317537
C_{p_H}	Heating Heat Capacity	4168	4153.497983

The corrupted numerical solutions with $\sigma = 0.05$ have been used to identify the model's parameters and the results show that all parameters are very close to its true values with the reference to the results shown in Table 20. It can be seen that the predictive model's solutions (dashed red color) are very close to the model exact solutions (solid blue line) as well. Therefore, this model displays a good fitting to the data according to the curves of volume, concentration, temperature and the heating temperature shown in Fig. 21. While the Least Squares results of the volume, the concentration and the heating temperature of CSTR are the same as their corresponding numerical solutions, the Least Squares results of temperature of the reacting tank are nearly close to its corresponding numerical solutions.

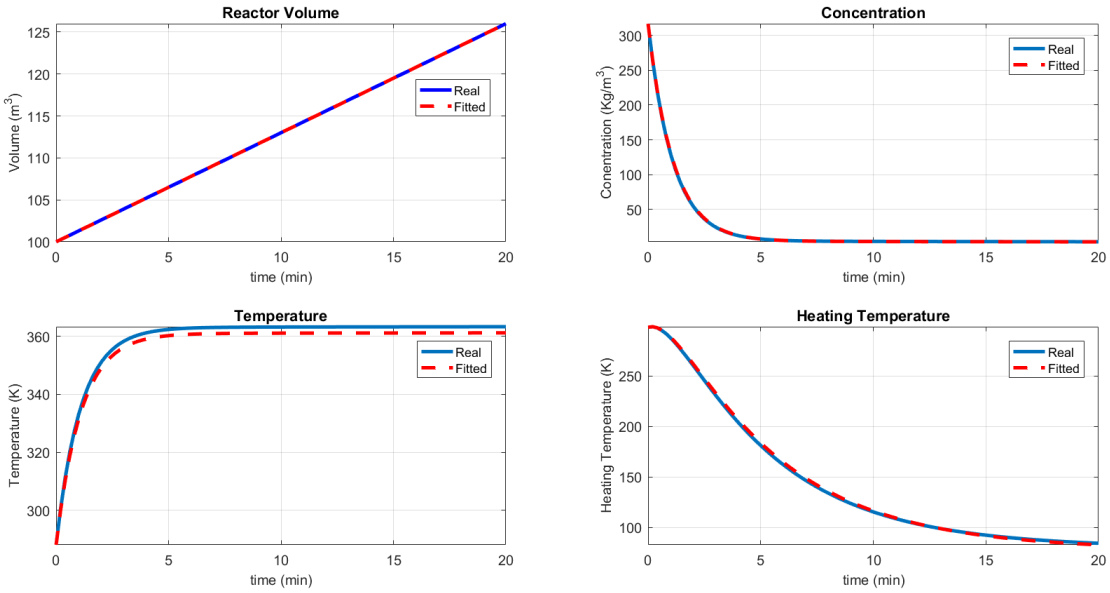

Figure 21: Fitted CSTR model Equation (36) when $\sigma = 0.05$

Table 20: Table of estimated model parameters when $\sigma = 0.05$

Parameter symbol	**Parameter Physical Meaning**	**Initial value**	**Estimated**
F_{out}	Outlet Velocity	130×10^{-6}	127.429×10^{-6}
F	Feeding Velocity	130×10^{-2}	122.894×10^{-2}
k_0	Pre-Arrhenius Frequency	0.9	0.888095389
E	Activation Energy	0.5	0.50971455
T_{mean}	Reference Temperature	298.15	295.2869142
H^*	Enthalpy	1004.3×10^3	997 444.3212
ρ	Density	1000	1094.290957
C_p	Heat Capacity	4186	3911.158011
U	Heat Transfer Coefficient	10 000	9931.53421
A	Cross-sectional Area	0.015	0.014838647
F_H	Heating Velocity	46.5×10^{-6}	46.4×10^{-6}
V_H	Heating Reactor Volume	50×10^{-6}	50.4×10^{-6}
ρ_H	Density of the Heating Substance	1000	977.7974624
C_{p_H}	Heating Heat Capacity	4168	4174.378311

The random noise of intensity $\sigma = 0.1$ has been also introduced in the numerical solutions of the CSTR model Equation (36) to obtain the experimental measurements taken as real data of

the process. Those real data have been used to estimate the model's parameters which show the convergence as it can be seen from the results that are displayed in Table 21. Based on the curves (solid blue line and dashed red line) in Fig. 22, it can be viewed that the measurements of volume, concentration, temperature and the heating temperature fit the model numerical solutions well.

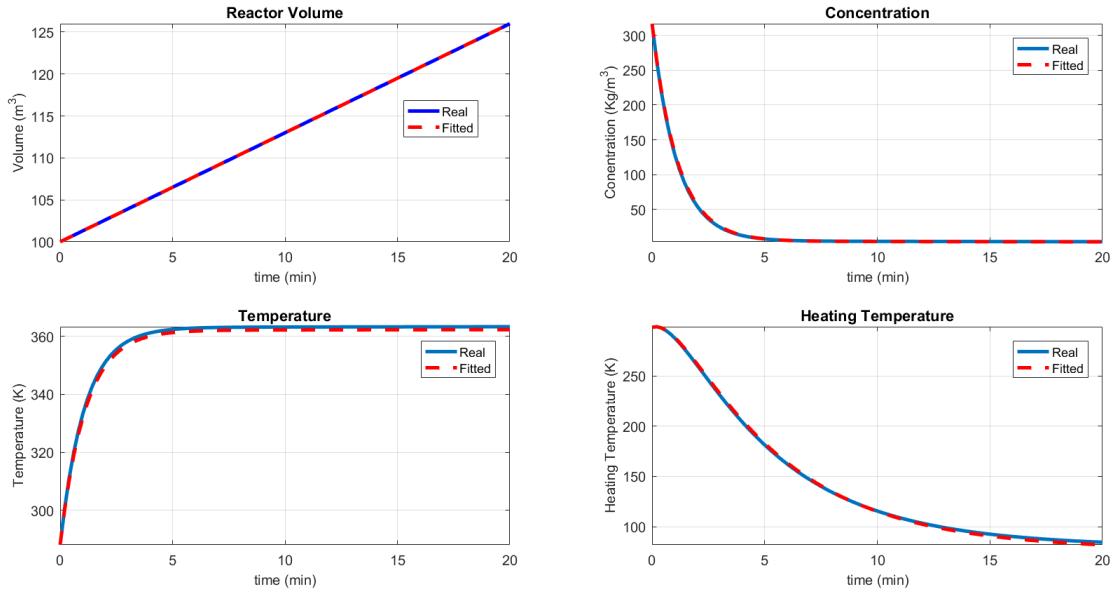

Figure 22: Fitted CSTR model Equation (36) when $\sigma = 0.1$

Table 21: Table of estimated model parameters when $\sigma = 0.1$

Parameter symbol	Parameter Physical Meaning	Initial value	Estimated
F_{out}	Outlet Velocity	130×10^{-6}	127.077×10^{-6}
F	Feeding Velocity	130×10^{-2}	119.092×10^{-2}
k_0	Pre-Arrhenius Frequency	0.9	0.878266408
E	Activation Energy	0.5	0.562648664
T_{mean}	Reference Temperature	298.15	289.2325135
H^*	Enthalpy	1004.3×10^3	947 566.2601
ρ	Density	1000	1085.801577
C_p	Heat Capacity	4186	3689.762929
U	Heat Transfer Coefficient	10 000	9904.85817
A	Cross-sectional Area	0.015	0.014785247
F_H	Heating Velocity	46.5×10^{-6}	46.0×10^{-6}
V_H	Heating Reactor Volume	50×10^{-6}	49.9×10^{-6}
ρ_H	Density of the Heating Substance	1000	995.4546099
C_{p_H}	Heating Heat Capacity	4168	4124.186059

The noise of the standard deviation 0.5 is introduced in the numerical solutions of model Equation (36) and the corresponding model fitting and estimated values of model parameters are found in Fig. 23 and Table 22.

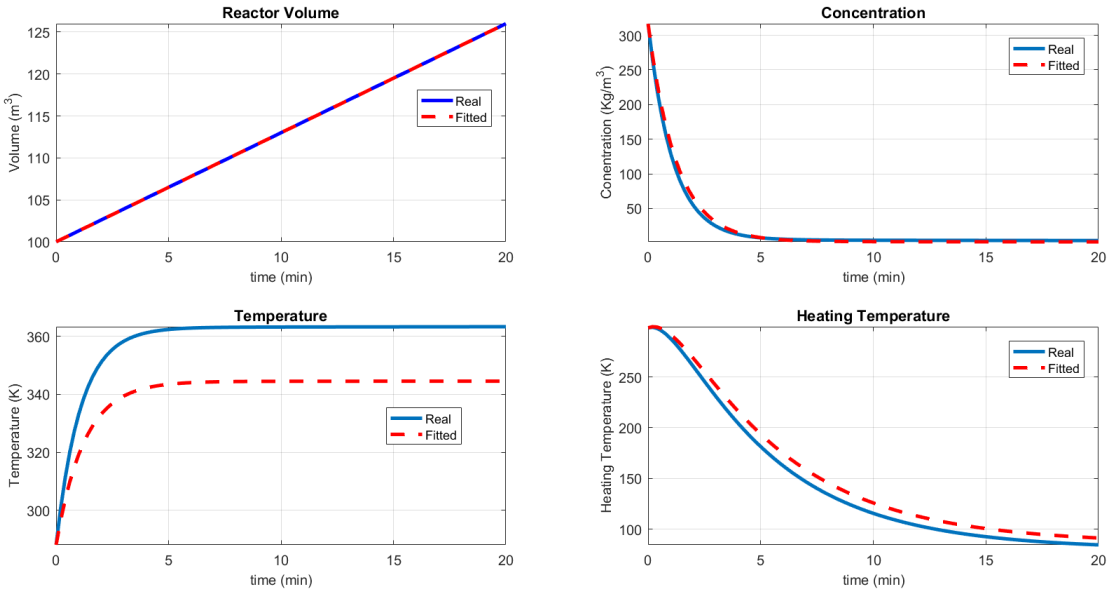

Figure 23: Fitted CSTR model Equation (36) when $\sigma = 0.5$

Table 22: Table of estimated model parameters when $\sigma = 0.5$

Parameter symbol	Parameter Physical Meaning	Initial value	Estimated
F_{out}	Outlet Velocity	130×10^{-6}	153.94×10^{-6}
F	Feeding Velocity	130×10^{-2}	55.021×10^{-2}
k_0	Pre-Arrhenius Frequency	0.9	0.795111739
E	Activation Energy	0.5	0.300459211
T_{mean}	Reference Temperature	298.15	409.8247248
H^*	Enthalpy	1004.3×10^3	808 294.8766
ρ	Density	1000	1167.962108
C_p	Heat Capacity	4186	3866.591573
U	Heat Transfer Coefficient	10 000	13 340.82233
A	Cross-sectional Area	0.015	0.014788745
F_H	Heating Velocity	46.5×10^{-6}	47.3×10^{-6}
V_H	Heating Reactor Volume	50×10^{-6}	41.7×10^{-6}
ρ_H	Density of the Heating Substance	1000	1329.654448
C_{p_H}	Heating Heat Capacity	4168	3821.050206

The noise of magnitude $\sigma = 0.5$ greatly affects the endothermic CSTR deterministic model (36) because most of the estimated parameters are far away from its initial values in according to the

results presented in Table 22. The predictive curves for the volume, the concentration and the heating temperature seem to be in good agreement with the measurements, however the other remaining state variable (temperature) shows poor fitting to the data as can be visualised in Fig. 23.

Figure 24 and Table 23 represent the Least Squares results obtained when the noise intensity is $\sigma = 1$.

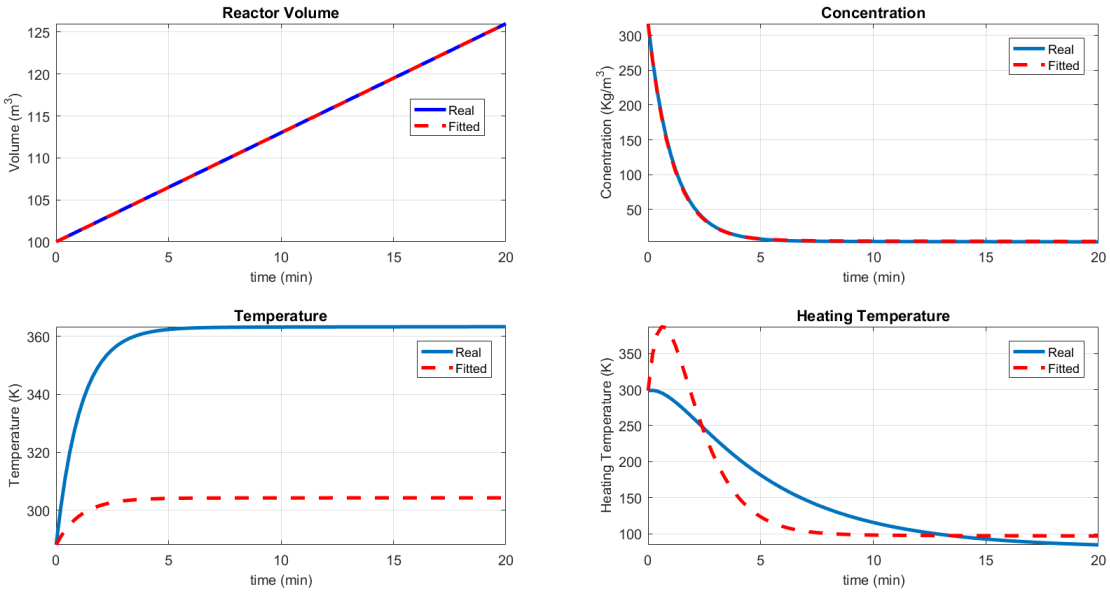

Figure 24: Fitted CSTR model Equation (35) when $\sigma = 1$

Table 23: Table of estimated model parameters when $\sigma = 1$

Parameter symbol	Parameter Physical Meaning	Initial value	Estimated
F_{out}	Outlet Velocity	130×10^{-6}	197.063×10^{-6}
F	Feeding Velocity	130×10^{-2}	154.711×10^{-2}
k_0	Pre-Arrhenius Frequency	0.9	0.918954071
E	Activation Energy	0.5	0.435849618
T_{mean}	Reference Temperature	298.15	292.9495998
H^*	Enthalpy	1004.3×10^3	393 172.6156
ρ	Density	1000	1156.565248
C_p	Heat Capacity	4186	6563.033057
U	Heat Transfer Coefficient	10 000	9727.782374
A	Cross-sectional Area	0.015	0.019190691
F_H	Heating Velocity	46.5×10^{-6}	51.3×10^{-6}
V_H	Heating Reactor Volume	50×10^{-6}	1.57×10^{-6}
ρ_H	Density of the Heating Substance	1000	965.7932723
C_{p_H}	Heating Heat Capacity	4168	3876.875097

Based on the results represented in Fig. 24, it can be seen that the model predictive results are not in good agreement with the experimental measurements of the model. Hence the deviation of the graphical representations is being supported by the parameter estimate results that are shown in Table 23. Most of the identified parameters diverge from its initial parameter values and this shows a significant effect of high intensity noise $(\sigma = 1)$ on the formulated CSTR model's temperature and the heating temperature. That is the Least Squares results for some CSTR physical values like the temperature and the heating temperature significantly differ from their corresponding numerical results as shown in Fig. 24.

4.2.3 Markov Chain Monte Carlo Results

For model Equation (36), initial number of samples generated was 500 000 and Gaussian distribution was initialized with mean 0 and covariance matrix $\Sigma_0 = \frac{0.00001 \times I_{p \times p}}{\sqrt{p}}$, where p represents the number of parameters to be identified, and $I_{p \times p}$ is the $p \times p$ identity square matrix. The

least squares results obtained when $\sigma = 0.05$ were treated as prior information to produce the MCMC results.

(i) Trace plots

The generated time series for parameters is plotted to diagnose whether the posterior parameter distributions are stationary. If the chain gets stuck somewhere during sampling period, then the chain does not move straightforward from one side to another and this makes the MCMC algorithm to produce a poor mixing chain. The poor mixing indicates that the parameters are not well identifiable. Therefore, further task of changing the ingredients of the algorithm should be done to correctly, efficiently and effectively identify the model parameters.

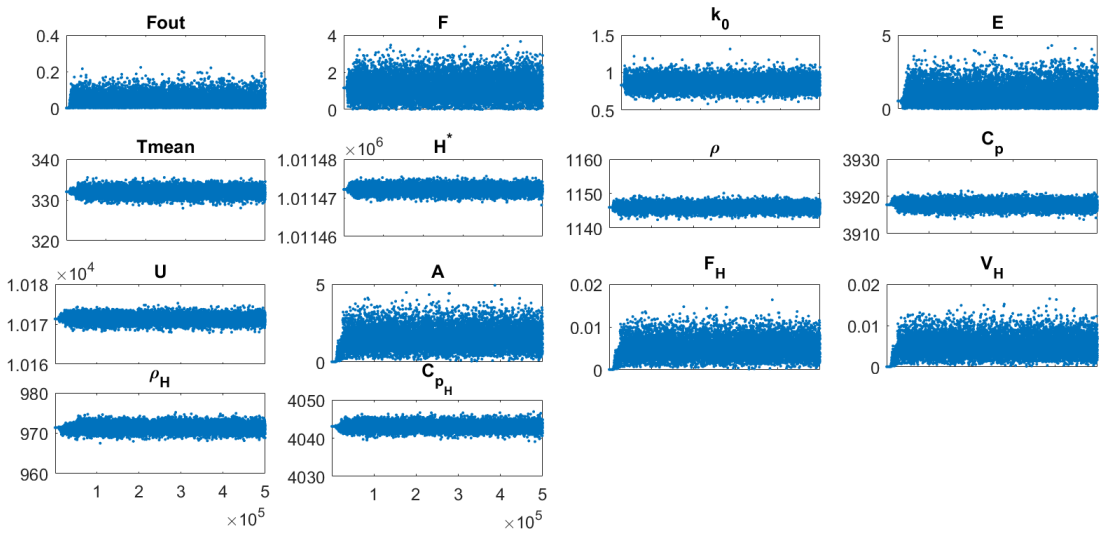

Figure 25: MCMC chain plots (time series plots) of samples CSTR model Equation (36)

Trace plots that are shown in Fig. 25 indicate that there are no high trends in sampled parameters since the chain is stationary and moves from one side to another. It is explored that DRAM does not stack in any place during sampling, which represents good mixing of the chain.

(ii) Scatter plots (pairs)

The scatter plots check the correlation index between pairs of samples. High correlation index among many pairs of samples can lead to poor identifiability of the model parameters. As a consequence, the model cannot be reliably applicable because small variation in a set of

correlated parameters can make the model corrupting. Low correlation index among pairs is preferably to be observed for a good mixing and for a well reliable and realistic model.

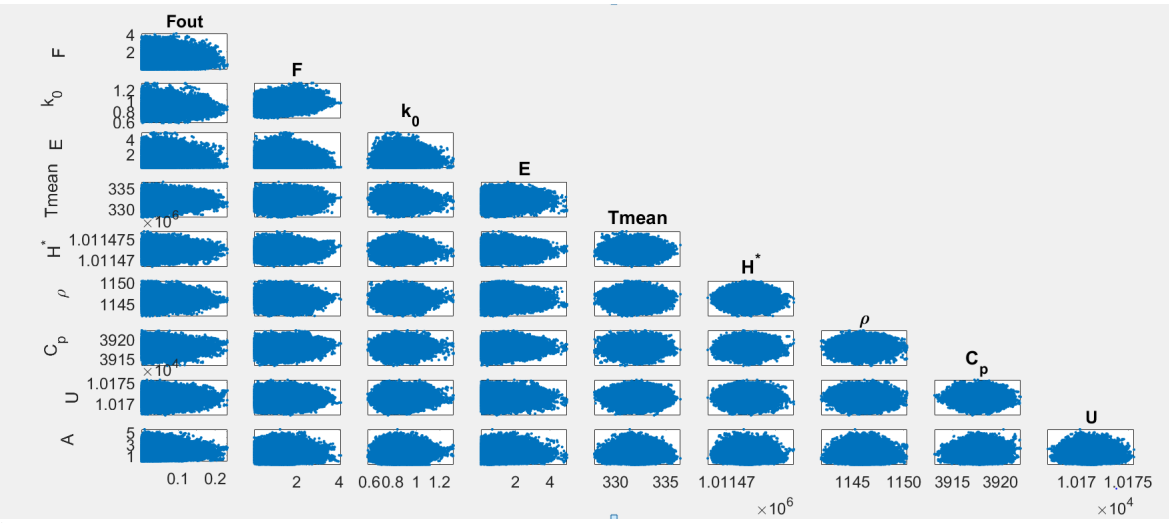

Figure 26: MCMC pairs plots of samples for CSTR model Equation (36)

As there are fourteen parameters to be identified from the data points, then there are as many as possible combinations of each pairs chosen from fourteen parameters which are equivalent to ninety one scatter plots. However, the graphical representation of the scatter plots is for the first ten parameter samples which are equivalent to forty five scatter plots. Figure 26 shows how pairs among those forty five scatter plots correlate and it can be seen that none of the parameters are strongly correlated with each another. If one observes strong correlation among sampled parameters, then it is the indication that the algorithm mixes badly and so a high number of simulations is required to at least increase the variance among samples.

(iii) Autocorrelation plots

The autocorrelation plots show how independent is the sampling process. If the coefficients of the autocorrelation functions (x-axis) for some of the posteriors do not decay toward zero as the number of lags (y-axis) increases, then it is the sign of having parameters dependence in sampling which causes the MCMC method not to converge to the target distribution. Thus, a decay of autocorrelation functions coefficients provides the accuracy and the certainty of obtaining a converging posterior distribution of parameters.

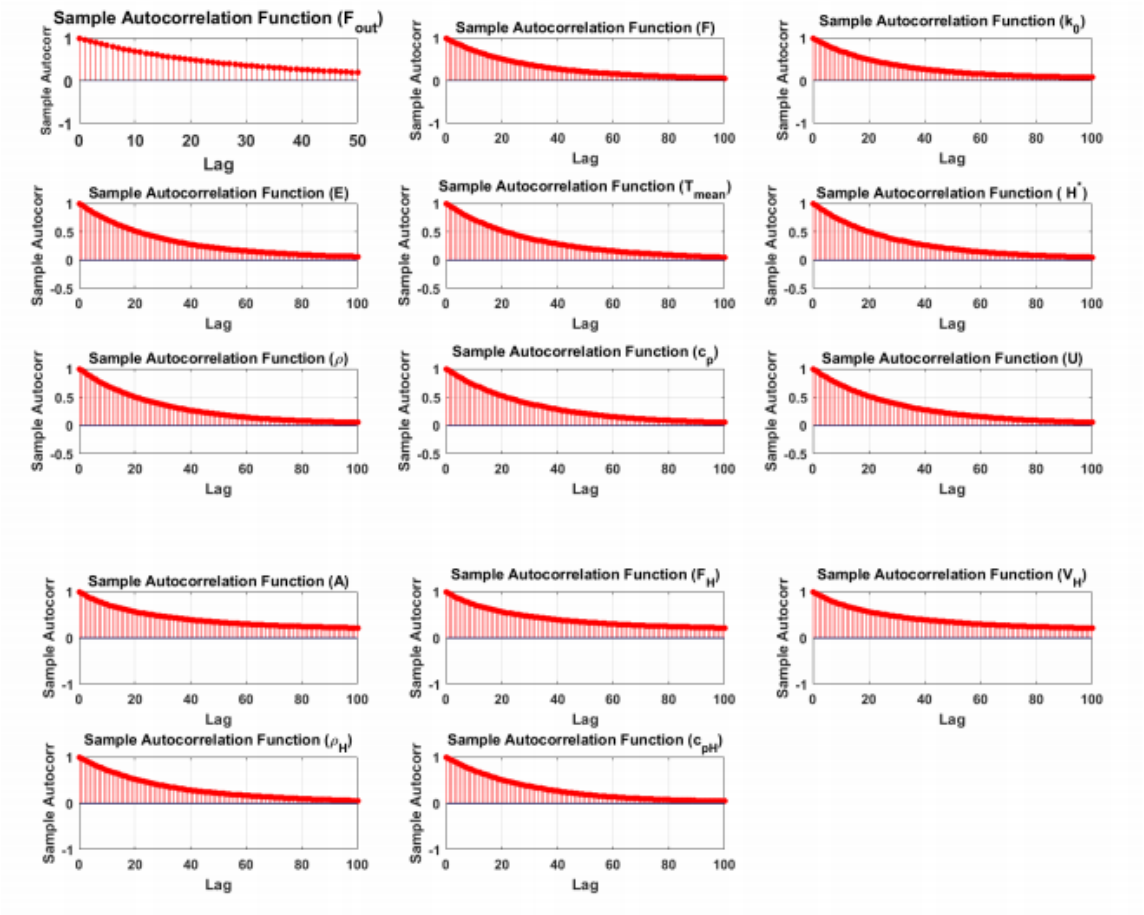

Figure 27: MCMC plots of autocorrelation functions for parameters samples of the model Equation (36)

From Fig. 27, it can be seen that all coefficients of autocorrelation functions (x-axis) are exponentially decaying as the number of lags (y-axis) increase. Therefore, the consecutive parameters are independently sampled during the run-time of the DRAM algorithm, and this determines the convergence of the generated chains.

(iv) Histograms for posterior samples of endothermic CSTR deterministic model

The histograms for sampled posterior parameters for a converging Markov chain must fairly follow the normal distribution curve. It is therefore a good practice to plot the histograms for all sampled parameters to make sure that all of them have bell shapes.

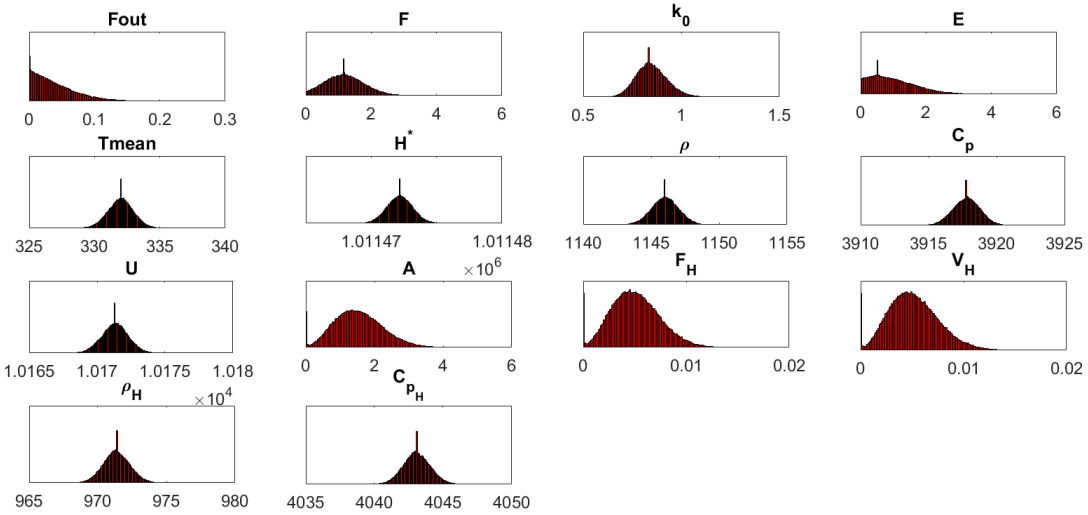

Figure 28: MCMC histograms plots of parameters posterior samples of the model Equation (36)

So, from Fig. 28, it is spotted that almost all sampled parameters follow the normal distributions, except for the parameters F_{out} and E which are slightly skewed in the right hand side. As results, DRAM method identified well other twelve parameters of the model Equation (36).

(v) Marginal density for posterior distributions

Figure 29 illustrates the density distributions of the estimated parameters of the model Equation (36). For well identified parameters, shapes of their kernel density distributions must follow Gaussian distribution.

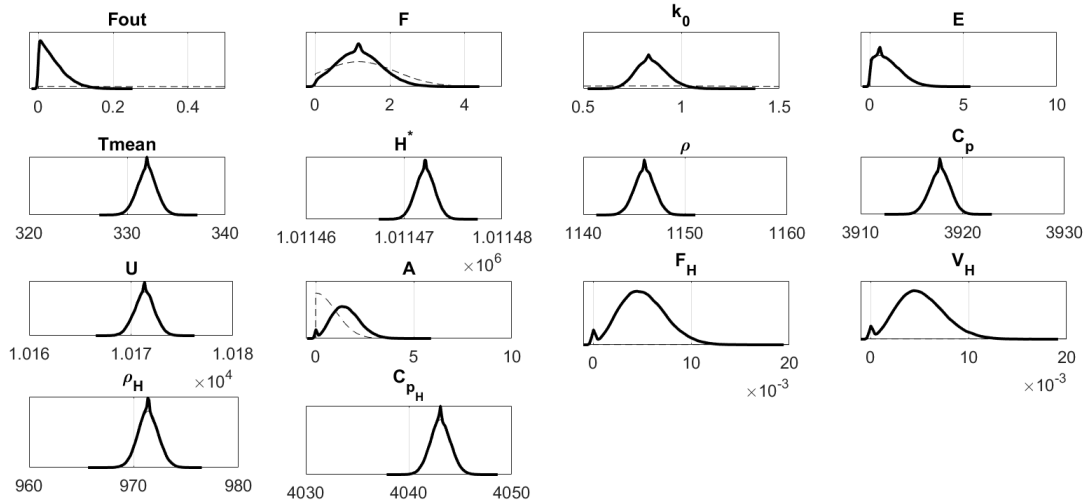

Figure 29: MCMC plots of Kenel density distributions parameters of the model Equation (36)

Figure 29 shows that the parameters are identified because all parameters seem to follow the Gaussian distribution except for parameters F_{out} and E. This Figure also displays the posterior means of all sampled parameters and are located in the symmetrical axes of their corresponding density distributions.

(vi) Empirical probability plot of posteriors

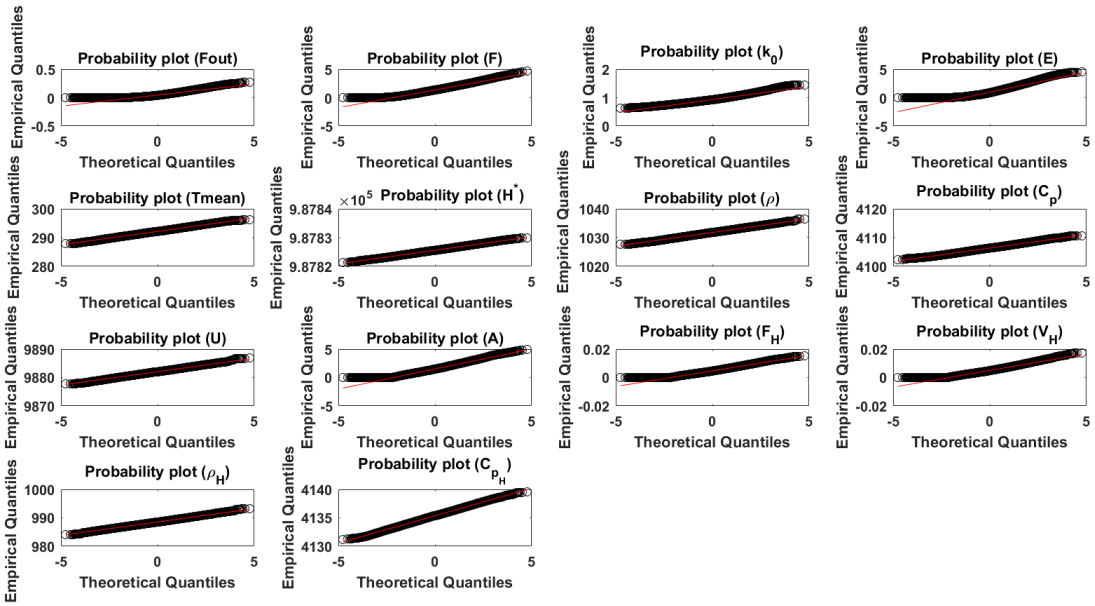

Figure 30: Probability plots for 500 000 posterior samples of parameters of the model Equation (36).

It is shown in Fig. 30 that quantiles of posterior chains of parameters F_{out} and E are not exactly following the theoretical normality of quantiles.

The overall MCMC quantitative results of model Equation (36) can be found in Table 24 - Table 26. The Table show that all posterior means are within their credible intervals. The MCMC results show convergence as the MCerror is minimized. Some curves for parameters posterior means have shown skewness and deviate from normal curves for example F_{out} and E. The kurtosis and the skewness values for probability distributions of posterior parameters that follow Gaussian distribution are conventionally expected to be around 3 and 0 respectively. It is clear that almost all parameters kurtosis and skewness values are approximately 3 and 0 except for F_{out} which is 4.3 and 1.15 respectively. The skewness for the parameter E is not approximately 0 but 0.849. It indicates that most of all model parameters follow Gaussian distribution. The geweke values for posterior distributions also check the convergence of the MCMC chain of

parameters and by default assuming that for a stationary distribution, the posterior means for two windows which are the start of sampling (10%) and the end of sampling (50%) of the posteriors are identical. When samples are drawn from a stationary distribution then geweke diagnostic statistical test approaches standard normal distribution and its statistical values are expected to be nearly the unity for converging chain. Tau values indicate the autocorrelation time and so the decrease in tau values implies the better mixing in sampling a certain posterior parameter from proposal distribution. It can be explored that tau values in the Table 26 are small and hence better mixing of the chain while estimating model parameters is attained.

Table 24: MCMC and LSQ estimated parameters of the model Equation (36) and their statistical inferences

Param	**Initial values**	**LSQ**	**Post mean**
F_{out}	130×10^{-6}	127.429×10^{-6}	0.040469
F	130×10^{-2}	122.894×10^{-2}	1.1983
k_0	0.9	0.8881	0.84984
E	0.5	0.5097146	0.99429
T_{mean}	298.15	295.29	332
H^*	1004.3×10^3	997.44432×10^3	1011500
ρ	1000	1017.16	1146
C_p	4186	4231.14	3917.8
U	10 000	10 681	10 171
A	0.015	0.014838	1.5279
F_H	46.56×10^{-6}	46.4×10^{-6}	0.005055
V_H	50×10^{-6}	50.4×10^{-6}	0.005124
ρ_H	1000	977.79746	971.37
C_{p_H}	4186	4174.3783	4043.1

Table 25: Table of posterior median, credible interval, standard deviation and Markov chain error for the MCMC results

Post Median	Credible Interval	Std	MCerr
130.016×10^{-6}	$[0.040377, 0.0405619]$	0.033356	0.000911
$129.9704569 \times 10^{-2}$	$[1.196687, 1.199921]$	0.58335	0.008309
0.900596750	[0.849618, 0.850056]	0.079068	0.000664
0.493470050	[0.992368, 0.996216]	0.69412	0.022557
298.151879315	[331.9976, 332.00305]	0.97761	0.011375
1028032.329677610	$[1011472.177, 1011572.182]$	0.96855	0.018189
1026.121304498	[1145.017, 1146.0223]	0.991195	0.016142
4217.368601824	[3917.778, 3917.884]	0.99181	0.022299
10 098.502551528	[10 170.319, 10 171.324]	0.97344	0.014898
0.014962113	[1.52593, 1.52989]	0.71386	0.061221
62.4641×10^{-5}	$[0.005048, 0.005062]$	0.002363	0.00020253
63.7067×10^{-5}	$[0.0051169, 0.005062]$	0.002436	0.00020553
994.859566589	[971.363,971.389]	0.96991	0.022239
4163.918608754	[4043.074,4043.179]	0.97664	0.015468

Table 26: Table of autocorrelation time, geweke, kurtosis and skewness for the MCMC results

tau	Geweke	Kurtosis	Skewness
72.252	0.75014	4.3	1.15
59.379	0.99404	2.9	0.3499
57.624	0.99733	3.4	0.398
71.166	0.782	3.4	0.849
66.184	0.99982	3.1	-0.0325
60.161	1	3.05	0.0119
59.628	0.99998	3.06	-0.00517
64.508	0.99992	3.08	-0.063
65.456	0.99998	3.09	-0.0125
452.28	0.39106	3.08	0.324
449.29	0.39138	3.08	0.326
392.98	0.38563	3.17	0.389
69.989	0.99957	3.13	0.0489
65.86	0.99996	3.12	0.0459

4.2.4 Sensitivity and Uncertainty Analysis Results

The sensitivity analysis is also applied to the model presented in Equation (36) to examine the influence of parameters uncertainty on the model response. The obtained PRCCs results are plotted in Fig. (31) and represented in Table (27).

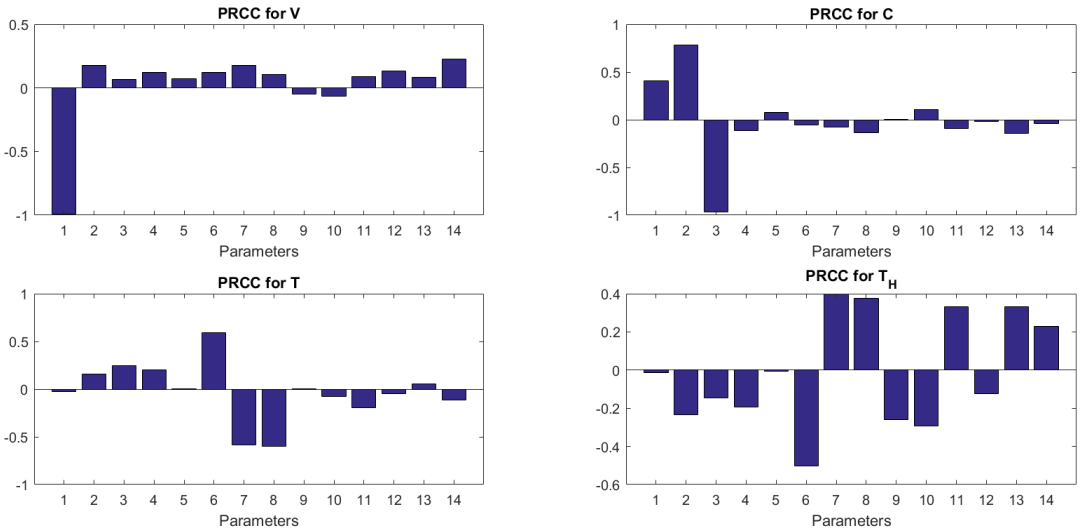

Figure 31: PRCCs plot for model Equation (36)

From Fig. 31, subplot 1-subplot 4 displays the PRCCs results for the volume, the concentration, the temperature and the heating temperature, respectively. This figure shows that the first parameter (F_{out}) is strongly and negatively correlated with the volume means that the increase in the values of F_{out} decreases the values of the volume in the reacting tank. Likewise, the second parameter (F) is positively correlated with the concentration whilst the third one is significantly and negatively correlated with the concentration, and consequently, the increase in the values of F will increase the values of the concentration in the model and the increase of k_0 will decrease the concentration values of the model as can be seen from subplot 2. In subplot 3, it can be explored that the increase of sixth parameter (H^*) values will increase the temperature of the tank whereas the increase of the seventh (ρ) and the eighth (C_p) parameters values will automatically decrease the temperature values in the formulated model. Sub-plot 4 of Fig. 31 shows that only the sixth parameter is negatively correlated with the heating temperature which explains that the increase in the enthalpy values will directly inhibit the increase of the heating temperature values. As a result, $F_{\text{out}}, F, k_0, H^*, \rho$ and C_p parameters are identified to be very sensitive to the model Equation (35) and hence much attention has to be quantitatively and qualitatively accorded to those influential model parameters.

Table 27: PRCCs results for model Equation (36)

Parameter	**PRCCs values for each state variable**			
Symbol	V	C	T	T_H
F_{out}	$-0.9890^{(*)}$	0.4067	-0.0263	-0.0126
F	0.1793	$0.7850^{(*)}$	0.1599	-0.2350
k_0	0.0645	$-0.9678^{(*)}$	0.2452	-0.1453
E	0.1209	-0.1126	0.1999	-0.1934
T_{mean}	0.0730	0.0739	0.0048	-0.0053
H^*	0.1246	-0.0532	$0.5897^{(*)}$	$-0.5029^{(*)}$
ρ	0.1777	-0.0739	$-0.5858^{(*)}$	0.3995
C_p	0.1076	-0.1335	$-0.6017^{(*)}$	0.3773
U	-0.0473	0.0001	0.0060	-0.2588
A	-0.0664	0.1083	-0.0800	-0.2929
F_H	0.0918	0.0950	-0.1923	0.3310
V_H	0.1325	-0.0212	-0.0447	-0.1234
ρ_H	0.0846	-0.1467	0.0563	0.3318
C_{p_H}	0.2289	-0.0405	-0.1175	0.2282

4.2.5 Conclusion

In this Section 4.2 of the dissertation, the variable-volume deterministic model for the endothermic continuously stirred tank reactor has been numerically solved and analysed by using the Least Squares and the Markov Chain Monte Carlo (MCMC) methods. The MCMC algorithm used in this Section is the delayed-rejection adaptive metropolis (DRAM). The results from DRAM have been graphically and statistically analysed to not only study the convergence of the results and the robustness of the model but to also examine the applicability and the reliability of the model by identifying unknown model physical parameters. The global sensitivity analysis is performed to quantify the effect of uncertainty in the model from the uncertainty of estimated parameters by using Latin Hypercube Sampling method. The partial rank correlation coefficients results and their significances to each variable of the model Equation (36) have been studied and analysed. Six parameters among fourteen identified parameters were shown to be correlated with the model variables and are very sensitive to the model responses. The numerical results revealed that the model is well identified and can be very beneficial to qualitatively, quantitatively and experimentally describe the dynamics of the variable-volume CSTR systems whenever the shown influential parameters are treated and controlled carefully.

4.3 Numerical Analysis of Exothermic CSTR Stochastic Models

Stochastic differential equations often do not have the exact solutions. The approximated solutions are obtained through numerical simulations. Therefore, the four scenarios of stochastic models presented in chapter 3 of this dissertation, that means Equations (83), (84), (85) and (95) were numerically solved and analysed by using Euler-Maruyama method with their corresponding deterministic models taken as benchmarks.

4.3.1 Numerical Results for Scenario A

In the simulation, the Brownian variables were chosen to be equally and normally distributed with mean 0 and standard deviation t, that means $\mathrm{d}B_V = \mathrm{d}B_C = \mathrm{d}B_T = \mathrm{d}B_{T_c} \backsim \mathbb{N}(0, \mathrm{d}t)$. The numerical results of stochastic model Equation (83) that were obtained for different values of volatility constants 0.1, 0.3, 0.5 and 1 are graphically displayed from Fig. 32 to Fig. 35.

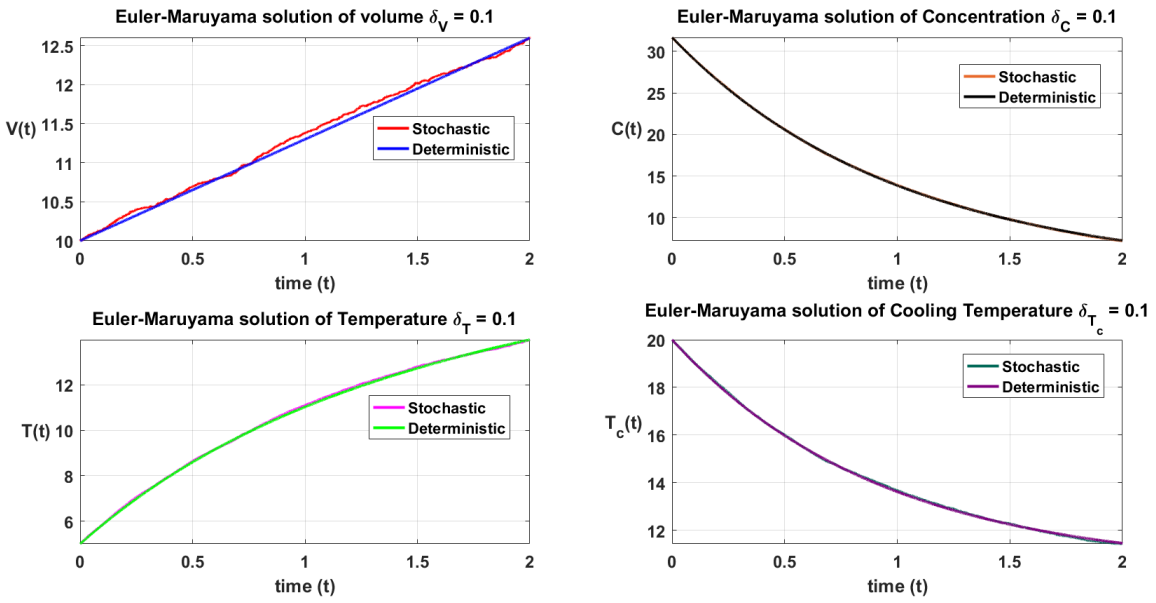

Figure 32: Stochastic solutions of the model Equation (83) obtained by using volatility constants $\delta = \delta_V = \delta_C = \delta_T = \delta_{T_c} = 0.1$ and the corresponding deterministic solutions

Figure 32 illustrates that the low random noise of uncertainty $\delta = 0.1$ that may be present in the CSTR's volume, concentration, temperature and cooling temperature does not much perturb their corresponding normal values as CSTR's physical quantities.

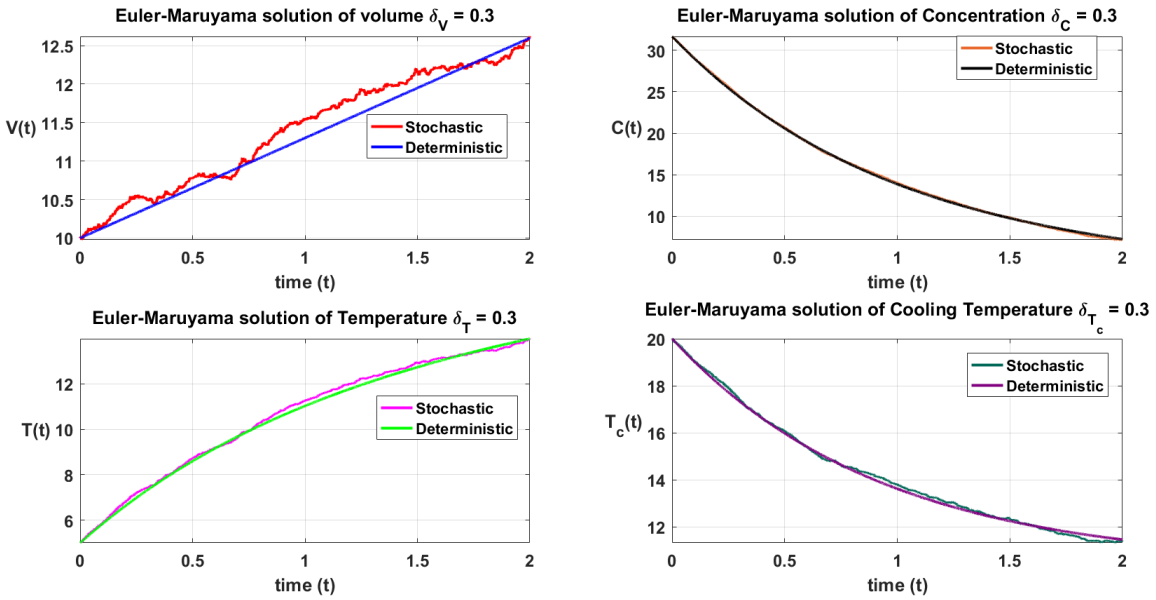

Figure 33: Stochastic solutions of the model Equation (83) obtained by using volatility constants $\delta = \delta_V = \delta_C = \delta_T = \delta_{T_c} = 0.3$ versus numerical solutions of its corresponding deterministic model Equation (35).

The results in Fig. 33 show that the volume is more affected by the uncertainty as compared with the concentration, temperature and the cooling temperature. It can be seen that the random fluctuation $\delta = 0.3$ in the deterministic CSTR model Equation (35) makes the volume values to slightly differ from its corresponding deterministic values as compared with the rest of the CSTR's physical quantities such as the concentration, the temperature and the cooling temperature.

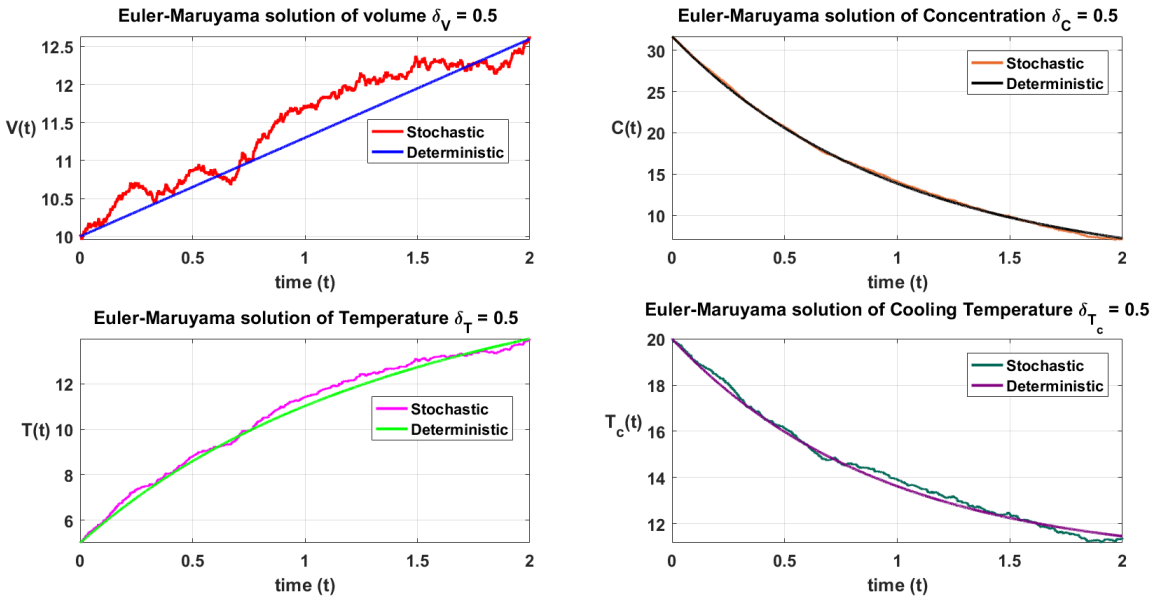

Figure 34: Stochastic solutions of the model Equation (83) obtained by using volatility constants $\delta = \delta_V = \delta_C = \delta_T = \delta_{T_c} = 0.5$ and the corresponding numerical solutions of its deterministic version

The results From Fig. 34 show that the volatility constants equivalent to 0.5 affect the numerical results of the CSTR's volume as compared with the effects in concentration, temperature and the cooling temperature results.

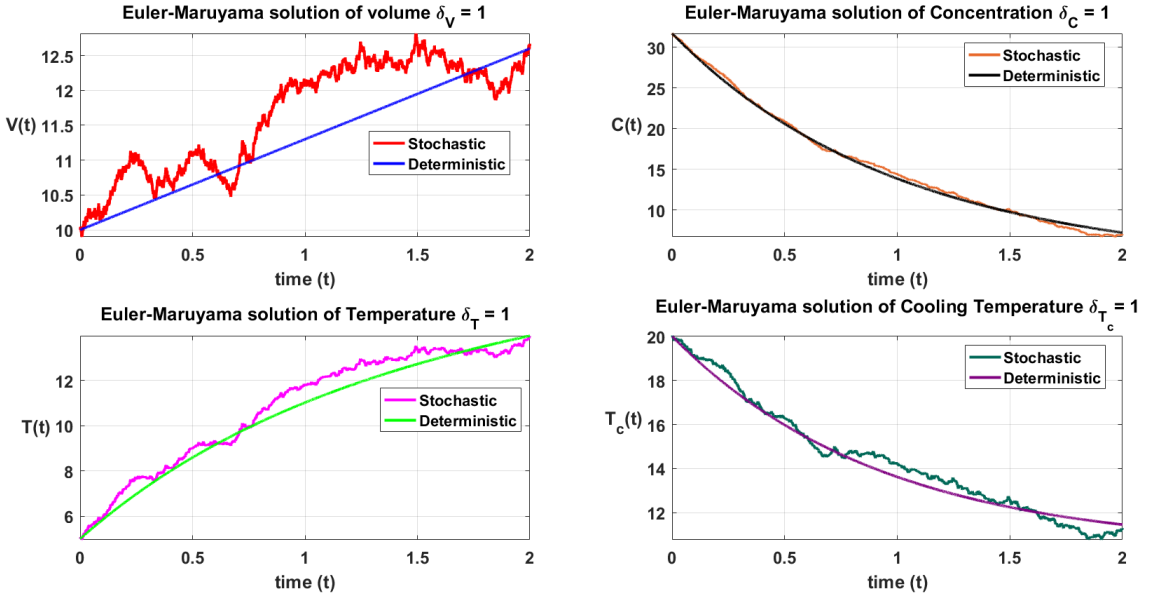

Figure 35: Stochastic solutions of the model Equation (83) obtained by using volatility constants $\delta = \delta_V = \delta_C = \delta_T = \delta_{T_c} = 1$ against numerical solutions of its corresponding deterministic deterministic model that is shown in system of Equations (35)

It can be observed that uncertainty in the tree CSTR's physical quantities, namely, the concentration values, temperature values and the cooling temperature values are not much affected as compared with the volume. For this case, it is expected that the CSTR'S volume values become very sensitive and be influenced by the high magnitude of the uncertainty.

In Fig. 32 - Fig. 35, it can be spotted that the higher the volatility constants values the much fluctuation of the stochastic model and hence this influences much variation between the deterministic and the stochastic CSTR models, especially for the CSTR's volume results. It is a good observation for scenario A, that small fluctuation values which may be present in the formulated CSTR stochastic model make it to behave like its corresponding deterministic model.

4.3.2 Numerical Results for Scenario B

The stochastic model presented in Equation (84) was also numerically simulated by using different volatility values as per scenario A. The numerical results are graphically plotted in Fig. 36 - Fig. 39.

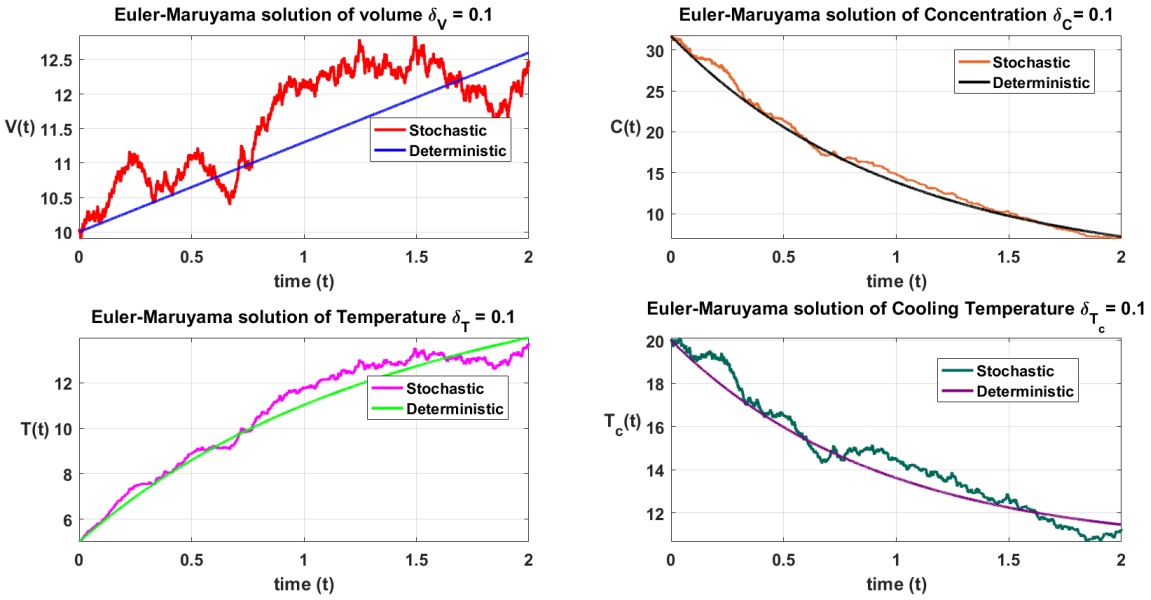

Figure 36: This figure demonstrates and compares stochastic solutions of model Equation(84) obtained by using volatility constants $\delta = \delta_V = \delta_C = \delta_T = \delta_{T_c} = 0.1$ and the analogous deterministic solutions

It can be seen from Fig. 36 that stochastic volume cannot fully capture all the uncertainties in the corresponding deterministic values of the volume whilst the stochastic concentration, temperature and the cooling temperature can capture the uncertainties in their corresponding deterministic curves.

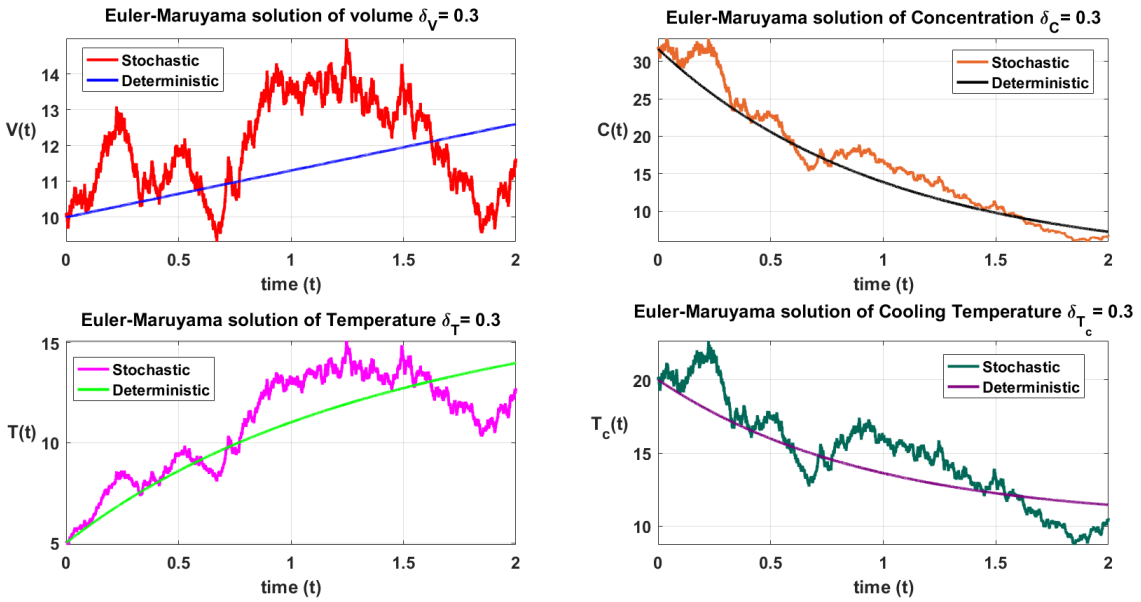

Figure 37: The illustration of stochastic solutions of the model Equation(84) obtained when volatility constants $\delta = \delta_V = \delta_C = \delta_T = \delta_{T_c} = 0.3$ against its deterministic numerical solutions

It is observed from Fig. 37 that all four stochastic CSTR's physical quantities fail to capture their uncertainties around the corresponding deterministic values. It means that the random noise of 0.3 will perturb the deterministic results of the CSTR'S volume, concentration, temperature and the cooling temperature.

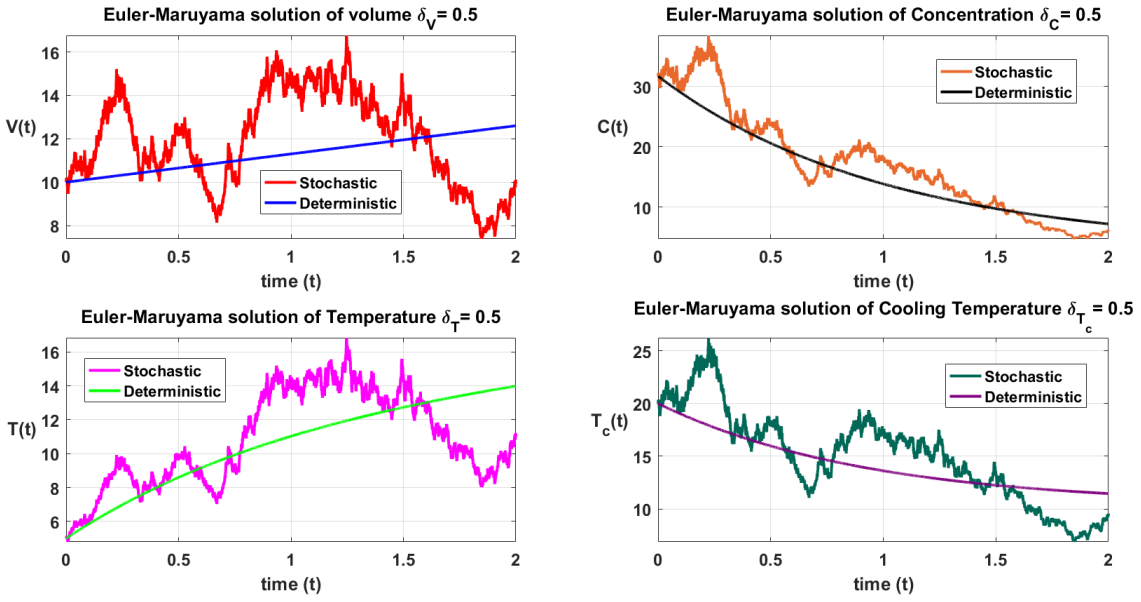

Figure 38: Numerical solutions of the stochastic model Equation(84) obtained when volatility constants are selected to be $\delta = \delta_V = \delta_C = \delta_T = \delta_{T_c} = 0.5$ against the respective deterministic numerical solutions

The same situation as it is in Fig. 37 is observed for Fig. 38, whereby the CSTR's stochastic volume, concentration, temperature and the cooling temperature are not fully capturing the uncertainties in their corresponding deterministic values.

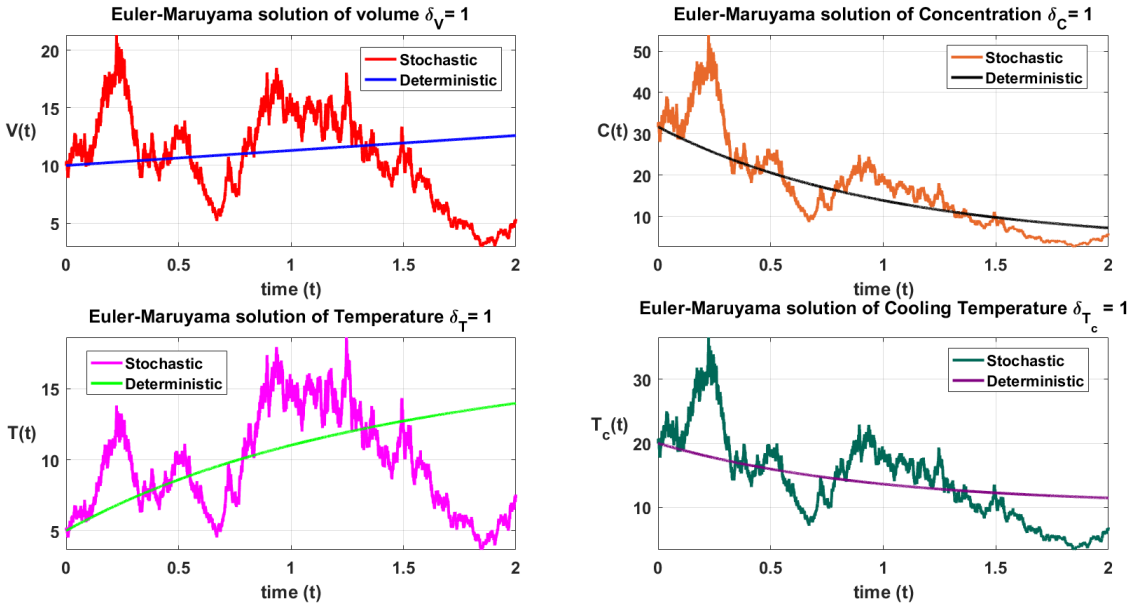

Figure 39: Stochastic solutions of the model Equation(84) which are obtained by using volatility constants $\delta = \delta_V = \delta_C = \delta_T = \delta_{T_c} = 1$ and numerical solutions of the corresponding deterministic model that is presented in Equation (35)

Figures 36, 37, 38, 39 are the numerical solutions of the derived stochastic model Equation (84) that is presented in scenario B and the corresponding numerical solutions of the deterministic model Equation (35). These figures show that small volatility constants values can not easily make the stochastic model to behave like its respective deterministic model. However, as compared with the numerical results obtained in scenario A with the same values of the volatility constants, stochastic model that is constructed in scenario B seems to be very sensitive to small values of the fluctuation constants. This could be an indication of having a high controllability of the physical quantities of the CSTR system model in the avoidance of some small stochastic excitement that may enter into the system if the model presented in scenario B is considered as piloting model during the application. Alternatively, high variation of the solutions may depend on the used scheme. It can be observed that Euler-Maruyama is not an effective method to tackle multiplicative SDEs.

4.3.3 Numerical Results for Scenario C

For this scenario, the parameter k_0 is very important and can be influenced by fluctuations such reactants impurities, environmental conditions and high temperature of the reaction. Therefore, this parameter has been perturbed and becomes $k_0 + \delta\frac{\mathrm{d}B}{\mathrm{d}t}$. Figure 40 - Figure 43 represent the numerical results obtained for the stochastic model Equation (85). The results were produced by considering fluctuation constants $\delta = 0.1, 0.3, 0.5$ and 1 as it has been done for previous scenarios.

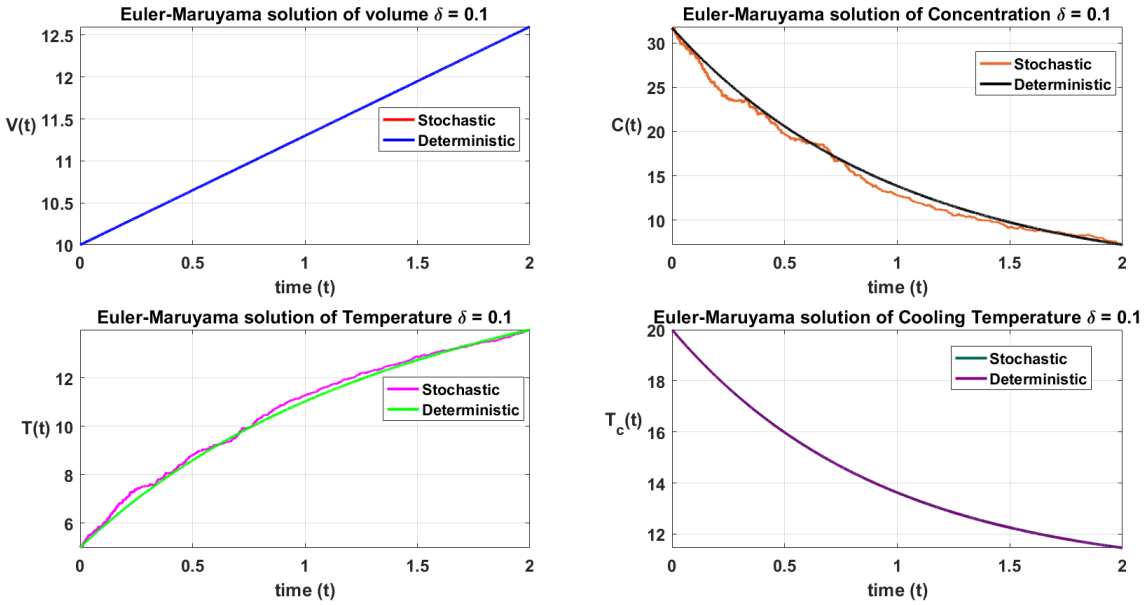

Figure 40: This figure points out stochastic numerical solutions of the model Equation(85) gotten by using volatility constants $\delta = 0.1$ versus numerical solutions of the corresponding deterministic model formulated in Equation (35)

Figure 40 illustrates that the perturbation of the pre-Arrhennius reaction rate together with low fluctuations do not alter the simulated physical values of the CSTR system such as the concentration and the temperature.

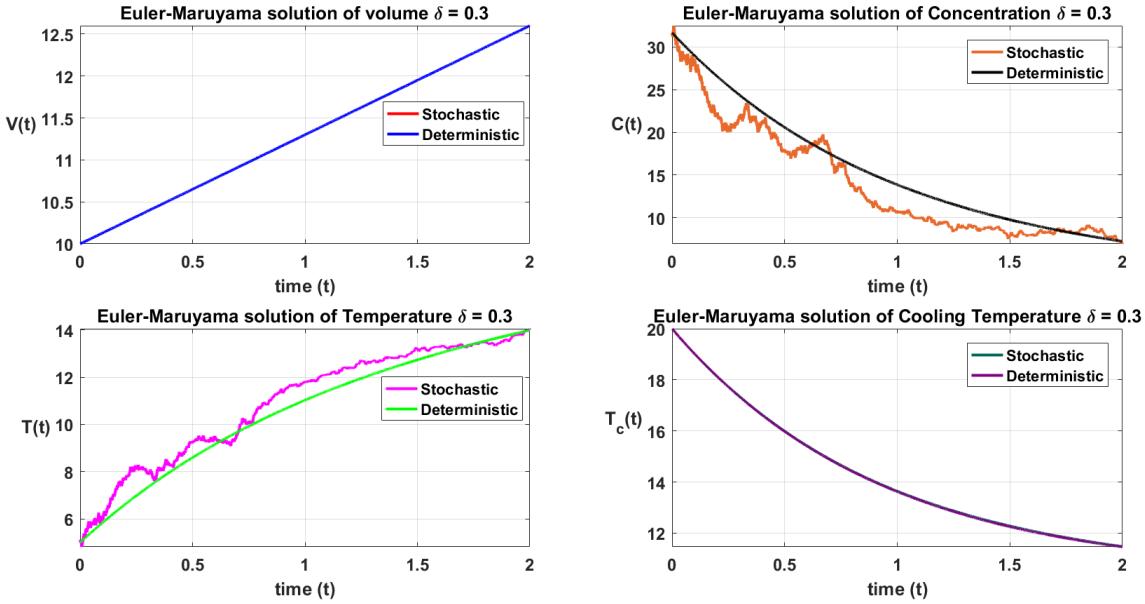

Figure 41: These are stochastic numerical solutions of the model Equation(85) produced by using volatility constants $\delta = 0.3$ against numerical solutions of the corresponding deterministic concentration and the temperature of the model Equation (35)

From Fig. 41, it can be spotted that the perturbation of the pre-Arrhennius reaction rate together with volatility constant $\delta = 0.3$ do not much alter the simulated CSTR's concentration and temperature values.

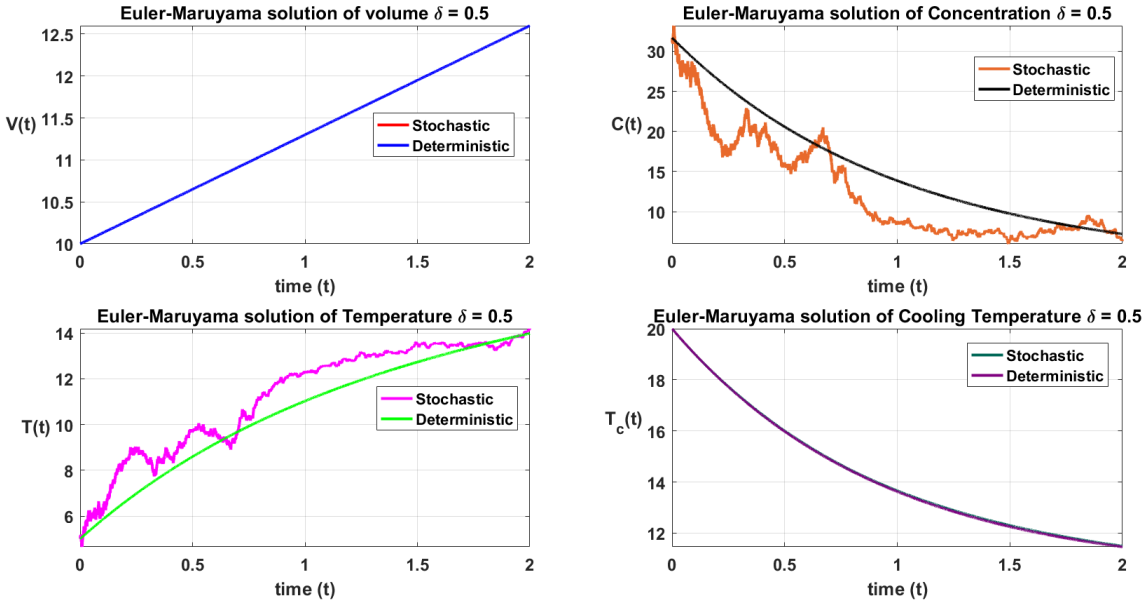

Figure 42: Stochastic numerical solutions of the model Equation(85) produced by using volatility constants $\delta = 0.5$ against its corresponding numerical solutions of the deterministic model presented in Equation (35)

The stochastic results of the physical concentration and the temperature of the CSTR system in Fig. 42 are not in a good agreement with their corresponding deterministic solutions.

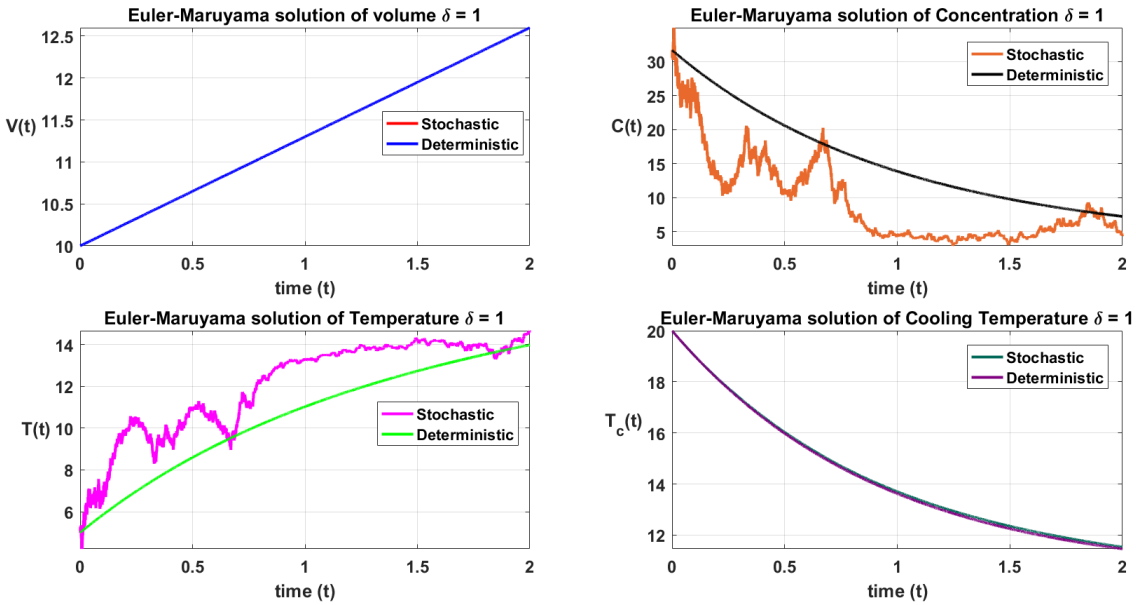

Figure 43: These are numerical results of the stochastic model Equation(85) obtained by using volatility constants $\delta = 1$ against its numerical solutions of the corresponding deterministic model Equation (35)

From Fig. 40 - Fig. 43, it is observed that sample trajectories of the stochastic model Equation (85) follow the results of deterministic model when fluctuation constants becomes small. However, the results displayed have shown stochastic effects on two differential Equations of the system, namely $\frac{\mathrm{d}C}{\mathrm{d}t}$ and $\frac{\mathrm{d}T}{\mathrm{d}t}$. This is because parameter k_0 appears in only those two mentioned differential Equations and this conducts to partial perturbation of the model.

4.3.4 Numerical Results for Scenario D

Numerical solutions of the stochastic model that is shown in system of Equations (89) were obtained in Fig. 44. This Figure shows that the uncertainty affects much more the CSTR's volume than the rest of the physical quantities of the system.

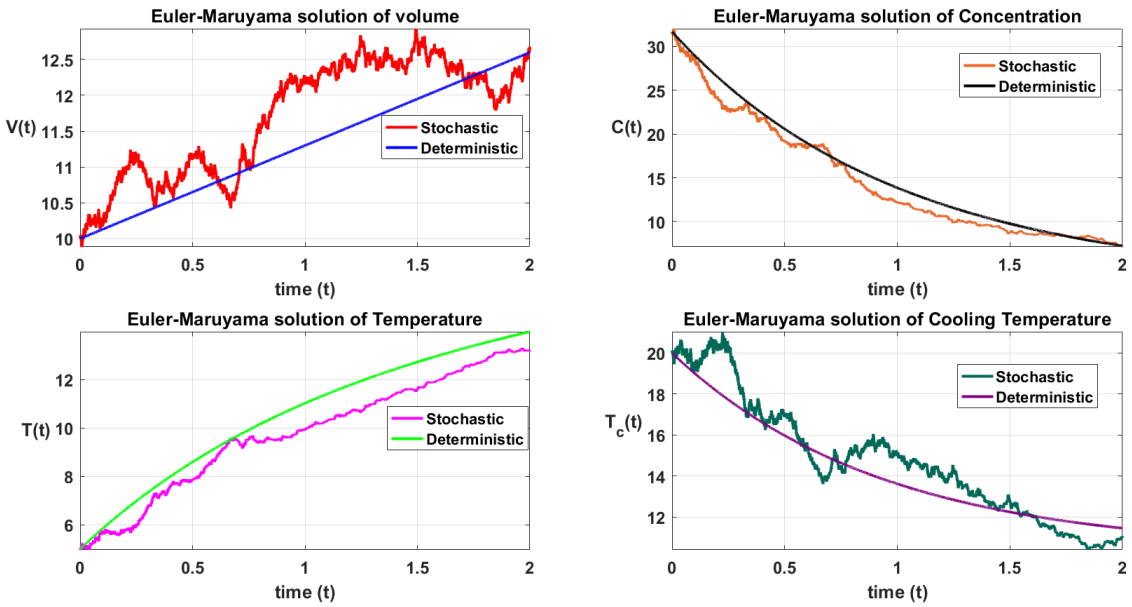

Figure 44: The plot that is illustrating stochastic numerical results of the system of Equations (89) against the corresponding deterministic numerical solutions of the model Equation (35)

To obtain the results in Fig. 44, the parameters, $F_{\text{in}} = 1.3; F = 1.3; F_{\text{out}} = 1.3 \times 10^{-4}; k_0 = 0.9; E = 0.5; T_{\text{mean}} = 29.815; H^* = -1004.3 \times 10^{-3}; \rho = 1; C_p = 4.186; U = 10; A = 0.015; F_c = 46.56 \times 10^{-2}; V_c = 50 \times 10^{-2}; \rho_c = 1; C_{p_c} = 4.186; T_{c_{\text{in}}} = 10; R = 8.341; C_{\text{in}} = 31.68; T_{\text{in}} = 20.0;$ step size for time $h = 2/10000;$ step size for Brownian $\xi = 2/80000$ have been fixed and the initial solutions of the model were fixed to be $X_0 = [10; 31.68; 5; 20]$.

4.4 Numerical Analysis of Endothermic CSTR Stochastic Models

In the same way, numerical analyses of the endothermic stochastic models which are presented in system of Equations (90) for scenario A, (91) for scenario B, (92) for scenario C, and (96) for scenario D are performed. The obtained stochastic numerical results and the corresponding deterministic numerical solutions from numerical simulations are graphically displayed in Fig. 45 - Fig. 48 for scenario A, Fig. 49 - Fig. 52 for scenario B, Fig. 53 - Fig. 56 for scenario C and Fig. 57 for scenario D.

4.4.1 Numerical Results for Scenario A

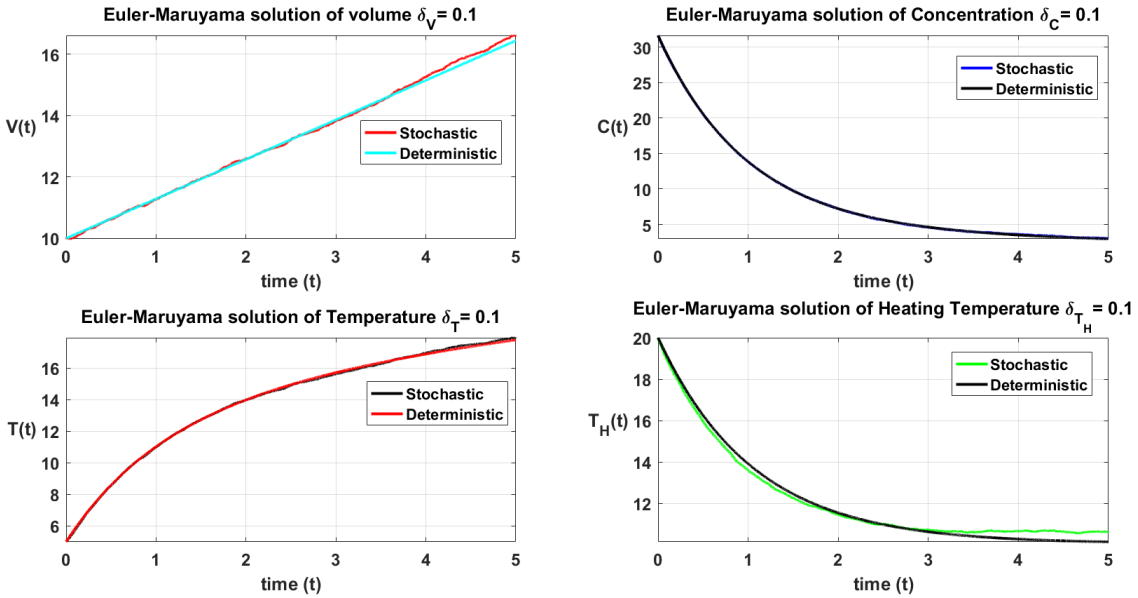

Figure 45: Stochastic numerical solutions of the model Equation (90) acquired by using fluctuation constants $\delta = \delta_V = \delta_C = \delta_T = \delta_{T_H} = 0.1$ and numerical results of the deterministic model Equation (36)

In Fig. 45, the endothermic CSTR's stochastic results of the volume, the concentration, the temperature and the heating temperature are in a good agreement with their corresponding deterministic CSTR's physical quantities.

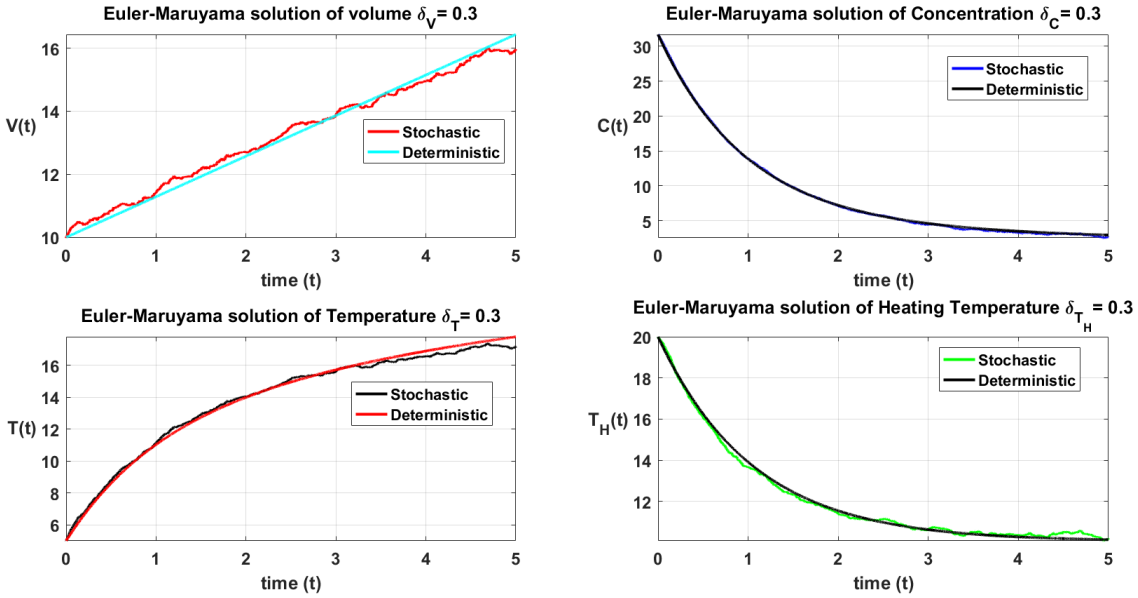

Figure 46: Stochastic numerical solutions of the model Equation (90) acquired by using fluctuation constants $\delta = \delta_V = \delta_C = \delta_T = \delta_{T_H} = 0.3$ and numerical results of the deterministic model Equation (36)

According to the results obtained in Fig. 46, the perturbation of the endothermic CSTR's state variables with the fluctuation constants $\delta = 0.3$ does not significantly affect the CSTR's volume, concentration, temperature and the heating temperature.

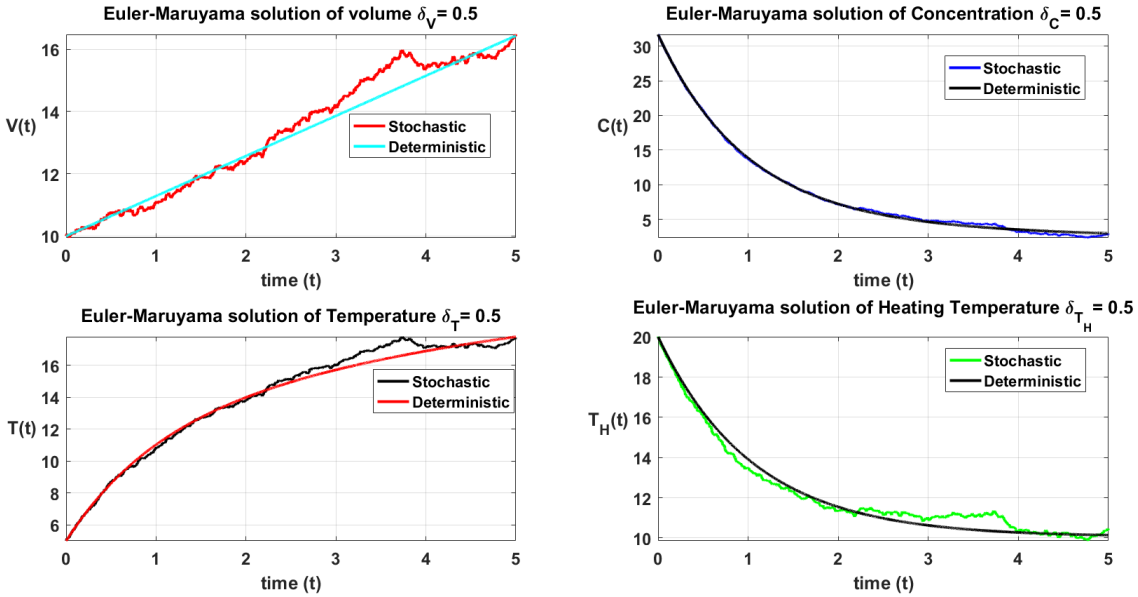

Figure 47: Stochastic numerical solutions of the model Equation (90) acquired by using fluctuation constants $\delta = \delta_V = \delta_C = \delta_T = \delta_{T_H} = 0.5$ and numerical results of the deterministic model Equation (36)

In Fig. 47, it is observed that the stochastic solutions of the volume, concentration, temperature and the heating temperature capture the uncertainties around the corresponding deterministic numerical results.

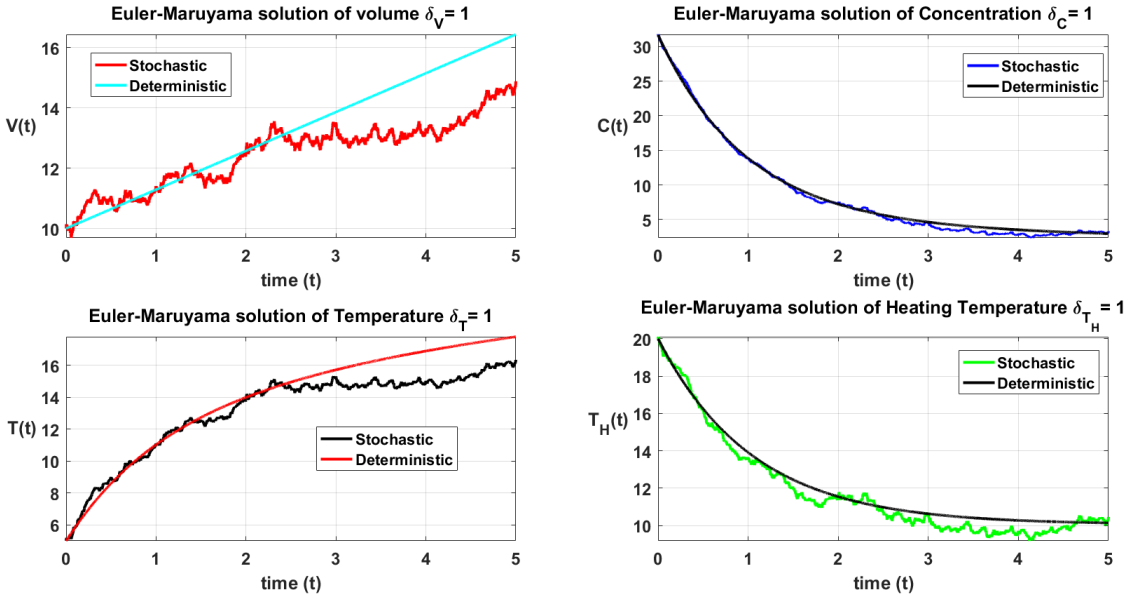

Figure 48: Stochastic numerical solutions of the model Equation (90) acquired by using fluctuation constants $\delta = \delta_V = \delta_C = \delta_T = \delta_{T_H} = 1$ and numerical results of the deterministic model Equation (36)

From Fig. 45 - Fig. 48, it can be observed that the stochastic numerical results of the CSTR's volume, concentration, temperature and the heating temperature agree with its corresponding deterministic results provided that the volatility constants are small. This makes both deterministic and non-deterministic results of the CSTR's state variables to coincide.

4.4.2 Numerical Results for Scenario B

The formulated stochastic model Equation (91) is numerical solved and analysed by using Euler-Maruyama method and the obtained numerical solutions are shown in Fig. 49 - Fig. 52.

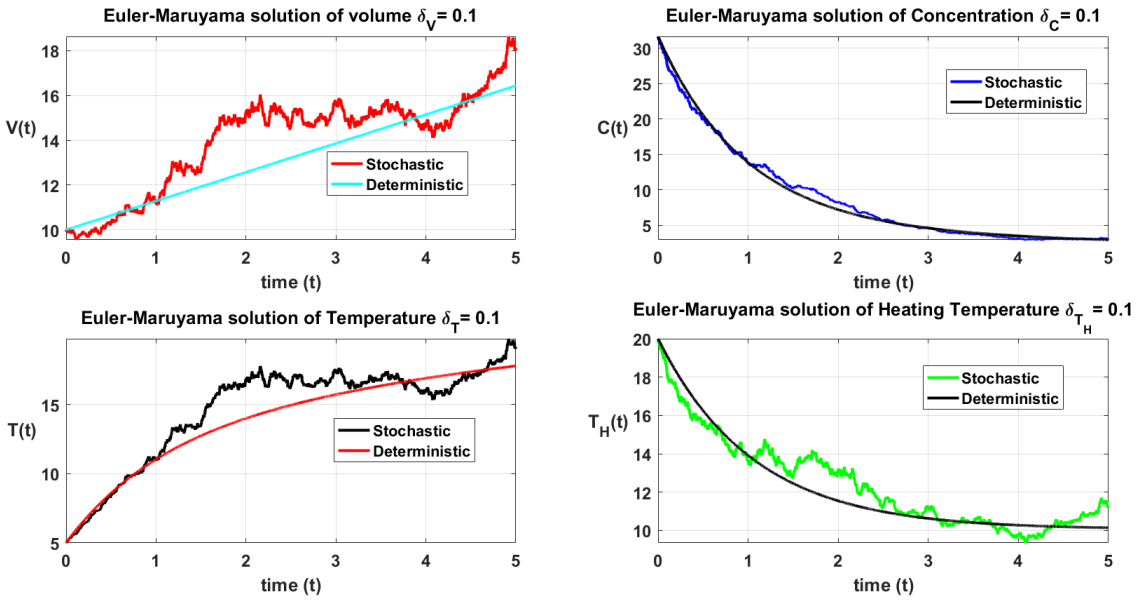

Figure 49: Stochastic numerical solutions of the model Equation (91) produced by using fluctuation constants $\delta = \delta_V = \delta_C = \delta_T = \delta_{T_H} = 0.1$ and numerical results of the deterministic model Equation (36)

The numerical results of multiplicative stochastic model in Fig. 49 show that only the concentration agrees with its corresponding deterministic solution. The stochastic results for the other three CSTR state variables (volume, temperature and the heating temperature) do not agree with their deterministic values respectively.

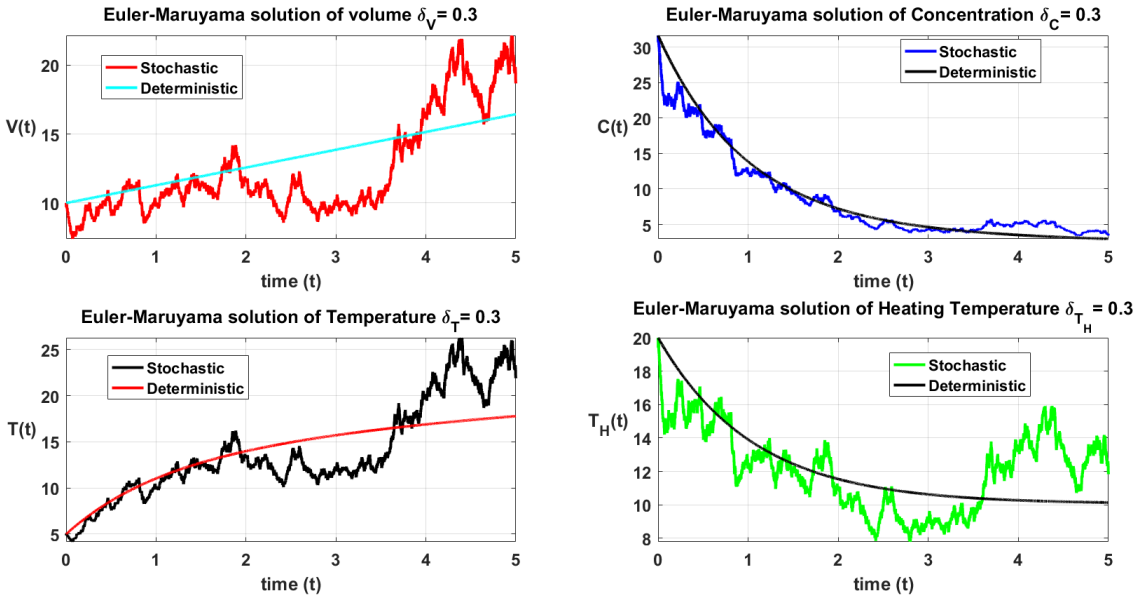

Figure 50: Stochastic numerical solutions of the model Equation (91) produced by using fluctuation constants $\delta = \delta_V = \delta_C = \delta_T = \delta_{T_H} = 0.3$ and numerical results of the deterministic model Equation (36)

In Fig. 50, the volatility constants of 0.3 in the multiplicative SDE affect the volume, temperature and the heating temperature of the deterministic CSTR with the endothermic reaction.

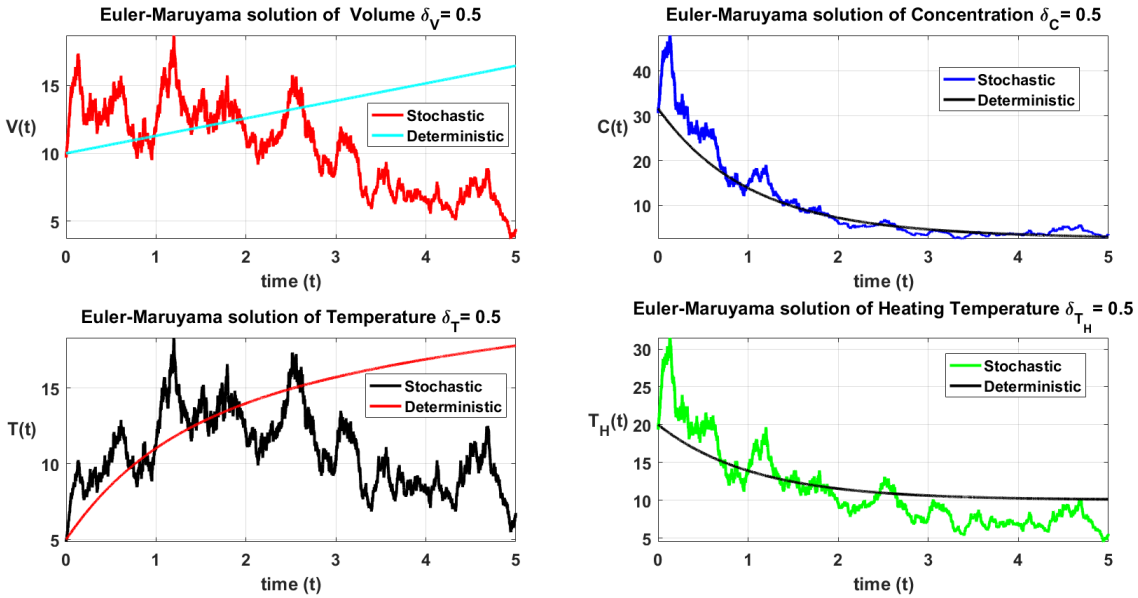

Figure 51: Stochastic numerical solutions of the model Equation (91) produced by using fluctuation constants $\delta = \delta_V = \delta_C = \delta_T = \delta_{T_H} = 0.5$ and numerical results of the deterministic model Equation (36)

Depending on the results obtained in Fig. 51, it can be seen that the volatility constants $\delta = 0.5$ perturb all the endothermic CSTR state variables, namely, the volume, the concentration, the temperature and the heating temperature of the system.

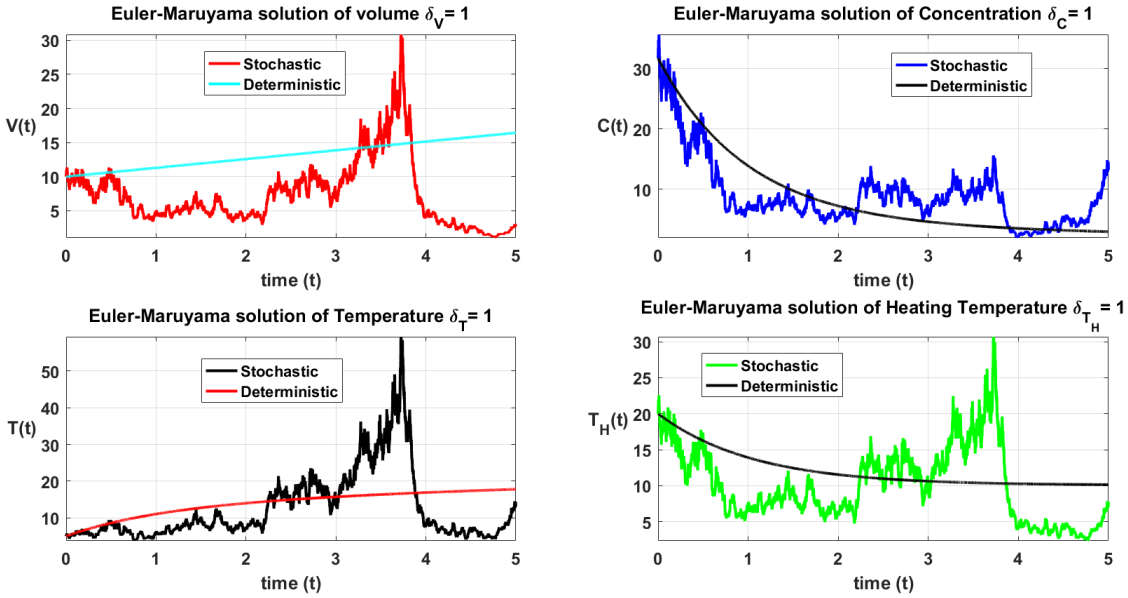

Figure 52: Stochastic numerical solutions of the model Equation (91) produced by using fluctuation constants $\delta = \delta_V = \delta_C = \delta_T = \delta_{T_H} = 1$ and numerical results of the deterministic model Equation (36)

Similarly, much variations of solutions are seen in Fig. 49 - 52 as the volatility constants becomes bigger. This is the same situation as for Scenario B in Section 4.3. Thus, Euler-Maruyama method is not an effective method to numerically solve the multiplicative SDEs.

4.4.3 Numerical Results for Scenario C

Figures 53 - 56 encapsulate the numerical results of both stochastic model that is shown in Equation (92) and its corresponding deterministic numerical solutions of model Equation (36).

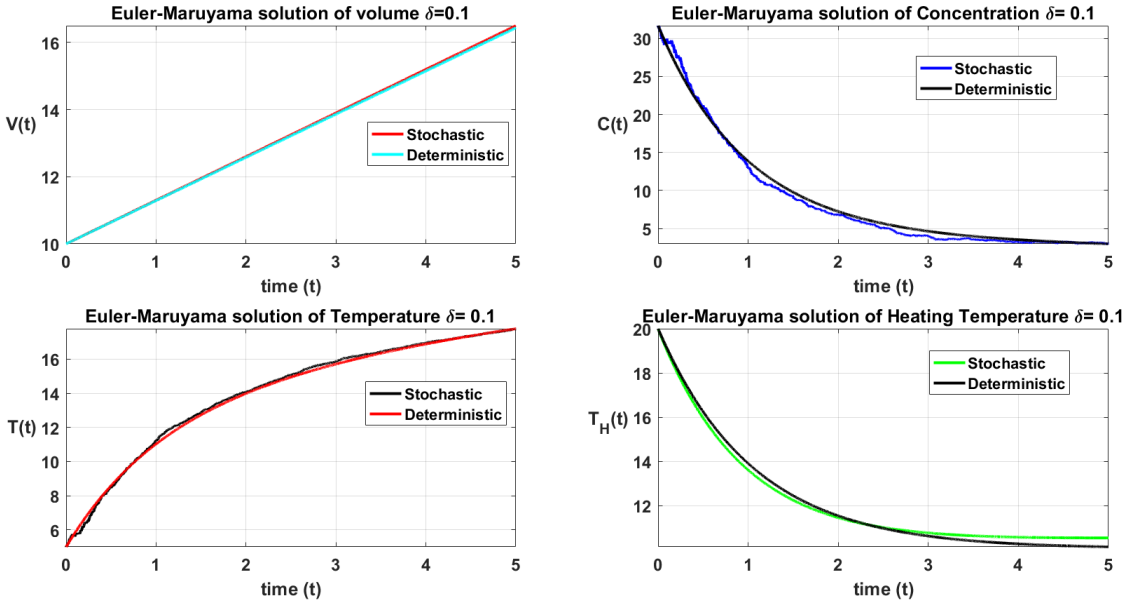

Figure 53: Stochastic numerical solutions of the model Equation (92) obtained when fluctuation constant $\delta = 0.1$ in comparison with the numerical solutions of the corresponding deterministic model presented in (36)

The numerical results that are shown in Fig. 53 reveal that the CSTR's concentration and the heating temperature are not significantly affected by the perturbation of the pre-Arrhennius reaction rate k_0 with the volatility constant $\delta = 0.1$.

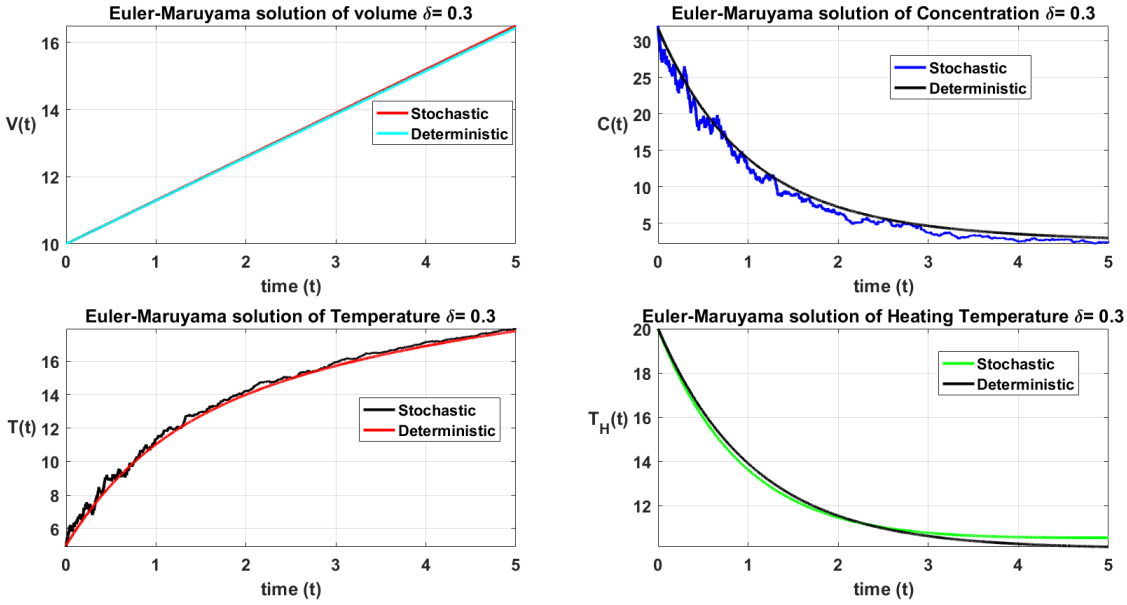

Figure 54: Stochastic numerical solutions of the model Equation (92) obtained when fluctuation constant $\delta = 0.3$ in comparison with the numerical solutions of the corresponding deterministic model presented in (36)

The perturbation of the pre-Arrhennius reaction rate with the fluctuation constant $\delta = 0.3$ leads to the same results of volume, concentration, temperature and the heating temperature for both deterministic and stochastic model Equations (36) and (92) respectively.

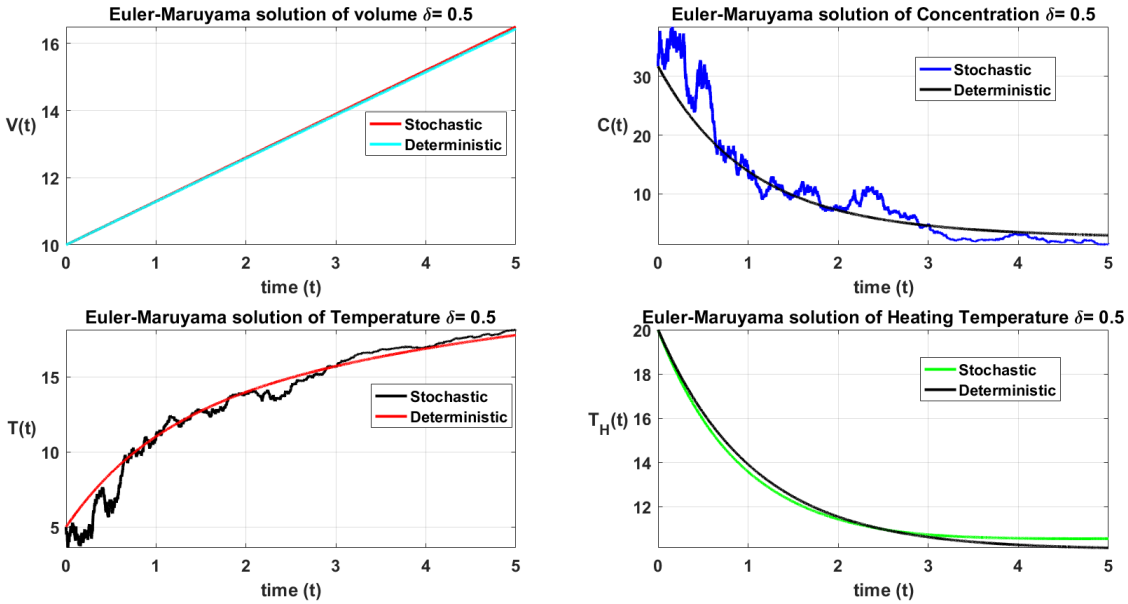

Figure 55: Stochastic numerical solutions of the model Equation (92) obtained when fluctuation constant $\delta = 0.5$ in comparison with the numerical solutions of the corresponding deterministic model presented in (36)

Based on the results obtained in Fig. 55, it can be noticed that the perturbation of the pre-Arrhennius reaction rate in the model Equation (36) with the volatility constant $\delta = 0.5$ have effects on the two CSTR's state variables such as the concentration and the temperature.

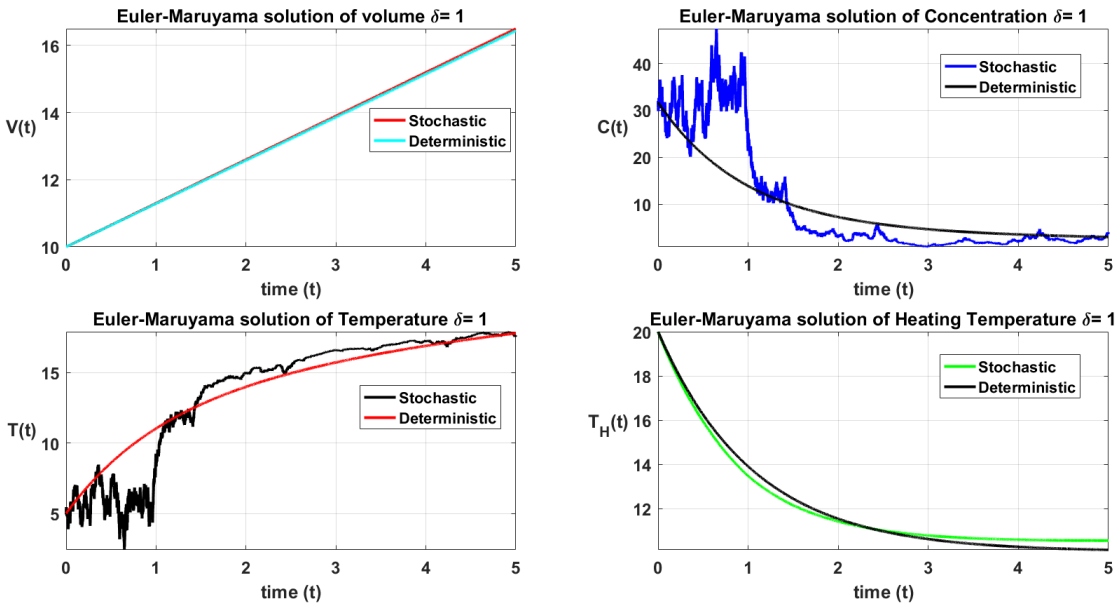

Figure 56: Stochastic numerical solutions of the model Equation (92) obtained when fluctuation constant $\delta = 1$ in comparison with the numerical solutions of the corresponding deterministic model presented in (36)

The perturbation of the pre-Arrhennius reaction rate by the fluctuation constant value 1 in the CSTR's model Equation (36) leads to high variation between stochastic and deterministic concentration and temperature of the CSTR system.

From Fig. 53 to Fig. 56, the results show that the perturbation of the pre-Arrhennius temperature dependent parameter k_0 still produce good results given that small values of the volatility constants are considered in the CSTR deterministic physical values of the concentration and the temperature.

4.4.4 Numerical Results for Scenario D

The Numerical results for this scenario is given in Fig. (57).

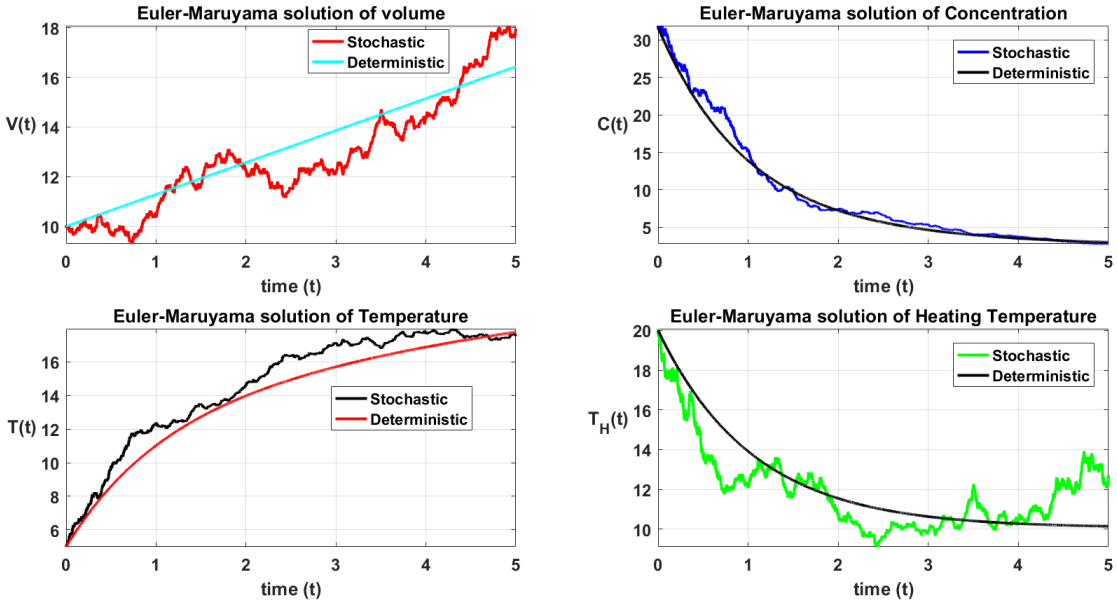

Figure 57: The plot is showing Euler-Maruyama stochastic solutions of the model Equation (96) and deterministic solutions of model Equation (36)

For this case, parameters used in the simulations are $F_{\text{in}} = 1.3; F = 1.3; F_{\text{out}} = 1.3\times10^{-4}; k_0 = 0.9; E = 0.5; T_{\text{mean}} = 29.815; H^* = 1004.3 \times 10^{-3}; \rho = 1; C_p = 4.186; U = 10; A = 0.015; F_H = 46.56\times10^{-2}; V_H = 50\times10^{-2}; \rho_H = 1; C_{p_H} = 4.186; T_{H_{\text{in}}} = 10; R = 8.341; C_{\text{in}} = 31.68; T_{\text{in}} = 20.0;$ step size for time $h = 5/10000;$ step size for Brownian $\xi = 5/80000$ and the initial solutions of the model are fixed as $X_0 = [10; 31.68; 5; 20]$.

As there is a sum of more than one diffusion parts with square root of volatility constants in the CSTR's model, this significantly make the CSTR stochastic physical quantities to differ from their corresponding CSTR's deterministic physical quantities for high values of the fluctuation constants.

4.5 Illustrative Example of Reaction Taking Place in CSTR as an Experimental Application

From chemical reaction point of view, the process of decomposition of a substance with water is called hydrolysis. Then, consider a fictitious but a real experiment of hydrolysis of acetic anhydride that forms the acetic acid (vinegar) in a CSTR of volume $1000m^3$. The introductory concentration feed is $2.6mol/m^3$ for the acetic anhydride and $50mol/m^3$ for water. The reaction rate k is approximately estimated to $0.0095m^3/mol.min$ and the feed flow is $15m^3/min$. Since

the reaction is exothermic, the CSTR is covered by the outer cooling jacket of volume $V_c = 2000m^3$ with the heat transfer coefficient $U = 10^3$. The cross-sectional area between CSTR and the cooling jacket is designed to be $S = 0.2m^2$ and the cooling volumetric flow F_c is $5m^3/min$ while the coolant density is $\rho_c = 997$. Specific heat capacities of the acetic acid and the coolant are 2043 and 4200 respectively. The heat produced from the reaction during the mixing is $-55.1kJ/mol$ at 60^oC with the coolant temperature at 20^oC and the activation energy which is equivalent to $-52.88kJ/mol$. If the reaction balance equation is chemically given by:

$$(CH_3CO)_2O + H_2O \rightleftarrows 2CH_3COOH, \tag{112}$$

and the reaction is considered to be first order in acetic anhydride and first order in water, then,

(i) Formulate a mathematical model for the reaction

(ii) Compute the fractional conversion of the acetic anhydride into the acetic acid

(iii) Graphically display the change of concentrations and temperature dynamics for the above experiment.

Solution

Let A represents the acetic anhydride, B be the water and C be the product which is acetic acid (vinegar). Since we are interested in the forward reaction of the balance Equation (112), then the reaction formula is given by:

$$A + B \rightarrow 2C, \tag{113}$$

with the following given data and unknowns with a question mark
$C_{A_0} = 2.6$, $C_A =?$, $C_{B_0} = 50$, $C_B =?$, $k = 0.0095$, $\chi_A =?$, $V = 1000$, $\chi_B =?$, $F_0 = 15$, $T =?$, $H^* = -55.1$, $T_c =?$, $E = -52.886$, $T_{c_0} = 20^oC = 293.15^oK$, $F_c = 5$, $U = 10^3$, $S = 0.2m^2$, $C_{p_c} = 4200$, $C_p = 2043$, $\rho = 1050$,$\rho_c = 997$, $T_0 = 60^oC = 333.15^oK$, $V_c = 2000$.
(i) Mathematical model that describes the dynamics of the above reaction in CSTR can be

formulated as follow:

$$\begin{cases} \frac{\mathrm{d}C_A}{\mathrm{d}t} = \frac{F_0}{V}(C_{A_0} - C_A) - kC_AC_B, \\ \frac{\mathrm{d}C_B}{\mathrm{d}t} = \frac{F_0}{V}(C_{B_0} - C_A) - kC_AC_B, \\ \frac{\mathrm{d}T}{\mathrm{d}t} = \frac{F_0}{V}(T_0 - T) + \frac{-H^*kC_AC_B}{\rho C_p} - \frac{US}{\rho C_pV}(T - T_c), \\ \frac{\mathrm{d}T_c}{\mathrm{d}t} = \frac{F_c}{V_c}(T_{c_0} - T_c) + \frac{US}{\rho_c C_{p_c} V_c}(T - T_c). \end{cases} \tag{114}$$

(ii) The acetic anhydride reactant conversion occurs at the steady-state, and then $\frac{\mathrm{d}C_A}{\mathrm{d}t} = \frac{\mathrm{d}C_B}{\mathrm{d}t} = 0$. Therefore,

$$\begin{cases} F_0C_{A_0} - F_0C_A - kC_AC_BV = 0 \equiv 39 - 15C_A - 9.5C_AC_B = 0 \\ F_0C_{B_0} - F_0C_B - kC_AC_BV = 0 \equiv 750 - 15C_B - 9.5C_AC_B = 0 \end{cases} \tag{115}$$

The system of Equations (115) is solved simultaneously. By solving for C_B from the first Equation of the system (115), we get

$$C_B = \frac{39 - 15C_A}{9.5C_A}. \tag{116}$$

Substituting the Equation (116) into the second Equation of the system (115), results to

$$750 - 15\frac{(39 - 15C_A)}{9.5C_A} - 9.5\frac{(39 - 15C_A)}{9.5C_A} = 0. \tag{117}$$

So, the simplified form of the Equation (117) leads to a quadratic polynomial in C_A variable presented in Equation (118) as follow,

$$142.50C_A^2 + 6979.5C_A - 585 = 0. \tag{118}$$

After solving the quadratic polynomial (118), the following results are obtained:

$$C_{A_1} = 0.083674mol/m^3,$$

$C_{A_2} = -49.063mol/m^3$ (to be rejected because in reality the concentration can not be negative).

Therefore, $C_A = 0.083674mol/m^3$ and $C_B = 47.484mol/m^3$.

As a result, the acetic anhydride fractional conversion into acetic acid in the presence of water of concentration $47.484mol/m^3$ is given by

$$\chi_A = \frac{C_{A_0} - C_A}{C_{A_0}} = \frac{2.6 - 0.083675}{2.6} = 0.96782.$$

It is clear that 96.782% of acetic anhydride is converted into product (vinegar). The remaining acetic anhydride portion equivalent to 3.218% is not converted into vinegar. This can be interpreted as impurity or more water is needed for a total conversion.

(iii) The simulation results that supplement the above calculations are graphically displayed in Fig. 58.

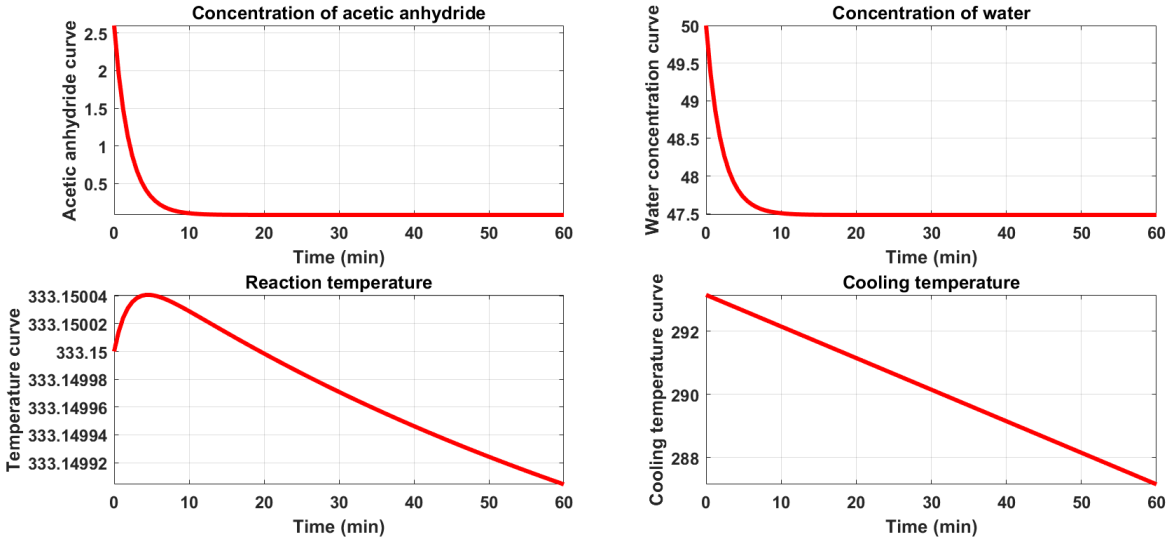

Figure 58: Simulation of the real example of formation of acetic acid (vinegar) from acetic anhydride and water.

From Fig. 58, it can be seen that the reactant concentration, which is the concentration of acetic anhydride, approaches $0.083674mol/m^3$ as the concentration of water becomes $47.484mol/m^3$ after $10min$ of the starting of the reaction (see sub-plots 1 and 2 of Fig. 58). The reaction temperature starts increasing and then returns to its lower temperature point due to the cooling effect. As a result, the vinegar production experiment from acetic anhydride and water was numerically simulated and the numerical solutions show that the optimal fractional conversion of 96.782% of vinegar from acetic anhydride is reached.

CHAPTER FIVE

CONCLUSION AND RECOMMENDATIONS

5.1 Conclusion

The aim of the current study was to develop deterministic and non-deterministic mathematical models for continuously stirred tank reactor (CSTR) and use the statistical and Bayesian methods to analyse and estimate the unknown physical parameters. The perturbed exothermic and endothermic CSTRs' mathematical models, for deterministic and stochastic, were formulated by using the Reynold transport theorem. This was an achievement of the first specific objective of this research project. The analyses of the formulated models, numerical simulations, parameters estimation and the determination of the effectiveness of different numerical methods in solving these models were achieved by using several statistical and Bayesian approaches. The methods used for parameters estimation were the classical least squares and Delayed-Rejection Adaptive Metropolis method which is the version of the Markov chain Monte Carlo (MCMC) methods. The partial rank correlation coefficients (PRCCs) with the Latin-Hypercube sampling technique was used for the sensitivity analysis and uncertainty quantification of the estimated parameters on models responses. The Euler-Maruyama method has been used as the numerical scheme for solving all formulated CSTR stochastic models which are presented in Chapter 3 of this dissertation. The results from the least squares showed that the models' estimates can be well fitting the theoretical models, provided that the noise intensity is minimized and ranges between 0 and 0.5. Moreover, the deterministic models' parameters identifiability, their statistical inferences and their credible intervals computed at the probability of 95% were obtained through MCMC results. The assessment of the effect of perturbation on the CSTRs' models was achieved by applying small Gaussian noises in the simulations of the deterministic models and by examining the effect of fluctuations in the stochastic models. It was observed that small perturbations in the CSTR deterministic models and the increase of fluctuations in the CSTR stochastic models can make the models' solutions to oscillate and significantly deviate from the corresponding theoretical deterministic models' solutions. As the state of the art, there must be always controllability and filtering of the noise of high magnitude that may enter the CSTR system from different sources. Furthermore, through simulations, it was observed that the deformation of the tanks is mainly based on the increase of the volume and it is possible

whenever the flow-out rate of input reactants exceeds the removal rate of the products. To address this problem there must be either a certain specific design of the tanks such that residence time of the products inside the tanks is taken into account or always make the removal rate to be at least faster than the supply rate or make the two to be at a constant rate. To simulate an actual real-life chemical problem as an application of CSTRs, the analytical and numerical experiments on the real life problem of production of vinegar (acetic acid) from water and the acetic anhydride was used. From the numerical simulations, it was observed that a portion of acetic anhydride remained unconverted and so, the full conversion into vinegar needs more water. The formulated CSTRs' models have been validated through simulations, model fitting, uncertainty quantification and sensitivity analyses whereby seven parameters were found to be highly correlated with the model Equation (35) while six parameters of the model Equation (36) highly correlated with it. All findings and contributions made in this dissertation can be used as a source of prior information for design engineers and scientists to correctly and effectively design suitable CSTRs without preliminary mathematical quantifications of variables and parameters which may be very costive. Therefore, the formulated models can be very useful in the description and modelling of the dynamics of various mechanical, chemical and biological systems.

5.2 Recommendations

Mathematical modelling approach is appreciated to solve and simulate challenging real life problems in science and engineering. Designing and development of manufacturing prototypes and physical tests are always very expensive. Mathematical and numerical models make it easy to analyse complex industrial problems. Within prior investment, industrialists prefer to use numerical modelling and simulations in design and development of their work, to analyse, optimise and verify the performance of designs. Thus, numerical models provide reliable and accurate simulations to mimic the real physical problem. Therefore, from this research, the following four recommendations are made.

(i) The formulated mathematical models and their estimated quantitative values provided in this dissertation can be industrially tested to get an insight of how they work. For instance, whenever possible in future, one can get real data from industry and try to fit those data to the formulated models for the prediction.

(ii) The formulated models can be adopted or extended whenever possible. For example, the formulated CSTR models can be extended to model a group of several connected CSTRs to switch from simple production to chain production.

(iii) Multiplicative stochastic differential equation (MSDE), refers to scenarios B, needs an effective stochastic scheme. It will be interesting to have a numerical scheme developed for simulating MSDE as Euler-Maruyama was not effective for providing good results.

(iv) Due to time constraint and the wideness of the project, researchers have been unable to estimate the parameters in stochastic models. Estimating parameters in stochastic models can be a whole separate topic in mathematics. This task is intended to be conducted in the future work.

REFERENCES

Aboelela, M. A., & Hennas, R. H. M. (2018). Development of a fractional-order pid controller using adaptive weighted pso and genetic algorithms with applications. *In:* Fractional Order Systems. Elsevier.

Ahmed, A., Gasmelseed, G., Karama, A., & Musa, A. (2013). Cascade control of a continuous stirred tank reactor (cstr). *Journal of Applied and Industrial Sciences*, **1**(4), 16–23.

Akiti, O. (2000). Turbulent mixing and chemical reaction in baffled stirred tank reactors: A comparison between experiments and a novel micromixing-based computational fluid dynamics model. New Jersey Institute of Technology.

Al-Araji, A. S. (2015). Modeling of continuous stirred tank reactor based on artificial neural network. *Al-Nahrain Journal for Engineering Sciences*, **18**(2), 202–207.

Allen, E. (2007). Modeling with Itô stochastic differential equations. Springer Science & Business Media.

Allen, L. J. (2017). A primer on stochastic epidemic models: Formulation, numerical simulation, and analysis. *Infectious Disease Modelling*, **2**(2), 128–142.

Baddour, N. (2008). Hamilton's principle for the derivation of equations of motion. Nova Science Publishers.

Ballesteros-Moncada, H., Herrera-López, E. J., & Anzurez-Marín, J. (2015). Fuzzy model-based observers for fault detection in cstr. *ISA Transactions*, **59**, 325–333.

Barnard, J. (1985). Types of ideal reactor. *In:* Comprehensive Chemical Kinetics. Elsevier.

Bird, R., Stewart, W., & Lightfoot, E. (2007). Transport phenomena, 2^{nd} Ed. New York, ny: John Wilwe & Sons.

Brooks, S. (1998). Markov chain monte carlo method and its application. *Journal of the Royal Statistical Society: Series D (the Statistician)*, **47**(1), 69–100.

Buehler, E. A., Paulson, J. A., & Mesbah, A. (2016). Lyapunov-based stochastic nonlinear model predictive control: Shaping the state probability distribution functions. In: *2016 American Control Conference (ACC)*. IEEE.

Burghardt, A. (2008). Mass transfer by diffusion.

Cahyari, K., Syamsiah, S., & Prasetya, A. (2016). Performance of continuous stirred tank reactor (cstr) on fermentative biohydrogen production from melon waste. In: *Materials Science and Engineering Conference Series*.

Couper, J. R., Penney, W. R., & Fair, J. R. (2009). Chemical Process Equipment-Selection and Design (Revised 2nd Edition). Gulf Professional Publishing.

Cui, M. H., Cui, D., Gao, L., Cheng, H. Y., & Wang, A. J. (2016). Efficient azo dye decolorization in a continuous stirred tank reactor (cstr) with built-in bioelectrochemical system. *Bioresource Technology*, **218**, 1307–1311.

Danish, M., Al Mesfer, M. K., & Rashid, M. (2015). Effect of operating conditions on cstr performance: An experimental study. *International Journal of Engineering Research and Applications*, **5**(2), 74–78.

Dias, R. C., & Costa, M. R. P. (2005). Transient behavior and gelation of free radical polymerizations in continuous stirred tank reactors. *Macromolecular Theory and Simulations*, **14**(4), 243–255.

Emmanuel, N. (2017). Pharmaceuticals factory to reduce 20% of rwanda's drug imports. `https://www.newtimes.co.rw/section/read/225685`. Accessed: 2019-10-22.

Etchells, J. (2005). Process intensification: Safety pros and cons. *Process Safety and Environmental Protection*, **83**(2), 85–89.

Finlayson, B. A. (2012). Introduction to chemical engineering computing. John Wiley & Sons.

Fonseca, L. J. P. (2019). Upscaling of mixing-limited chemical reactions from pore to continuum scale using the dispersive lamella concept. PhD thesis. Spanish National Research Council.

Foutch, G. L., & Johannes, A. H. (2003). Reactors in process engineering. *Encyclopedia of Physical Science and Technology*, **1**, 1–54.

Haario, H., Saksman, E., & Tamminen, J. (1999). Adaptive proposal distribution for random walk metropolis algorithm. *Computational Statistics*, **14**(3), 375–396.

Haario, H., Saksman, E., & Tamminen, J. (2001). An adaptive metropolis algorithm. *Bernoulli*, **7**(2), 223–242.

Hahl, S. K., & Kremling, A. (2016). A comparison of deterministic and stochastic modeling approaches for biochemical reaction systems: On fixed points, means, and modes. *Frontiers in Genetics*, **7**, 157.

Hill, C. G., & Root, T. W. (1977). An introduction to chemical engineering kinetics & reactor design. Wiley Online Library.

Ibrehem, A. S. (2011). Modified mathematical model for neutralization system in stirred tank reactor. *Bulletin of Chemical Reaction Engineering & Catalysis*, **6**(1), 47–52.

Jang, S., & Gopaluni, R. (2011). Parameter estimation in nonlinear chemical and biological processes with unmeasured variables from small data sets. *Chemical Engineering Science*, **66**(12), 2774–2787.

Jiang, J., Wu, J., Poncin, S., & Li, H. Z. (2016). Effect of hydrodynamic shear on biogas production and granule characteristics in a continuous stirred tank reactor. *Process Biochemistry*, **51**(3), 345–351.

Jingjing, D., Chunyue, S., & Ping, L. (2007). Modeling and control of a continuous stirred tank reactor based on a mixed logical dynamical model. *Chinese Journal of Chemical Engineering*, **15**(4), 533–538.

Kandiyoti, R. (2009). Fundamentals of reaction engineering. Bookboon.

Karadimou, D., Papadopoulos, P., & Markatos, N. (2019). Mathematical modelling and numerical simulation of two-phase gas-liquid flows in stirred-tank reactors. *Journal of King Saud University-Science*, **31**(1), 33–41.

Karimi, H., & McAuley, K. B. (2014). A maximum-likelihood method for estimating parameters, stochastic disturbance intensities and measurement noise variances in nonlinear dynamic models with process disturbances. *Computers & Chemical Engineering*, **67**, 178–198.

Karimi, H., & McAuley, K. B. (2015). A bayesian method for estimating parameters in stochastic differential. *IFAC-Papers On Line*, **48**(8), 147–152.

Kockmann, N. (2019). A brief history of chemical reactor and reaction technology. *Chemie Ingenieur Technik*, **91**(7), 941–952.

Laine, M. (2008). Adaptive MCMC methods with applications in environmental and geophysical models.

Lee, V. (1969). Transport phenomena equations of change. *Chemical Engineering Education*, **3**(3), 126–128.

López Buriticá, K., Casanova Trujillo, S., Acosta, C. D., & Granada Diaz, H. A. (2015). Dynamical analysis of a continuous stirred-tank reactor with the formation of biofilms for wastewater treatment. *Mathematical Problems in Engineering*, **2015**.

Lorenz, T. (2006). Reynold's transport theorem for differential inclusions. *Set-Valued Analysis*, **14**(3), 209–247.

Lu, Y., Fang, Z., & Gao, C. (2017). Stabilization of (state, input)-disturbed cstrs through the port-hamiltonian systems approach. *arXiv preprint arXiv:1707.01560*, **3**, 1–11.

Mao, Z., & Yang, C. (2017). Micro-mixing in chemical reactors: a perspective. *Chinese Journal of Chemical Engineering*, **25**(4), 381–390.

Marino, S., Hogue, I. B., Ray, C. J., & Kirschner, D. E. (2008). A methodology for performing global uncertainty and sensitivity analysis in systems biology. *Journal of Theoretical Biology*, **254**(1), 178–196.

Masoumi, S., Duever, T. A., & Reilly, P. M. (2013). Sequential markov chain monte carlo (mcmc) model discrimination. *The Canadian Journal of Chemical Engineering*, **91**(5), 862–869.

Mbalawata, I. S., Särkkä, S., & Haario, H. (2013). Parameter estimation in stochastic differential equations with markov chain monte carlo and non-linear kalman filtering. *Computational Statistics*, **28**(3), 1195–1223.

Mbalawata, I. S., Särkkä, S., Vihola, M., & Haario, H. (2015). Adaptive metropolis algorithm using variational bayesian adaptive kalman filter. *Computational Statistics & Data Analysis*, **83**, 101–115.

Moraes, A. (2015). Simulation and statistical inference of stochastic reaction networks with applications to epidemic models. PhD thesis.

Moran, S., & Henkel, K.-D. (2000). Reactor types and their industrial applications. *Ullmann's Encyclopedia of Industrial Chemistry*, **2**, 1–49.

Muhirwa, J. P., & Ndanguza, D. (2017). Effect of random noise, quasi random noise and systematic random noise on unknown continuous stirred tank reactor (cstr). *Applied Mathematical Sciences*, **11**(62), 3051–3071.

Naikwad, S. N., & Dudul, S. V. (2009). Identification of a typical cstr using optimal focused time lagged recurrent neural network model with gamma memory filter. *Applied Computational Intelligence and Soft Computing*, **2009**.

Nanda, S. (2008). Reactors and fundamentals of reactors design for chemical reaction.

Ndanguza, D., Muhirwa, J. P., & Uwimana, A. (2019). Modeling and parameters estimation of a spatial predator-prey distribution. *Rwanda Journal of Engineering, Science, Technology and Environment*, **2**(1).

Nicoulaud-Gouin, V., Garcia-Sanchez, L., Giacalone, M., Attard, J., Martin-Garin, A., & Bois, F. Y. (2016). Identifiability of sorption parameters in stirred flow-through reactor experiments and their identification with a bayesian approach. *Journal of Environmental Radioactivity*, **162**, 328–339.

Niederberger, T. (2012). Markov chain Monte Carlo methods for parameter identification in systems biology models. PhD thesis. lmu.

Niven, R. K., Cordier, L., Kaiser, E., Schlegel, M., & Noack, B. R. (2018). Rethinking the reynolds transport theorem, liouville equation, and perron-frobenius and koopman operators. *arXiv preprint arXiv:1810.06022*, **18**(10), 6–22.

Øksendal, B. (2003). Stochastic differential equations. *In:* Stochastic differential equations. Springer.

Oksendal, B. (2013). Stochastic differential equations: an introduction with applications. Springer Science & Business Media.

Oravec, J., Bakošová, M., Hanulová, L., & Mészáros, A. (2018). Multivariable robust model predictive control of a laboratory chemical reactor. *In:* Computer Aided Chemical Engineering. Elsevier.

Osorio, B. G., Castro, H. B., & Torres, J. D. S. (2011). State and unknown input estimation in a cstr using higher-order sliding mode observer. In: *IX Latin American Robotics Symposium and IEEE Colombian Conference on Automatic Control, 2011 IEEE*. IEEE.

Poulopoulos, S. G., & Inglezakis, V. J. (2006). Adsorption, ion exchange and catalysis: design of operations and environmental applications. Elsevier.

Prokopová, Z., & Prokop, R. (2009). Modelling and simulation of chemical industrial reactors. In: *ECMS*.

Rajagopalan, T., & Seshadri, V. (1972). Analysis of continuous stirred tank reactor as a multivariable process and algorithms for computer determination of the equilibrium states. *International Journal of Control*, **15**(3), 497–507.

Ramli, N. M., & Mohamad, M. S. (2017). Modelling for temperature non-isothermal continuous stirred tank reactor using fuzzy logic. *International Journal of Environmental and Ecological Engineering*, **11**(2), 169–175.

Remo, F., Luboobi, L. S., Mabalawata, I. S., & Nannyonga, B. K. (2018). A mathematical model for the dynamics and mcmc analysis of tomato bacterial wilt disease. *International Journal of Biomathematics*, **11**(01), 1850001.

Renard, P., Alcolea, A., & Gingsbourger, D. (2013). Stochastic versus deterministic approaches. *In:* Environmental Modelling: Finding Simplicity in Complexity, Second Edition (eds J. Wainwright and M. Mulligan). Wiley Online Library.

Rowse, L. E. (2011). Design of small scale anaerobic digesters for application in rural developing countries. University of South Florida.

Roy, V. (2020). Convergence diagnostics for markov chain monte carlo. *Annual Review of Statistics and Its Application*, **7**, 387–412.

Russo, L. P., & Bequette, B. W. (1993). Cstr performance limitations due to cooling jacket dynamics. *In:* Dynamics and Control of Chemical Reactors, Distillation Columns and Batch Processes. Elsevier.

Salmi, T. O., Mikkola, J. P., & Warna, J. P. (2010). Chemical reaction engineering and reactor technology. CRC Press.

Sauer, T. (2012). Numerical solution of stochastic differential equations in finance. *In:* Handbook of computational finance. Springer.

Sethi, S. P., & Lehoczky, J. P. (1981). A comparison of the ito and stratonovich formulations of problems in finance. *Journal of Economic Dynamics and Control*, **3**, 343–356.

Shakeri, E., Latif-Shabgahi, G., & Abharian, A. E. (2018). Design of an intelligent stochastic model predictive controller for a continuous stirred tank reactor through a fokker-planck observer. *Transactions of the Institute of Measurement and Control*, **40**(10), 3010–3022.

Sharma, S. (2017). Markov chain monte carlo methods for bayesian data analysis in astronomy. *Annual Review of Astronomy and Astrophysics*, **55**, 213–259.

Sinha, A., & Mishra, R. K. (2018). Control of a nonlinear continuous stirred tank reactor via event triggered sliding modes. *Chemical Engineering Science*, **187**, 52–59.

Sinharay, S. (2003). Assessing convergence of the markov chain monte carlo algorithms: A review. *ETS Research Report Series*, **2003**(1), i–52.

Stepanov, I. A. (2017). Exact calculation of the internal energy of the ideal gas in statistical mechanics. *Physical Science International Journal*, **14**(5), 1–5.

Telen, D., Vercammen, D., Logist, F., & Van Impe, J. (2014). Robustifying optimal experiment design for nonlinear, dynamic (bio) chemical systems. *Computers & Chemical Engineering*, **71**, 415–425.

Theodore, L. (2012). Chemical reactor analysis and applications for the practicing engineer. Wiley Online Library.

Tofighi, S. R., Bayat, F., & Merrikh-Bayat, F. (2017). Robust feedback linearization of an isothermal continuous stirred tank reactor: H-infinity mixed-sensitivity synthesis and dk-iteration approaches. *Transactions of the Institute of Measurement and Control*, **39**(3), 344–351.

Tronci, S., Grosso, M., Alvarez, J., & Baratti, R. (2009). Stochastic dynamical nonlinear behavior analysis of a class of single-state cstrs. *IFAC Proceedings Volumes*, **42**(11), 697–702.

Uppal, A., Ray, W., & Poore, A. (1974). On the dynamic behavior of continuous stirred tank reactors. *Chemical Engineering Science*, **29**(4), 967–985.

Valderrama Bahamondez, G. I., & Fröhlich, H. (2019). Mcmc techniques for parameters estimation of ode based models in systems biology. *Frontiers in Applied Mathematics and Statistics*, **5**, 55.

Vojtesek, J., & Dostal, P. (2008). Simulation analyses of continuous stirred tank reactor. *IEEE Transactions Automatic Control*, **24**, 27–31.

Vojtesek, J., & Dostal, P. (2009). Simulation of adaptive control of continuous stirred tank reactor. *International Journal of Simulation Modelling (IJSIMM)*, **8**(3).

Wilhelm, R. (1962). Progress towards the a priori design of chemical reactors. *Pure and Applied Chemistry*, **5**(3-4), 403–422.

Yamamoto, T., Fang, Y., & Komarov, S. V. (2019). Surface vortex formation and free surface deformation in an unbaffled vessel stirred by on-axis and eccentric impellers. *Chemical Engineering Journal*, **367**, 25–36.

Zhang, S., Müller, D., Arellano-Garcia, H., & Wozny, G. (2013). Cfd simulation of the fluid hydrodynamics in a continuous stirred-tank reactor. *Chemical Engineering*, **32**.

APPENDICES

Research Output

(i) Publication 1: Markov Chain Monte Carlo Analysis of the Variable-Volume Exothermic Model for a Continuously Stirred Tank Reactor

Engineering, Technology & Applied Science Research *Vol. 11, No. 2, 2021, 6919-6929* 6919

Markov Chain Monte Carlo Analysis of the Variable-Volume Exothermic Model for a Continuously Stirred Tank Reactor

Jean Pierre Muhirwa
Department of Applied Mathematics and Computational Science (AMCS), Nelson Mandela African Institution of Science and Technology Tanzania (NM-AIST)
Arusha, Tanzania and
Department of Mathematics, University of Rwanda, College of Science and Technology (UR-CST), Kigali, Rwanda
muhirwaj@nm-aist.ac.tz

Isambi Sailon Mbalawata
Research Department
African Institute for Mathematical Sciences (AIMS)
Kigali, Rwanda
imbalawata@nexteinstein.org

Verdiana Grace Masanja
Department of Applied Mathematics and Computational Science (AMCS)
Nelson Mandela African Institution of Science and Technology Tanzania (NM-AIST)
Arusha, Tanzania
verdiana.masanja@nm-aist.ac.tz

Abstract-In this paper, a variable-volume Continuously Stirred Tank Reactor (CSTR) deterministic exothermic model has been formulated based on the Reynold Transport Theorem. The numerical analysis of the formulated model and the identifiability of its physical parameters are done by using the least squares and the Delayed-Rejection Adaptive Metropolis (DRAM) method. The least square estimates provide the prior information for the DRAM method. The overall numerical results show that the model gives an insight in describing the dynamics of CSTR processes, and 14 parameters of the CSTR are well identified through DRAM convergence diagnostic tests, such as trace, scatter, autocorrelation, histograms, and marginal density plots. Global sensitivity analysis was further performed, by using the partial rank correlation coefficients obtained from the Latin hypercube sampling method, in order to study and quantify the impact of estimated parameters, uncertainties on the model outputs. The results showed that 7 among the 14 estimated model parameters are very sensitive to the model outcomes and so those parameters need to be handled and treated carefully.

Keywords-parameter identifiability; variable volume; exothermic; CSTR; RTT; MCMC; DRAM

I. INTRODUCTION

During the past decades, Continuously Stirred Tank Reactors (CSTRs) have gained research momentum as important industrial and chemical production tools. For controlling the reactors, various methods have been proposed to tackle the complexity and the non-linearity operational behaviors that are present in the tank reactor during the production processes [1-6]. Discussions about CSTRs seem to be broad and range from general to specific purposes. For example, mathematical modeling and numerical simulations of two-phases which are gas-liquid flow in the CSTR can be found in [7] and the Fokker-Plank Equation was applied for a two-state stochastic CSTR system in [8]. In [9], the robust feedback linearization of an isothermal CSTR was conducted by using the mixed sensitivity synthesis and iteration approaches in the presence of uncertainties. A one state variable, temperature, of a non-isothermal CSTR was analyzed by using Proportional Integral Derivative (PID) and fuzzy logic controllers, and the results from simulations and temperature control show that fuzzy logic can be adopted as a good controller of the process compared with the PID controller [10, 17]. The effects of hydrodynamic shear on biogas production in the CSTR using the Metzner-Otto method were analyzed and discussed in [11]. The Bayesian approach was used in [12] as the sorption parameter identifiability tool. The research outputs showed that the Bayesian inference is a more preferable method for the analysis of CSTR experiments as per numerical identifiability as well as the sorption parameter identifiability. The efficient Azo Dye color identification in the CSTR with the built-in bio-electrochemical system was developed for Azo dye alizarin Yellow R (AYR) which in turn can help in waste-water treatment [13]. Authors in [14] investigated the performance of CSTR as bioreactor for producing biohydrogen from water melon waste in the anaerobic digester. The Lyapunov-based stochastic non-linear model predictive control was used in [15] to shape the state probability density functions in the CSTR with the exothermic reaction $A \xrightarrow{k} B$, where k is the reaction rate, A is the reactant and B is the product. The

(ii) Publication 2: Sensitivity and Uncertainty Analysis of Variable-Volume Deterministic Model for Endothermic Continuously Stirred Tank Reactor

Journal of Mathematics and Informatics
Vol. 20, 2021, 73-89
ISSN: 2349-0632 (P), 2349-0640 (online)
Published 4 May 2021
www.researchmathsci.org
DOI: http://dx.doi.org/10.22457/jmi.v20a08189

Journal of
Mathematics and Informatics

Sensitivity and Uncertainty Analysis of Variable-Volume Deterministic Model for Endothermic Continuously Stirred Tank Reactor

***Jean Pierre Muhirwa*[1,2,*], *Isambi Sailon Mbalawata*[3] and *Verdiana Grace Masanja*[1]**

[1]Nelson Mandela African Institution of Science and Technology Tanzania
School of Computational and Communication Science and Engineering
Department of Applied Mathematics and Computational Science
Arusha-Tanzania,
[2]University of Rwanda-College of Science and Technology, School of Science
Department of Mathematics, Kigali-Rwanda,
[3]African Institute for Mathematical Sciences-Secretariat, Research Department,
Kigali-Rwanda
[2]E-mail: verdiana.masanja@nm-aist.ac.tz; [3]E-mail: imbalawata@nexteinstein.org,
[*]Corresponding author. Email: muhirwaj@nm-aist.ac.tz,

Received 7 March 2021; accepted 29 April 2021

Abstract. This paper deals with the formulation and the identifiability of the variable-volume deterministic model for the endothermic continuously stirred tank reactor (CSTR). The identifiability of physical parameters of the formulated model is done by using the least squares and the delayed rejection adaptive algorithm version of the Markov chain Monte Carlo (MCMC) method. The least square estimates are used as prior information for the MCMC method. To measure the model output associated with the perturbed model parameters, we use global sensitivity analysis implemented in Latin Hypercube Sampling method. The obtained results from partial rank correlation coefficients show that six parameters are very sensitive and correlated with the model outputs. Finally, we show that the least square and the MCMC numerical results impart the model to be realistic, reliable and worthwhile to describe the dynamics of CSTR processes as physical parameters of the model are well identified and their uncertainties in the model response are analysed and quantified.

Keywords: Variable-volume; Markov chain Monte Carlo; Endothermic; continuously stirred tank reactor

AMS Mathematics Subject Classification (2010): 65C05, 78M31

Selected Matlab Codes

```
%% Euler-Maruyama Matlab codes for stochastic model
%% in Scenario A (exothermic) but it can be adopted
% to other SDEs in this dissertation accordingly.
%% Model function
function ds = exomodel(t,y,theta)

V = y(1);C = y(2);T = y(3); Tc = y(4);

Tcin = 10; R = 8.341; Cin = 31.68; Tin = 20.0; Fin = 1.3;
Fout = theta(1);F = theta(2);k0 = theta(3);E = theta(4);
Tmean = theta(5);deltaH = theta(6);rho = theta(7);
Cp =  theta(8);U = theta(9);A = theta(10);Fc = theta(11);
Vc = theta(12);rhoc = theta(13);Cpc =  theta(14);

k = k0*exp(-E/R*(1/T-1/Tmean));
rate = k*C;% reaction rate

dVdt =Fin-Fout;
dCdt = (F/V).*(Cin-C)- rate;
dTdt = (F/V).*(Tin-T)- deltaH*rate/(rho*Cp)-((U*A)/(rho*V*Cp))
.*(T-Tc);
dTcdt = (Fc/Vc).*(Tcin-Tc) + U*A/(rhoc*Vc*Cpc).*(T-Tc);

ds = [dVdt;dCdt;dTdt;dTcdt]; %solutions vector
end

clc
clear all; close all;
% Parameter values
theta(1)= 1.3*10^(-4); theta(2)= 130e-2; theta(3) = 0.9;
```

```
theta(4)= 0.5; theta(5)= 29.815; theta(6)= -1004.3*10^(-3);
theta(7) = 1; theta(8)  = 4.186; theta(9)  = 10;
theta(10) = 0.015;
theta(11) = 46.5e-2;theta(12) = 50e-2; theta(13) = 1;
theta(14) = 4.186;

%time = linspace(0,20);%time space
n = 10000;
tmax = 2.0;
time = linspace ( 0, tmax, n + 1 );
 y0 = [10 31.68 5 20 ]';% initial solutions vector
% Numerical solver
[t, s] = ode45(@exomodel,time, y0,[],theta);
x0 =[ 10,31.68,5,20];
 r = 8;
 seed = 123456789;

 rng ( seed )
%
%  Set time steps.
%
  dt_large = tmax / n;
  dt_small = tmax / n / r;
%
%  Carry out the Euler-Maruyama approximate
%integration process.
%
  t = linspace ( 0, tmax, n + 1 );
  x1 = zeros ( 1, n + 1 );
  x2 = zeros ( 1, n + 1 );
  x3 = zeros ( 1, n + 1 );
  x4 = zeros ( 1, n + 1 );
```

```
  x1(1) = x0(1);
  x2(1) = x0(2);
  x3(1) = x0(3);
  x4(1) = x0(4);
Fin = 1.3; F = 1.3; Fout = 1.3*10^(-4); k0 = 0.9;
E = 0.5;
Tmean  = 29.815;H = -1004.3*10^(-3);rho = 1;
Cp = 4.186;
U = 10; A = 0.015; Fc = 46.56*10^(-2);
Vc = 50*10^(-2);
rhoc = 1; Cpc = 4.186; Tcin = 10; R = 8.341;
Cin = 31.68;
Tin = 20.0;
for j = 1 : n
  sigma = 0.1;
  dw = sqrt ( dt_small ) * randn ( 1, r );
  x1(j+1) = x1(j) + dt_large * (Fin-Fout) +
  sigma * sum ( dw(1:r) );
  x2(j+1) = x2(j) + dt_large *((F/x1(j))*(Cin-x2(j))
  -k0*exp((-E/R)
  *(1/x3(j) - 1/Tmean))*x2(j)) + sigma* sum ( dw(1:r) );
  x3(j+1) = x3(j) + dt_large * ((F/x1(j))*(Tin-x3(j))-
  (H*k0*exp((-E/R)*(1/x3(j) - 1/Tmean))*x2(j))/(rho*Cp) -
  U*A*(x3(j)-x4(j))/(rhoc*Cp*x1(j)))+ sigma *
   sum ( dw(1:r) );
  x4(j+1) = x4(j) + dt_large *((Fc/Vc).*(Tcin-x4(j))+
  U*A*(x3(j)-x4(j))/(rhoc*Vc*Cpc))+ sigma* sum ( dw(1:r) );
  end
 %Plot the approximate solution.
  subplot(2,2,1)
  plot ( t, x1, 'r-', 'LineWidth', 2 ), hold on, grid on
```

```
plot(t,s(:,1),'b-','LineWidth', 2);axis tight; grid on
xlabel ( 'time (t)', 'FontSize', 16 )
%legend('V(t)','C(t)','T(t)','T_c(t)')
ylabel ( 'V(t)', 'FontSize', 16, 'Rotation', 0,
'HorizontalAlignment', 'right')
legend('Stochastic', 'Deterministic')
title ( 'Euler-Maruyama solution of volume',
 'FontSize', 12 )
subplot(2,2,2)
plot ( t, x2, 'Color',[0.9100 0.4100 0.1700],
'LineWidth', 2 )
, hold on,  grid on
plot(t,s(:,2), 'k-','LineWidth', 2);axis tight; grid on
xlabel ( 'time (t)', 'FontSize', 16 )
ylabel ( 'C(t)', 'FontSize', 16, 'Rotation', 0,
'HorizontalAlignment', 'right')
legend('Stochastic', 'Deterministic')
title ( 'Euler-Maruyama solution of Concentration',
 'FontSize', 12 )
subplot(2,2,3)
plot ( t, x3, 'm-', 'LineWidth', 2 ),
hold on, grid on
plot(t,s(:,3),'g-','LineWidth', 2);axis tight;
 grid on
xlabel ( 'time (t)', 'FontSize', 16 )
ylabel ( 'T(t)', 'FontSize', 16, 'Rotation', 0,
'HorizontalAlignment', 'right')
legend('Stochastic', 'Deterministic')
title ('Euler-Maruyama solution of Temperature',
'FontSize', 12 )
subplot(2,2,4)
plot ( t, x4,'Color',1/255*[0,104,87], 'LineWidth', 2 ),
```

```
 hold on, grid on
plot(t,s(:,4),'Color',[.5 0 .5],'LineWidth', 2);axis
tight; grid on
xlabel ( 'time (t)', 'FontSize', 16 )
ylabel ( 'T_c(t)', 'FontSize', 16, 'Rotation', 0,
'HorizontalAlignment',  'right' )
legend('Stochastic', 'Deterministic')
title ('Euler-Maruyama solution of Cooling Temperature',
'FontSize', 12 )
```

Poster Presentation: Mathematical Modelling and Analysis of Deformable Perturbed Continuously Stirred Tank Reactor (CSTR)

Introduction

Continuously Stirred Tank Reactors (CSTRs) are very useful chemical reactors that produce chemical products from the given inputs of reactants [1]. The complexity and the non-linearity dynamical behaviours of CSTRs have attracted many researchers, especially mathematicians who can contribute to determining, predicting, estimating parameters and controlling the states of these reactors. This research aims at formulating CSTRs' deterministic and stochastic models and the use of Bayesian and statistical methods to analyse them.

Materials and Methods

The following figures were used for models formulations for both exothermic and endothermic reactions.

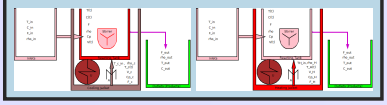

Mathematical Models

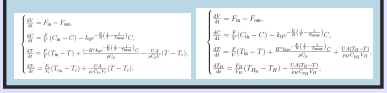

Conclusion

The aim of the current study was to develop deterministic and non-deterministic mathematical models for continuously stirred tank reactor (CSTR) and use the statistical and Bayesian methods to analyse and estimate the unknown physical parameters. The results from the least squares showed that the models' estimates can be well fitting the theoretical models, provided that the noise intensity is minimized and ranges between 0 and 0.5. It was observed that stochastic results agree with deterministic models' solutions if the volatility constants are small. Furthermore, through simulations, it was observed that the deformation of the tanks can be caused by the increase of the volume. The formulated models can be used to describe biological, chemical and mechanical processes as they were validated by using Markov chain Monte Carlo and Latin Hypercube Sampling techniques via sensitivity and uncertainty analysis.

References

[1] Telen, D., Vercammen, D., Logist, F., and Van Impe, J. (2014). Robustifying optimal experiment design for nonlinear, dynamic (bio) chemical systems. Computers chemical engineering, 71, 415-425.

Acknowledgements

My acknowledgements go to my sponsor, DAAD, my employer, UR-CST, my host University, NM-AIST and publication support from AIMS Secretariat.

Deterministic Results

we can see that the concentration of the reactants is decreasing inside the tanks for both exothermic and endothermic reactions. As the reactants react inside the tanks its concentration decreases and stabilize around 0 moles/m^3. Also these Figures show that as the temperature of the systems rises/decreases, there must be a cooling/heating process which decreases/increase the temperature of the reacting tank towards its stable point. In this case, the temperature at the cooling/heating jacket also increases/decrease and both temperature stabilize to their working points after 5 minutes of the start of the reaction. The volume of the reacting tanks increases from $100m^3$ to $126m^3$ as the inlet feeding rates becomes greater than the outlet feeding rates. If the volume continues to increase linearly, this may lead to deformation. To avoid this inconvenience, there should be system regularization and designation of the feeding which maintains the feeding rates and the outlet rates at constant values.

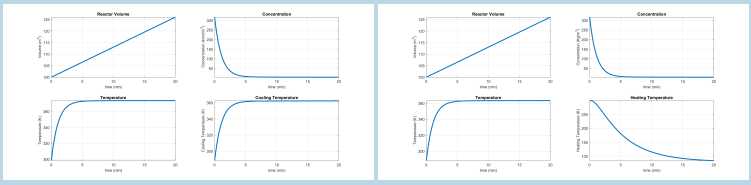

Stochastic Results

In below Figures, there are the numerical solutions of the derived stochastic model Equations and the corresponding numerical solutions of the deterministic model Equations. These figures show that stochastic model results behave like its respective deterministic models as their results are coinciding.

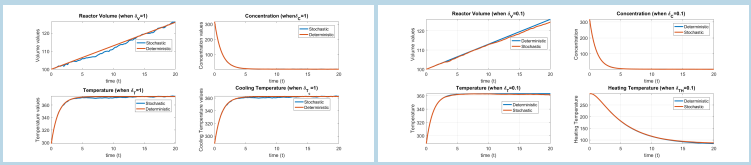

We have carried out sensitivity and uncertainty analysis of the estimated parameters on the formulated model and the results are displayed. The figures show that the first parameter (F_{out}) is strongly and negatively correlated with the volume means that the increase in the values of F_{out} decreases the values of the volume in the reacting tank. Likewise, the second parameter (F) is positively correlated with the concentration whilst the third one is significantly and negatively correlated with the concentration, and consequently, the increase in the values of F will increase the values of the concentration in the model and the increase of k_0 will decrease the concentration values of the model. We can further explore that the increase of sixth parameter (H^*) values will increase the temperature of the tank whereas the increase of the seventh (ρ) and the eighth (C_p) parameters values will automatically decrease the temperature values in the formulated model. The Figures show that only the sixth parameter is negatively correlated with the cooling/heating temperature which explains that the increase in the enthalpy values will directly inhibit the increase of the cooling/heating temperature values. As a result, $F_{out}, F, k_0, H^*, \rho$ and C_p parameters are identified to be very sensitive to the model Equation and hence much attention has to be quantitatively and qualitatively accorded to those influential model parameters.